UNIVERSITY OF CALIFORNIA,

IRVINE

Electrospray Thrusters for Attitude Control of a 1-U CubeSat

THESIS

submitted in partial satisfaction of the requirements

for the degree of

MASTER OF SCIENCE

in Mechanical and Aerospace Engineering

by

Navin Timilsina

Thesis Committee:

Associate Professor Manuel Gamero-Castano, Chair

Professor Roger H. Rangel

Associate Professor Lorenzo Valdevit

2014

TABLE OF CONTENTS

Page

LIST OF TABLES

Page

LIST OF FIGURES

Page

ACKNOWLEDGEMENTS

I would like to thank my advisor and thesis committee chair, Associate Professor Manuel Gamero-Castano, for all his continuous help, support and guidance during the past two years at the University of California, Irvine.

Thanks to the Department of Mechanical and Aerospace Engineering for providing me the fellowship to pursue this Master of Science at the University of California, Irvine. Special thanks also to Professor Roger H. Rangel for his guidance and support for obtaining the fellowship. Without this support, it would be unimaginable for me to obtain my Master's degree.

My kindest gratitude to my fellow lab mates Rafael Borrajo and Enric Grustan for their support and help in the laboratory. I can't stop thanking Gleb Melnikov, the undergraduate researcher who designed the preliminary version of Wireless Control used in this thesis. I would also like to show appreciation to Mr. David Hartwig for teaching me how to use different fabricating tools.

Last but not least, my eternal gratitude to my family and friends all around the world for giving me constant help and motivation to get to this point.

ABSTRACT OF THE THESIS

Electrospray Thrusters for Attitude Control of a 1-U CubeSat

by

Navin Timilsina

Master of Science in Mechanical and Aerospace Engineering

University of California, Irvine, 2014

Associate Professor Manuel Gamero-Castano, Chair

With a rapid increase in the interest in use of nanosatellites in the past decade, finding a precise and low-power-consuming attitude control system for these satellites has been a real challenge. In this thesis, it is intended to design and test an electrospray thruster system that could perform the attitude control of a 1-unit CubeSat.

Firstly, an experimental setup is built to calculate the conductivity of different liquids that could be used as propellants for the CubeSat. Secondly, a Time-Of-Flight experiment is performed to find out the thrust and specific impulse given by these liquids and hence selecting the optimum propellant. On the other hand, a colloidal thruster system for a 1-U CubeSat is designed in Solidworks and fabricated using Lathe and CNC Milling Machine. Afterwards, passive propellant feeding is tested in this thruster system. Finally, the electronic circuit and wireless control system necessary to remotely control the CubeSat is designed and the final testing is performed.

Among the propellants studied, Ethyl ammonium nitrate (EAN) was selected as the best propellant for the CubeSat. Theoretical design and fabrication of the thruster system was

performed successfully and so was the passive propellant feeding test. The satellite was assembled for the final experiment but unfortunately the microcontroller broke down during the first test and no promising results were found out. However, after proving that one thruster works with passive feeding, it could be said that the ACS testing would have worked if we had performed vacuum compatibility tests for other components beforehand.

1. INTRODUCTION

The concept of CubeSats was introduced in late 90s and more than 100 successful launches have been made by the end of 2012 [1]. Among these CubeSats, most don't have any Attitude Control System (ACS) incorporated in them, while some of them have used Magnetic Torquers or Reaction Wheels [2]. As Earth's magnetic field varies with time, use of Magnetic Torquers for ACS is not feasible when we are looking for a very precise attitude control. In the case of Reaction Wheels, they can work for a limited amount of time as they have a limited capacity to accumulate angular momentum and have to be "unloaded" to continue working [3]. Given this scenario, an ACS system using Electrospray thrusters could solve all these problems as we can obtain a precise attitude control with very low available power which could work for a longer period of time given that these thrusters have high Specific Impulse (Isp). This thesis is based on designing, fabricating and testing an Electrospray thruster system for the Attitude Control of a 1U CubeSat and finding the best propellant among various for its use in the CubeSat. We will discuss shortly about Electrospray technique and CubeSats and later elaborate the objectives of the thesis.

1.1 Electrospray Technique

Electrospray is a technique in which charged droplets are produced from liquid and later accelerated applying high electric field. When the electric field applied to a liquid surface is higher than its surface tension, the liquid surface deforms, forming a cone-like structure called Taylor cone. If a proper liquid flow is fed to the cone simultaneously, a steady jet comes out from its apex, which eventually breaks down into charged droplets [4].

Propellant feeding in an electrospray thruster can be done in two ways: Active Feeding or Passive Feeding. The propellant tank is pressurized thus making the liquid flow due to pressure difference

in active feeding. While in passive feeding, the propellant reaches the tip of the emitter due to capillary action and is driven or stopped by the electric field applied to the emitter. Passive feeding requires only one shutoff valve for the whole propellant delivery system and simple voltage signals to drive the propellant to each emitter, while the other requires the use of a pressurizing mechanism and a regulating valve for each emitter in the system. Generation of bubbles and trapping of gas in the propellant lines is one of the common malfunctions in electrospray thrusters using active feeding and the risk of having this problem is multiplied when we use electrospray thrusters for attitude control because at least six thrusters are required for it. Though current implementations use active feeding systems, because of lower cost, weight, power requirements and risks of malfunctioning, we will choose a passive propellant feeding system for our use.

Besides electric propulsion, electrospray technique can be used in various other fields listed below.

- Electrospray Ionization: This technique is used in mass spectrometry in order to produce ions, especially from macromolecules [5].
- Electrospinning: The application of high voltage to a polymer solution forms a cone-jet geometry which, if converted into very fine fibers instead of being broken into small droplets, is called Electrospinning [6].
- Nanotechnology: This technique can be used to deposit particles in nanostructures [7].
- Bio-electrospraying: Bio-electrospraying is a new technology that enables the deposition of living cells on various targets. Using this technology along with mass spectrometry, healthy and unhealthy cells could be differentiated. This technology has been applied tremendously in the current Health Care industry [5].
- Liquid Metal Ion Sourcing: Liquid metals can be used to create ion sources for ion implantation techniques and to focus ion beam instruments [8].

1.2 CubeSat

CubeSat is a type of miniaturized satellite for space research that has a volume of 10 cubic centimeters and a mass up to 1.33 kg. The concept was begun at California Polytechnic State University, San Luis Obispo and Stanford University in 1999 with the primary mission of providing access to space for small payloads. Over these years, the use of CubeSat has been broadened and over 75 successful launches have been made. Earth remote sensing (Data collection on the environment, geology, climate and other characteristics of Earth) and Genetics Research are among the various purposes for which these mini satellites are being launched. Even though the primary configuration is of $10\ cm^3$ and 1 kg (1-Unit CubeSat), these units can be combined to make larger satellites that are double the size (2-U /10X10X20 cm & 2.66kg), triple the size (3-U/10X10X30 cm & 4kg) or even bigger.[1]

1.3 Objectives of the Thesis

As the title states, 'Electrospray Thrusters for Attitude Control of a 1-U CubeSat', a complete design, fabrication and testing of an electrospray thruster system for ACS of a 1-U CubeSat will be done after choosing the best propellant for this use. To start, an experimental setup is built up in order to measure the conductivity of various liquids which would be the prospective propellants for the use in our CubeSat. After this, a Time-Of-Flight experiment is carried out in order to find out the mass flow rate, specific impulse, thrust, etc. provided by a thruster. This experiment is repeated for various mass flow rates and various liquids, in order to find out the best liquid that would suit for the CubeSat. For the satellite's design, all possible thruster configurations will be considered and further design of the chosen configuration will be done using Solidworks. Once this phase is completed, using Lathe and Milling Machine, all the parts of the thruster system will be fabricated using proper material for each of them. Afterwards, a test for passive feeding system will be done using one of the thrusters designed earlier in a vacuum. Proper functioning and stability of the thruster will be checked before performing the final assembly of all the thrusters in the cubic structure representing the CubeSat. Finally, the satellite will be hung using a wire in one of the vacuum chambers and using an Arduino based wireless controller developed using LabView. The thrusters will be turned on and off and the wire will be twisted at a certain angle which can be visually seen. Knowing the thrust produced by each thruster and the properties of the wire, the angle obtained can be compared to the theoretical angle to be turned and hence to ensure the proper functioning of the system. An accelerometer is also going to be inserted into the satellite to find out the angular accelerations of the satellite at every moment.

2. CONDUCTIVITY MEASUREMENT OF PROPELLANTS

2.1 Introduction

Conductivity is the ease at which electric current or charge can pass through a material. For the liquids we will be testing afterwards as propellant of our Colloidal thrusters, an experiment will be carried out in order to measure their Electric conductivity.

2.2 Theory

Certain Potential difference will be applied between the two ends of a tube filled with the propellant liquid. The current passed through the liquid will be measured using an Ammeter and knowing the diameter and length of the tube and using Ohm's Law, the conductivity of the liquid can be found out.

Let

$$V = Voltage\ difference\ between\ the\ two\ liquids$$

$$I = Total\ current\ flown$$

$$A = Cross-sectional\ area\ of\ the\ tube$$

$$L = Length\ of\ tube$$

We know that the resistance of a liquid contained in a tube of length L and cross-sectional area A is

$$R = \frac{\rho L}{A} = \frac{L}{\sigma A}$$

where ρ & σ $are\ resistivity\ and\ conductivity\ of\ the\ liquid\ respectively$

Now, by Ohm's law,

$$R = \frac{V}{I} = \frac{L}{\sigma A} \rightarrow \boldsymbol{\sigma = \frac{I}{V} \cdot \frac{L}{A}}$$

Current will be measured for different applied voltage and then the ratio $\frac{I}{V}$ will be calculated using the regression line of all these points.

2.3 Experimental Setup

The high voltage end is connected to (5) in Figure 1 which is internally connected to the liquid through a platinum wire. The tube (4) in Figure 1 is filled with this charged liquid and submerged into another bottle. The other end of the tube is grounded so that current flows due to the potential difference, which can be measured with the help of an Electrometer.

To fill the tube with the desired liquid, first the bottle (let's say bottle 1) is connected with a high-pressure line through valve (3) Figure 1. Now due to the difference in pressure between the extreme and bottle, the liquid flows through the tube. Once we see the droplets, we submerge that end of tube in the liquid of bottle (2) and stop applying the pressure in bottle 1. Bottle 1 will have the liquid we want to measure conductivity and bottle 2 will have any other passive liquid, for example acetone.

Once the setup is ready, various potential differences are applied and the corresponding current is noted down. These data are used to find a regression line which will later give us the Current-Voltage relation needed for the conductivity calculation.

In the figure,

1, 2: Plastic Holders to place the bottles with desired liquid

3: Orifice to enter air (change pressure in the bottle)

4: Tube to transfer the liquid

5: Tip to connect the current

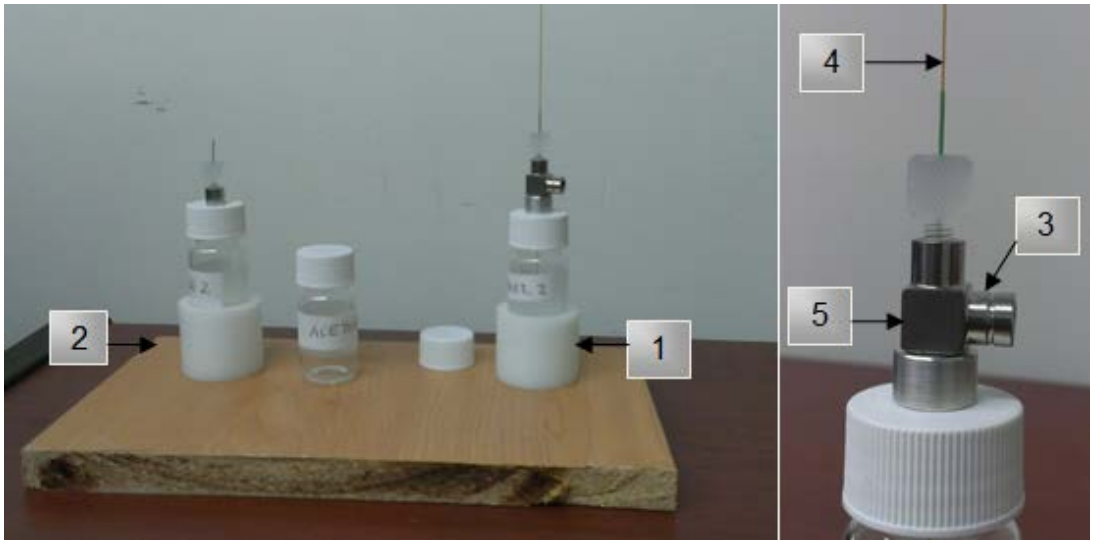

Figure 1. Equipment to measure conductivity of a liquid

2.4 Results

The propellant fluids for which this experiment is carried out are:

Table 1. Liquids whose conductivity is measured

Liquid	Full Name	Formula	Density $g\ ml^{-1}$
EAN	Ethylammonium nitrate	$C_2H_8N_2O_3$ $[(C_2H_5)NH_3]^+[NO_3]^-$	1.261
Emi IM	1-ethyl-3-methylimidazolium bis (trifluoro-methylsulfonyl) imide	$C_8H_{15}F_6N_3O_4S_2$ $[C_6H_{11}N_2]^+[N(SO_2CF_3)_2]^-$	1.53
Emi BF4	1-ethyl-3-methylimidazolium tetrafluoroborate	$C_6H_{11}BF_4N_2$	1.294
Emi TF	1-ethyl-3-methylimidazolium trifluoromethanesulfonate	$C_7H_{11}F_3N_2O_3S$	1.387
TES	Triethylsulfonium bis(trifluoromethylsulfonyl)imide	$C_8H_{15}F_6NO_4S_3$ $[C_6H_{15}S]^+[N(SO_2CF_3)_2]^-$	1.47
Formamide G	4%EAN in Formamide		
Formamide H	7%EAN in Formamide		

In Annex 7.2, all the calculations are carried out and the final conductivity of the liquids is given in Table 2.

Table 2. Conductivities of some liquid propellants to be used in Colloidal Thrusters

Liquid	Conductivity (Si/m)	Lab Temperature while measurement
EAN	2.03	19.8ºC
Emi IM	0.77	20.2ºC
Emi BF4	1.31	19.9ºC
Emi TF	1.24	19.7ºC
TES	0.64	19.9ºC
Formamide G	0.96	22.8ºC
Formamide H	1.50	20.2ºC

3. TIME-OF-FLIGHT TECHNIQUE

3.1 Introduction

In order to find out which liquid will be the best one for its use as propellant in Colloidal thrusters, it is essential to know the thrust, mass flow rate, specific impulse, and efficiency that are obtained for each liquid. According to [4], the approximate relations for thrust and specific impulse yielded by electrosprays are:

$$T \sim [2V_A \rho f(\epsilon)]^{\frac{1}{2}} \left(\frac{K\gamma Q^3}{\epsilon}\right)^{\frac{1}{4}} \qquad (1)$$

$$I_{sp} \sim \left(\frac{1}{g}\right)\left[\frac{2V_A f(\epsilon)}{\rho}\right]^{\frac{1}{2}} \left(\frac{K\gamma}{Q\epsilon}\right)^{\frac{1}{4}} \qquad (2)$$

where:

$$V_A = \ acceleration\ voltage$$

$$\rho = \ Liquid\ Density$$

$$f(\epsilon) = Dimensionless\ function$$

$$K = liquid\ electrical\ conductvity$$

$$\gamma = liquid\ surface\ tension$$

$$Q = liquid\ volumetric\ flow\ rate$$

$$\epsilon = liquid\ dielectric\ constant$$

$$g = gravity's\ acceleration$$

For a propellant liquid of fixed conductivity, the increase in flow rate translates into larger thrust output. However, the specific impulse decreases at the same time. Again, according to [4], the ranges of Q for which stable cone-jets are formed are

$$\frac{\rho Q_{min} K}{\gamma \epsilon_0 \epsilon} \sim 1 \qquad (3)$$

while the maximum value is some 20-40 times larger than Q_{min}.

Using equations (1),(2), and (3), it can be found out that the dependence of thrust and specific impulse on solution conductivity is $T \sim K^{-\frac{1}{2}}$ and $I_{sp} \sim K^{\frac{1}{2}}$. Hence, the higher the electric conductivity of the liquid more is the specific impulse.

Normally, thrust balances can be used to find more accurate values of Thrust but in this case as thrust produced are of few micronewtons, no balance is available to measure it. Moreover, it would also have been difficult to measure the mass flow rate and thrust simultaneously.

Hence, in order to find more accurate values of T and I_{sp} , experiments have to be done. Time-of-flight technique is one of the experimental methods to measure $T, \dot{m}, I_{sp}\ and\ \eta$ of charged, colloid beams accelerated by an electric field. A TOF measurement is a time dependent spectrum of a current signal associated with the electrospray beam $I(t)$ following its instantaneous interruption. From the data obtained, i.e $I(t)\ vs\ t$, the specific charge distribution, thrust, specific impulse, mass flow rate and efficiency can be found out. In Annex 7.3.1, the formulae to calculate each of the above parameters are derived and below they are listed.

$$\frac{q}{m} = \left(\frac{1}{2V_A}\right)\left(\frac{L}{t_f}\right)^2 \qquad (4)$$

$$T = -\frac{2V_A}{L}\int_{t=0}^{t=\infty} I(t)dt \qquad (5)$$

$$\dot{m} = -\frac{4V_A}{L^2}\int_{t=o}^{t=\infty} t \cdot I(t)dt \qquad (6)$$

$$I_{sp} = \frac{T}{\dot{m}g} \qquad (7)$$

$$\eta = \frac{T^2}{2\dot{m}V_A I} \qquad (8)$$

where:

$\frac{q}{m} = charge - to - mass\ ratio$

$V_A = acceleration\ Voltage$

$L = distance\ between\ emitter\ and\ the\ collector$

$t_f = time\ required\ for\ particles\ to\ cover\ the\ distance\ L\ (TOF)$

$T = thrust$

$I(t) = current\ signal\ associated\ with\ the\ electrospray\ beam$

$\dot{m} = mass\ flow\ rate$

$g = gravity's\ acceleration$

$\eta = efficiency$

3.2 Experimental Hardware

The study of the electrosprays has been made in vacuum conditions and the setup is shown in Figure 2. All these experiments will be done with active propellant feeding even though later on a passive propellant feeding will be used for the satellite.

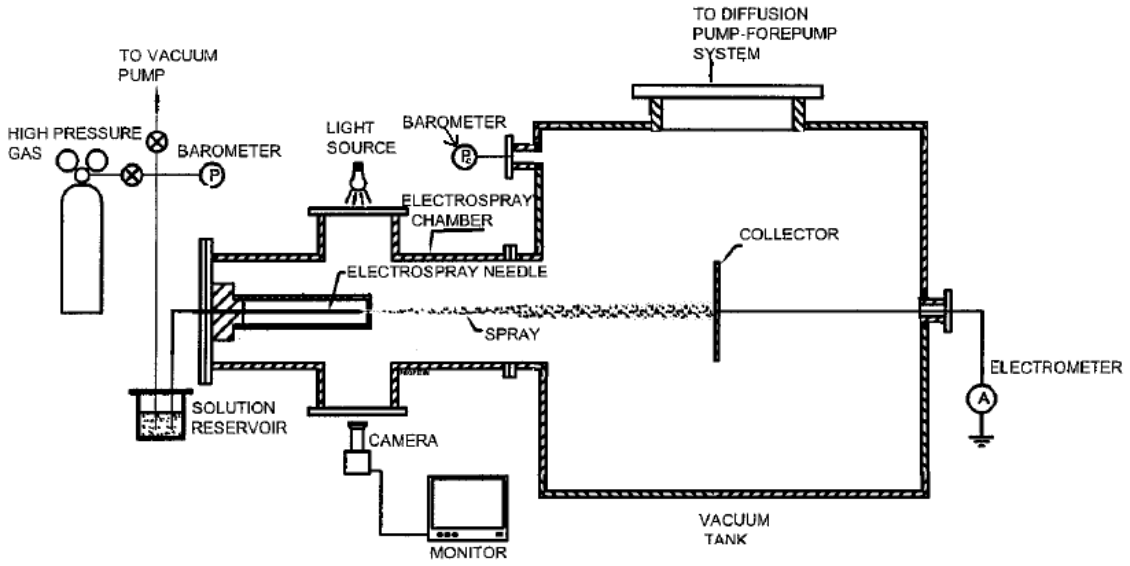

Figure 2. Schematic of the experimental setup used in the research to study electrosprays [4]

The liquid to be analyzed is kept in a glass bottle which is inserted inside another bottle that can resist a higher pressure difference with the atmosphere. The bottle is connected to a line which is later connected to vacuum and high pressure gas through different valves. A barometer is located between the vacuum and high pressure lines and the solution reservoir in order to find out the pressure at the reservoir. An electrospray needle of inner diameter = 40 μm (Polymicro technologies, 18019 N. 25th Ave., Phoenix, AZ 85023) is used and it is inserted inside a 10 cm cross, which is mounted on a cylindrical tank of diameter = 45 cm and length = 80 cm. A background pressure of 10^{-5} Torr is achieved with the help of a Mechanical Pump (S/N: 2653-2V; Welch Manufacturing company, Illinois) and a Turbo molecular pump(S/N: 220853; Model: 9698830; TU-301 Navigator). Another barometer measuring up to milli torrs is used to measure the pressure inside the vacuum tank.

The needle tip has been sharpened into a cone and made it electrically conducting depositing a layer of tin oxide in it. Also, an Optical microscope equipped with a color video camera is used to observe the needle tip on a nearby monitor.

In order to make the liquid reach from the bottle to the needle tip, there must be a pressure difference between the bottle and the vacuum tank. Once the liquid reached the needle tip, to form a cone-jet, an appropriate voltage difference between the electrospray needle and a nearby electrode, extractor hereafter, must be set. Furthermore, as the electrospray beam has to be studied far from the emission point, the extractor must have a hole in order to let the entire beam pass through it. The hole shall neither be too small to block the beam nor too big so that the electric field between the needle and the extractor may not be uniform. This electrode arrangement and the TOF apparatus are shown in Figure 3. The charged beam exiting the extractor-needle region eventually reached the collector C_{TOF} which is connected to an electrometer.

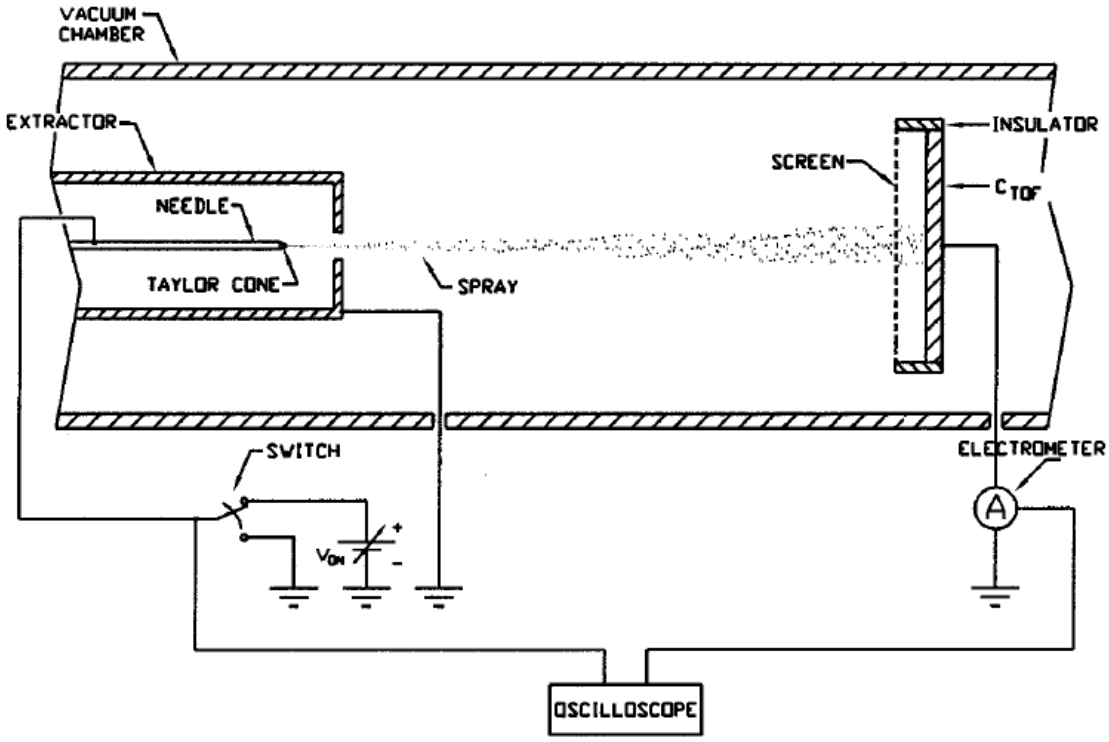

Figure 3. Sketch of the electrode geometry and electric connections employed to record time of flight spectra of colloid beams [4]

A high-speed, high-voltage switch is used to periodically short the needle voltage to ground. The falling time of the needle voltage is negligible to the time of flight of the droplets we measure during our experiments. During the interval in which the needle is shorted, the electrospraying process is interrupted, and a beam wake moves towards the collector. An oscilloscope connected to the electrometer output and triggered by the voltage signal of the electrospray needle measures the TOF of this wake. The settling time of the electrometer is also fast enough to measure these electrospray beams.

For all the experiments carried out, we will consider that the acceleration voltage is the same as the needle voltage. Also, the possible error that could be occurred because of loss of the liquid due to evaporation is ruled out according to [4].

3.3 Steps to initiate and end properly an experiment

The turbo molecular pump used to decrease the pressure in the vacuum tank to 10^{-5} Torrs is very sensitive to air molecules and can only start working at very low pressures (few milli Torrs). So, if for any reason, atmospheric air is in contact with the turbo molecular pump while it's working, the pump gets destroyed.

On the other hand, the emitter and the extractor are separated by a distance of few millimeters and a high voltage (order of kilovolts) has to be applied in between them. Hence, in order to avoid sparks in between the emitter and the extractor, the power supply of high voltage shall be turned on once the pressure inside the vacuum tank is approximately zero.

These are two of the many problems that we can encounter with while performing an electrospray experiment. Hence, it is good to follow some rules in order to start and end an experiment to avoid any problems in the experimental procedure.

Figure 4 shows some important valves to assure a proper functioning of electrosprays which are described hereafter.

- Valve 1: At the entrance of the tube connecting the vacuum chamber with the mechanical pump.
- Valve 2: Connects vacuum chamber to the atmosphere.
- Valve 3: Connects the vacuum chamber to the bottle containing liquid (propellant)
- Valve 4: Allows switching high pressure or atmospheric pressure which finally goes to the bottle via Valve 7.
- Valve 5: Valve joining another vacuum pump to the bottle
- Valve 6: Joins high pressure line to valve 4
- Valve 7: Allows connection between bottle and Valve 4/Valve 5.

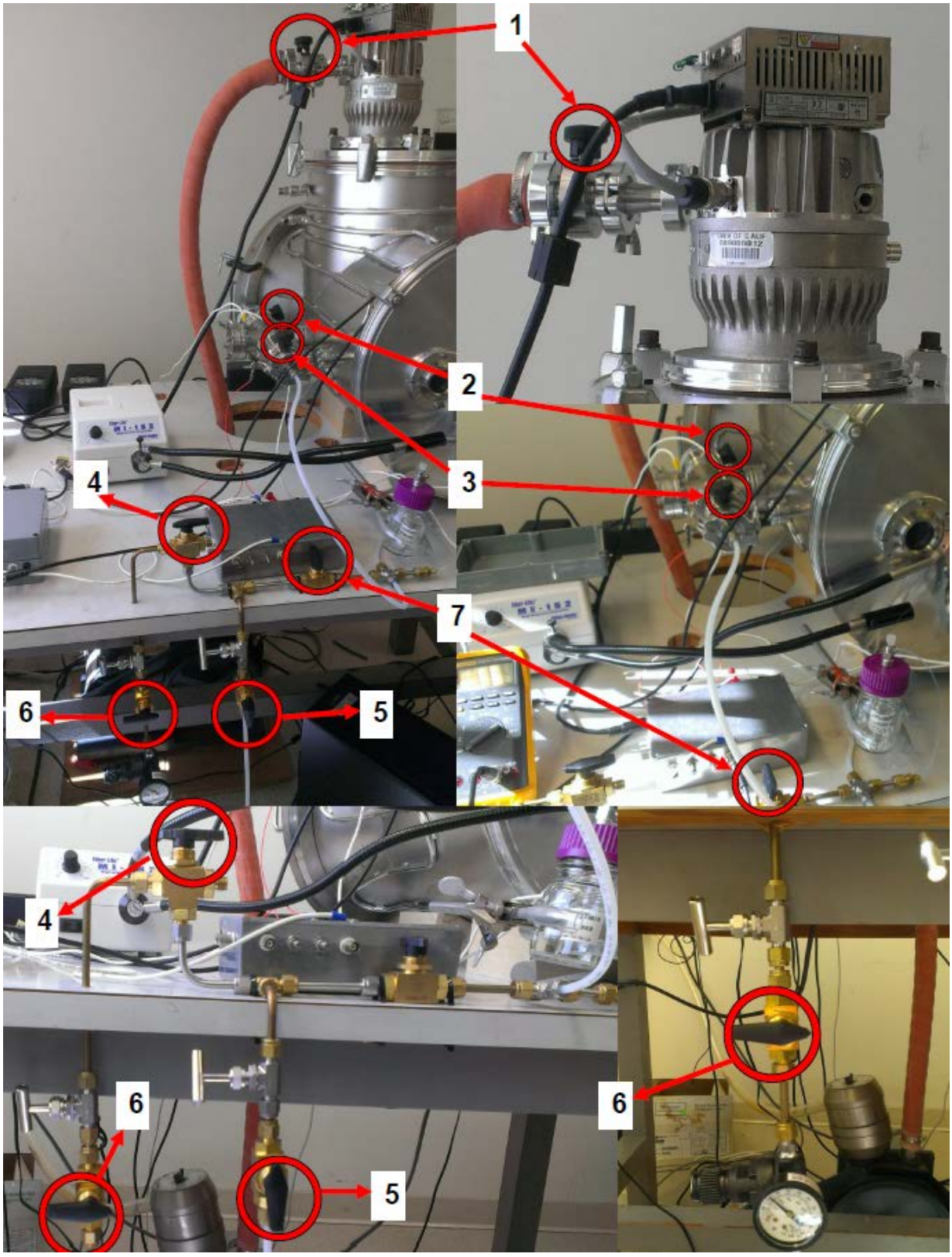

Figure 4. Important valves to assure the proper functioning of the vacuum chamber and the pumps

3.3.1 Steps to Initiate

1) Open Valve 3 and close the valves 1, 2 & 7.
2) Open the mechanical pump (I).
3) Open Valve 1
4) Check that the pressure goes on decreasing in the pressure sensor(I) and continue till the pressure is between 300 to 500 milliTorrs (this can be noticed in the another pressure sensor (II) located above the vacuum cylinder)
5) Open the turbo-molecular pump and wait till the pressure sensor II reads practically zero.
6) Apply the voltage difference and check in the oscilloscope that the voltage change effects are the proper ones. (Caution: Don't do this before the pressure inside the cylinder is absolutely zero)
7) Close the valve 3 and (open the other mechanical pump (II))
8) Open valve 7 with valves 4, 5 &6 closed.
9) Open valve 6 & switch valve 4 to high pressure line (this way the bottle will be in high pressure and liquid will flow from bottle to the electrospray source. The pressure change shall be noticed in sensor I. At the same time, it has to be checked that the pressure in sensor II has to be practically zero.
10) Once the liquid reaches the tip, close the high pressure line and leave valve 4 at atmospheric pressure. This is the regime where experiments will be conducted.

Note: If the line already has liquid, in step 9, put it in atmospheric pressure instead of high pressure

3.3.2 Steps to Close

1) Close Valve 4 and Open Valve 5.
2) Wait till the Pressure sensor I reads pressure of approximately -760 Torrs. As the atmospheric pressure changes every day, make sure that the sensor is more or less stabilized.
3) Close Valve 7 and open Valve 3. (High change in pressure shall not be noticed in both sensors).
4) Close mechanical pump II and the high voltage line.
5) Close Turbo-molecular pump.(It takes 15-20 minutes to completely stop)
6) Close Valve 1.
7) Close Mechanical pump I. You shouldn't note a rapid decrease in pressure in Sensor II.
8) If this is the case, the air is entering the cylinder and as the rotors in turbo-molecular pump are still moving, it might get damaged, so start the mechanical pump and open Valve 1.Now you'll have to wait till the turbo-molecular pump is completely closed (You will stop hearing its sound) or find the leak and arrange it.
9) If not, you're done!! Remember that if you want to leave your apparatus in atmospheric pressure, you have to wait till the turbo-molecular pump stops running and later open the Valve 2.

3.4 Experimental Procedure

3.4.1 Liquids analyzed and measurements done

The liquids whose TOF measurement is done are:

Table 3. Characteristics of Liquids used for TOF experiment.

Liquid	Full Name	Formula	Density $g\ ml^{-1}$	Conductivity (σ) (Si/m)
EAN	Ethylammonium nitrate	$C_2H_8N_2O_3$ $[(C_2H_5)NH_3]^+[NO_3]^-$	1.261	2.03 at 19.8ºC
Emi IM	1-ethyl-3-methylimidazolium bis (trifluoro-methylsulfonyl) imide	$C_8H_{15}F_6N_3O_4S_2$ $[C_6H_{11}N_2]^+[N(SO_2CF_3)_2]^-$	1.53	0.77 at 20.2ºC
Emi BF4	1-ethyl-3-methylimidazolium tetrafluoroborate	$C_6H_{11}BF_4N_2$	1.294	1.31 at 19.9ºC
Emi TF	1-ethyl-3-methylimidazolium trifluoromethanesulfonate	$C_7H_{11}F_3N_2O_3S$	1.387	1.24 at 19.7ºC
TES	Triethylsulfonium bis(trifluoromethylsulfonyl)imide	$C_8H_{15}F_6NO_4S_3$ $[C_6H_{15}S]^+[N(SO_2CF_3)_2]^-$	1.47	0.64 at 19.9ºC
Formamide G	4%EAN in Formamide			0.96 at 22.8ºC
Formamide H	7%EAN in Formamide			1.50 at 20.2ºC
Formamide 1	50% Emi IM in Formamide			1.57
Formamide 2	25% Emi IM in Formamide			1

A voltage cut off switch is designed using LabView program. Once the spray is formed, using the program, the voltage is cut off and the corresponding beam is captured in the Oscilloscope. An USB data acquisition device is used to pass this information to the computer.

For each liquid, TOF measurement is made for different mass flow rate. Mass flow rate is a parameter that we can't control directly through the experimental setup, but varying the pressure difference between the liquid bottle and the vacuum tank, a change in mass flow rate can be obtained.

Measurements are done starting from the minimum flow rate for which a Taylor cone can be formed.

In order to find out the minimum flow rate, the best idea is decrease slowly the pressure difference between the liquid bottle and the vacuum tank and find out the point when the current measured in the oscilloscope is oscillating. It has to be taken in account that, the oscillating feature is not found for every liquid. In such case, the minimum point is when a cone is stable initially but after switching the power off, the cone dies and can't get back on its own without changing voltage difference or flow rate.

The maximum flow rate can be one where the cone angle is not very small.

In between these two points: minimum flow rate and maximum, measurement is done for various flow rates and for each flow rate various measurements are taken in order to approximate better the results.

3.4.2 Correction of data obtained

The information passed from the oscilloscope to computer after a TOF experiment is in the form of a matrix with value of time in the first column and the Intensity of current in the other one. In fact the current measured is in Volts which later shall be multiplied by the gain of the circuit to get the Current in Amperes. The number of rows depends on the time fraction we have established to measure value of I (current).

A graph plotted with the initial data seems to be as in Figure 5.

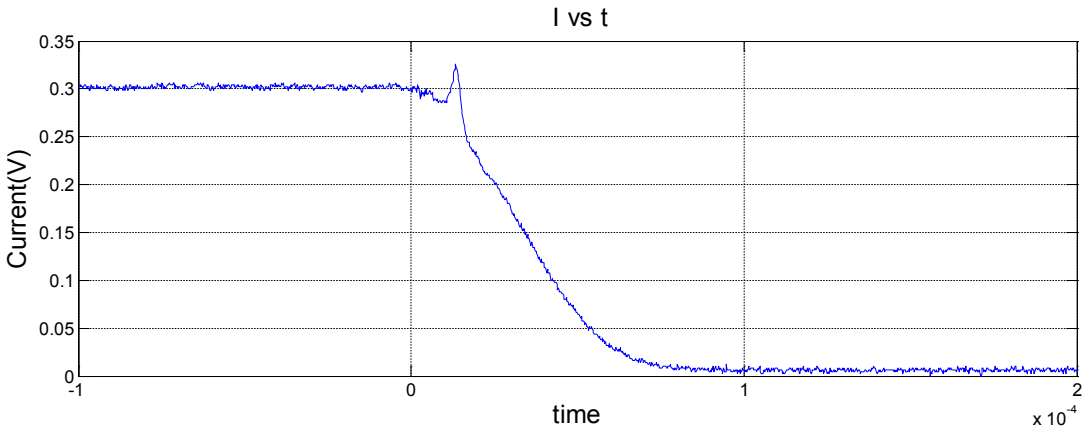

Figure 5. Evolution of current with respect to time after a voltage cut off

As we see in the graph, the voltage cut-off is carried out at time (t) = 0. The current before time = 0 represents the current due to the charge carried out by all the droplets and ions to the collector and it is uniform as expected. We need the value of this current to find out the gain of the circuit to calculate Current values in amperes. This current value is assumed to be an average of the first 50 values. Let's call it $\boldsymbol{tot\_volt}$.

Now, we have the value of total voltage seen in the electrometer. Let's call it $\boldsymbol{I1}$. Our electronic circuit is designed such that $\boldsymbol{1mV = 1.01nA}$. Hence, $\boldsymbol{I1}$ has to be multiplied by $\boldsymbol{1.01e-09}$. Let's call it $\boldsymbol{I_{amm}}$; $\boldsymbol{I_{amm} = I1 * 1.01e-09}$.

If we think, we are seeing $\boldsymbol{tot\_volt}$ in the graph instead of $\boldsymbol{I_{amm}}$.

Hence, to take this in account, all the current values of the graph has to be applied by the factor $\boldsymbol{I_{amm}/tot\_volt}$.

Secondly, we see that there is an offset in the current values different than zero which shall be removed for the calculation of thrust, specific impulse etc given by the liquid. In order to do this, an average of the last 50 values of current is calculated which will be the offset and later this offset is subtracted from all the current values.

Finally, there is a drop in voltage in between the source and the needle tip so that the value of voltage that we apply is not what is available at the needle. In Annex 7.3.2, a relation between the voltage applied at the source and voltage at the needle is found out and it is:

$$\boldsymbol{Needle\ voltage = 0.9265 * Source\ voltage + 1.7203}$$

3.5 Programming Code

In order to analyze the experimental results, we have developed some codes in MATLAB which will be shortly explained hereafter.

First of all, no all the experiments give perfect data. Hence, all the graphs have to be checked one by one and eliminate the bad ones from the list. The code developed to perform this task is presented in Annex 7.3.3.1. This code uses two functions named 'reading_filename' and 'arrange_data' which are explained later and presented in Annex 7.3.3.2 and 7.3.3.3 respectively.

Then there is a main code which calculates the average of each measurement and finds out values of Thrust, Specific Impulse, mass flow rate etc for each of them and also prints the required graphs.

3.5.1 Function 'reading_filename'

While the graph from oscilloscope passes to the computer, the filename where the data is saved is designed in such a way that it contains many experimental parameters separated between them by an '_'.An example is given in Figure 6.

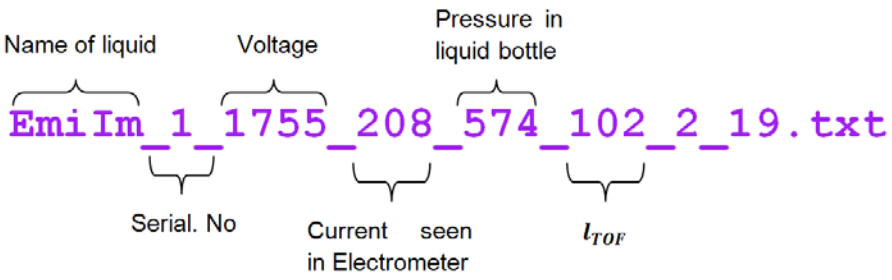

Figure 6. Filename created with the experimental parameters in it.

The serial number goes from 1 to the total number of measurements done for a same pressure and voltage. The pressure in the bottle is given in Torrs and it can be positive or negative which has to be corrected later while finding the results. l_{TOF} is given in millimeters. Current seen in Electrometer and the Voltage applied are both in Volts.

In order to take advantage of these parameters in the codes to be developed later, these values have to be taken out from the filename which is done by the function 'reading_filename'. In Annex 7.3.3.2, the code is presented.

3.5.2 Function 'arrange_data'

As explained before in 3.4.2 'Correction of data obtained', any possible offset has to be removed from the current values calculated and also whole beam has to be multiplied by the gain factor. Furthermore, all data obtained before cutting the voltage applied (i.e before time (t) = 0) also has to be removed. All these things are carried out in the function ' arrange_data' which is presented in Annex 7.3.3.3.

3.5.3 Main Code

The main code first reads all the files present in a certain directory and then, the functions 'reading_filename' and 'arrange_data' are called in order to get the corrected values of Current vs time for each and every measurements made for a liquid.

After this, an average is calculated for various measurements done where the experimental conditions were same. Using such average values for all experimental conditions, useful parameters for the colloidal thruster analysis like thrust, specific impulse, mass flow rate, etc are calculated and the graphs interested are drawn.

The code is presented in Annex 7.3.3.4. This code uses another small function to calculate the integral called 'calc_integral' which is presented in Annex 7.3.3.5.

3.6 Results

3.6.1 Colloid Beam Phenomenology

In this section, TOF curves for each liquid studied will be presented and according to the nature of the graphs, different types of charged particles will be identified.

At t=0 the needle voltage is shorted to ground, and the spray is interrupted. Because the droplets travel toward the collector with finite speed v, it takes time L/v for the electrometer to measure null electric current, where L is the distance between emitter and the collector. Once the voltage is shorted, the particles with high charge-to-mass ratio reach faster to the collector and vice versa. Some common charged particles that can be seen in an electrospray beam are:

- Ions: They have high but normally constrained charge-to-mass ratio. Hence, in a TOF graph, they will present a sharp drop in the total current reaching the collector.
- Main droplets: They are the heavier particles with low charge than in the ions, and the range of charge-to-mass ratio can be higher. Hence, they reach later to the collector than ions and cover a big area with less steep drops in the curves.
- Secondary and Satellite droplets: For higher mass flow rates, the jet break in cone-jet mode is not uniform and smaller droplets in comparison to the main droplets are formed

in between the main droplets at the time of break up. These droplets are called secondary/satellite droplets. Satellite droplets are even smaller than secondary droplets and the way to differentiate them is presented in [9].

Not always the graphs obtained are free of errors. Some of the common errors that can be found doing an electrospray experiment which will later have serious effects in the TOF graphs are:

- Capacitive Coupling: Sometimes, various distortions are present near the origin unrelated to the actual TOF waves. They are caused by a type of antenna effect in electronics in between the emitter and the collector called Capacitive Coupling.
- Voltage Shorting: The time required to short the voltage to ground has to be very small in comparison to the time required for the charged particles to reach the collector. It is very hard to short a voltage of order of kilovolts to zero in infinitesimal time. Hence, this has some negative effects in the TOF graph. From the time when the voltage shorting is started till it really gets zero, some particles will be still being emitted from the emitter. These particles mix up with the charged particles on their way to the collector.
- Electronic noise

3.6.1.1 Emi IM

Time of Flight spectra of solution Emi Im is shown in Figure 7. The needle voltage for this experiment is of $1628\ Volts$ and $L_{TOF} = 102.14\ mm$.

Graphs are drawn for various mass flow rates of the propellant.

There are mainly 5 different regions in the graph which are identified as follows:

- Region 1: Electronic Noise
- Region 2: This region is supposed to be created due to the inefficient voltage shorting. The width of this region goes on increasing while the flow rate increases.

- Region 3: This distortion is supposed to be due to Capacitive Coupling.

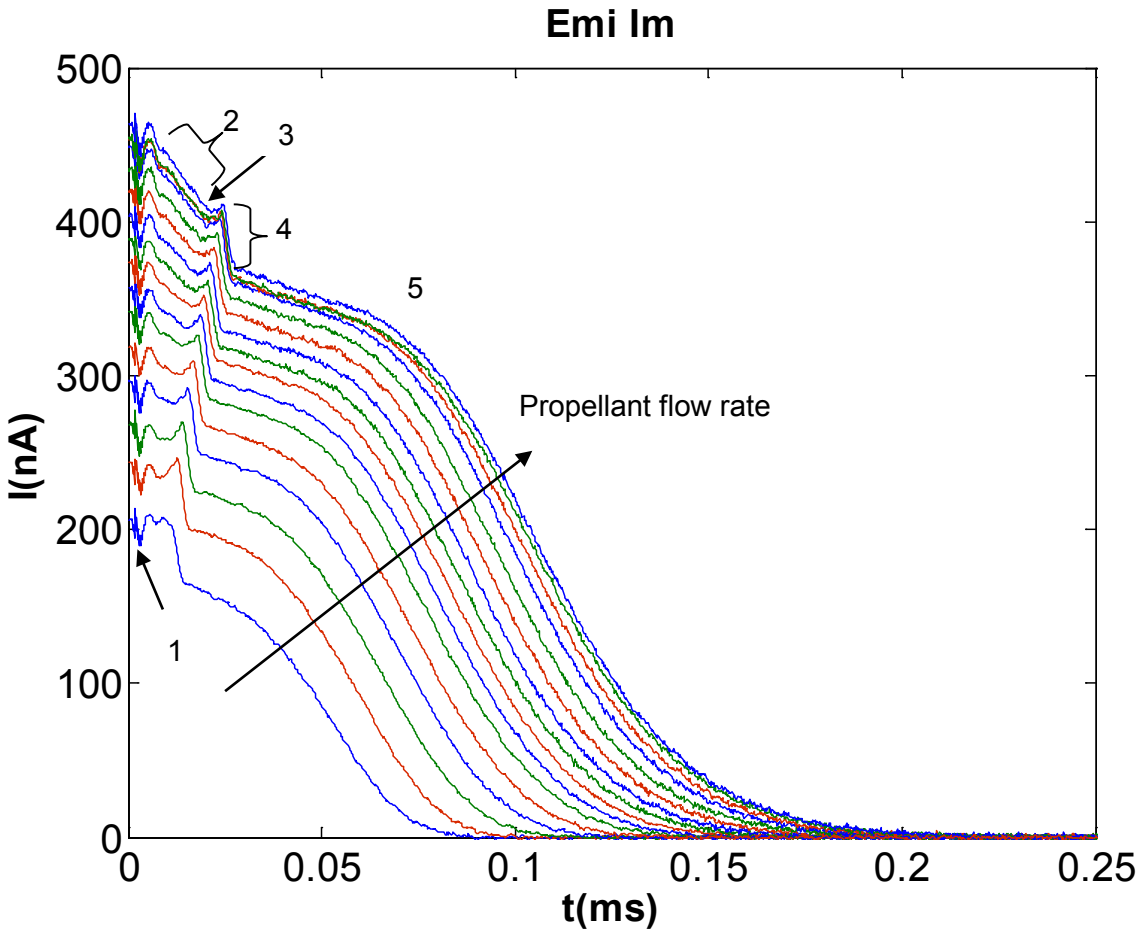

Figure 7. Time of Flight Spectra for solution Emi Im

- Region 4: These are the ions as they show a sharp drop in the Current. Because of the voltage shorting error, the TOF goes on increasing with the flow rate. If the voltage shorting would be corrected, all the ions should have same TOF which would be similar to the TOF of the beam with $I \cong 210\, nA$ i.e. that one with minimum flow rate as the voltage shorting error is minimum here which is approximately $0.013\, ms$. Hence, the specific charge of these ions is:

$$\frac{q}{m} = \frac{1}{2 \cdot V_{acc}} \left(\frac{L_{TOF}}{TOF}\right)^2 \cong \frac{1}{2 \cdot 1628} \left(\frac{102.14e-03}{0.013e-03}\right)^2 \cong 19000\, C/kg$$

- Region 5: These are the slow charge carrying entities or the main droplets. They cover a larger area due to a broader distribution of their Specific Charge. It can also be noted that the TOF associated with them increases while the current increases and it occupies a broader area in the graph.

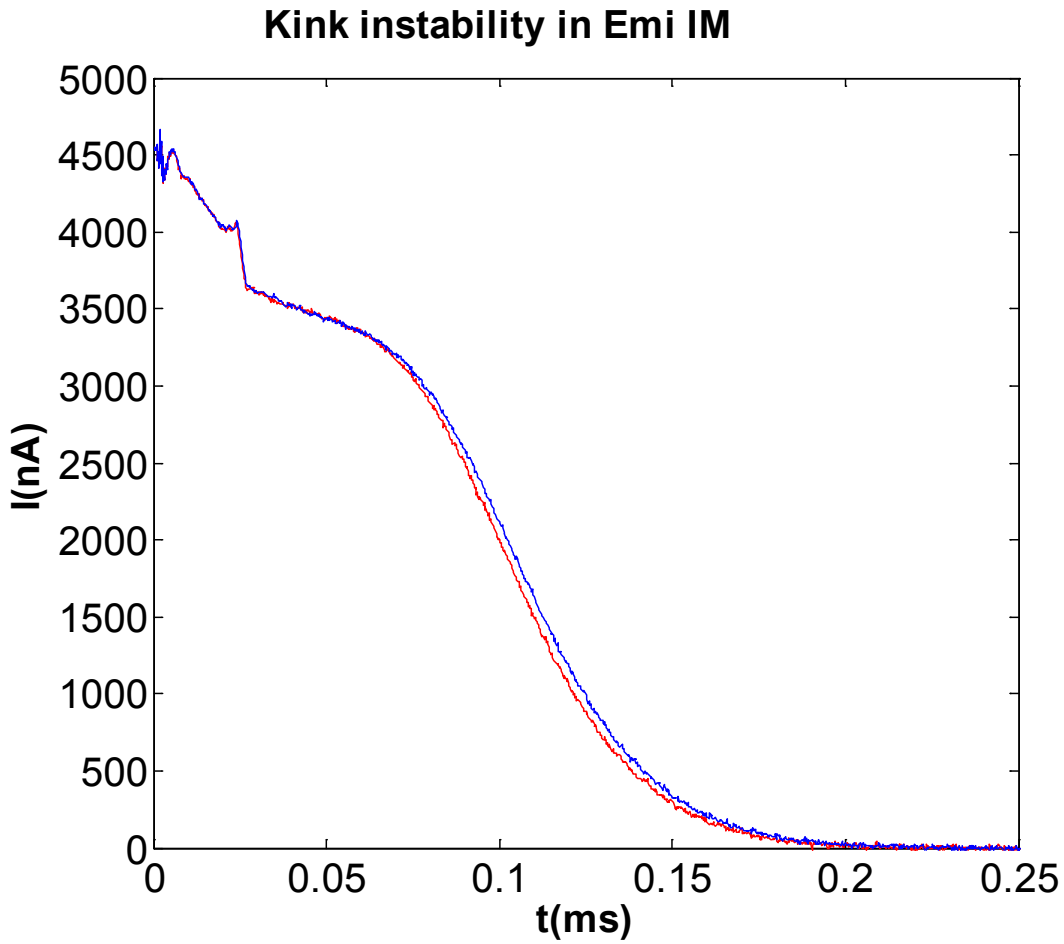

Figure 8. Kink instability in Emi Im

For $I \cong 450\ nA$, it can be seen that two graphs arise from the same point and later get separated. A closer view is shown in Figure 8. As shown in Annex 7.3.4.1, these graphs belong to two different mass flow rates (1.36E-09 kg/s and 1.44E-09 kg/s). The reason of this might be the transition from axisymmetric or varicose instabilities into the jet break-up to the lateral or kink instabilities as explained in [9].

3.6.1.2 EAN

Time of Flight spectra of solution EAN is shown in Figure 9. The needle voltage for this experiment is of $1800\ Volts$ and $L_{TOF} = 102.14\ mm$.

Graphs are drawn for various mass flow rates of the propellant. There are mainly 5 different regions in the graph which are identified as this way.

- Region 1: Electronic Noise
- Region 2: This region is supposed to be created due to the inefficient voltage shorting. The width of this region goes on increasing while the flow rate increases.
- Region 3: This distortion is supposed to be due to Capacitive Coupling.
- Region 4: These are the ions as they show a sharp drop in the Current. Because of the voltage shorting error, the TOF goes on increasing with the flow rate. If the voltage shorting would be corrected, all the ions should have same TOF which would be similar to the TOF of the beam with $I \cong 660\ nA$ i.e. that one with minimum flow rate as the voltage shorting error is minimum here which is approximately $0.01\ ms$. Hence, the specific charge of these ions is:

$$\frac{q}{m} = \frac{1}{2 \cdot V_{acc}}\left(\frac{L_{TOF}}{TOF}\right)^2 \cong \frac{1}{2 \cdot 1800}\left(\frac{102.14e-03}{0.01e-03}\right)^2 \cong 29000\ C/kg$$

- Region 5: These are the slow charge carrying entities or the main droplets. They cover a larger area due to a broader distribution of their Specific Charge. It can also be noted that the TOF associated with them increases while the current increases and it occupies a broader area in the graph.

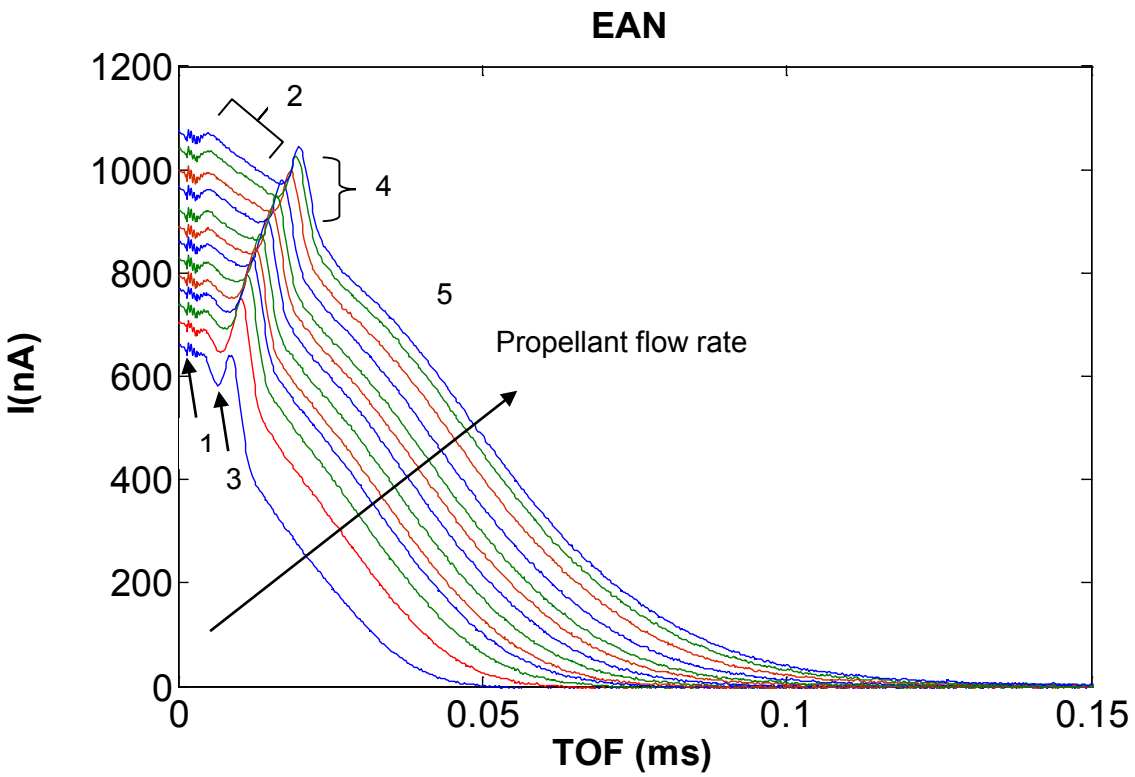

Figure 9. Time of Flight Spectra for solution EAN

3.6.1.3 Emi BF4

Time of Flight spectra of solution EMI BF4 is shown in Figure 10. The needle voltage for this experiment is of $1917\ Volts$ and $L_{TOF} = 102.14\ mm$.

Graphs are drawn for various mass flow rates of the propellant and presented in Figure 10. There can be seen various unwanted disturbances in the graph. For smaller flow rates, the initial current apparently seems to be higher and it goes on decreasing while the flow rate increases till a moment comes when once again the current increases with the flow rate (See Annex 7.3.4.3). The conclusion drawn is that the spray wasn't stable till the pressure in the liquid bottle was some 55 Torrs and these graphs were part of an unstable spray. For all following analyses, the data within the unstable spray range is neglected. Removing all these graphs with, we can observe that the graph obtained is Figure 11.

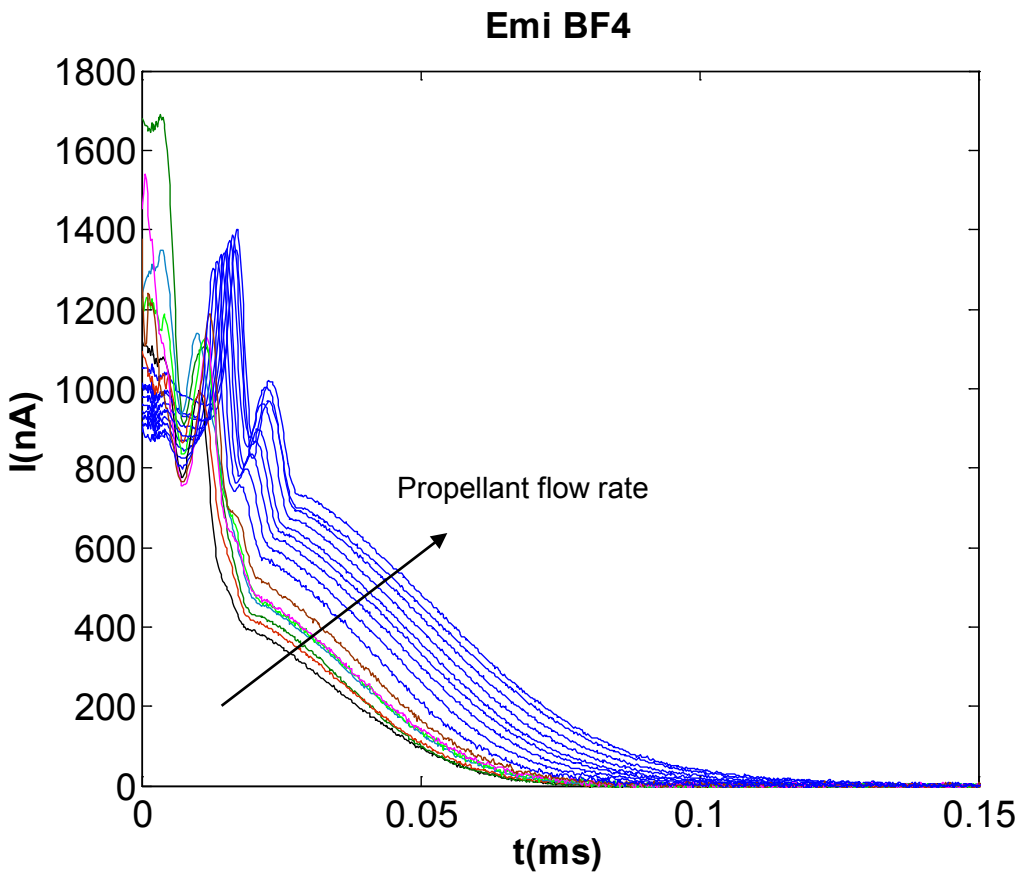

Figure 10. Time of Flight Spectra for solution EMI BF4

There are mainly 4 different regions in the graph which are identified as this way.

- Region 1: Electronic Noise
- Region 2: This region is supposed to be created due to the inefficient voltage shorting. The width of this region goes on increasing while the flow rate increases.
- Region 3: These are the ions as they show a sharp drop in the Current. Because of the voltage shorting error, the TOF goes on increasing with the flow rate. If the voltage shorting would be corrected, all the ions should have same TOF which would be similar to the TOF of the beam with $I \cong 900\, nA$ i.e. that one with minimum flow rate among the stable sprays, as the voltage shorting error is minimum here, which is approximately $0.02\, ms$. Hence, the specific charge of these ions is:

$$\frac{q}{m} = \frac{1}{2 \cdot V_{acc}} \left(\frac{L_{TOF}}{TOF}\right)^2 \cong \frac{1}{2 \cdot 1917} \left(\frac{102.14e-03}{0.02e-03}\right)^2 \cong 6800\ C/kg$$

- Region 4: These are the slow charge carrying entities or the main droplets. They cover a larger area due to a broader distribution of their Specific Charge. It can also be noted that the TOF associated with them increases while the current increases and it occupies a broader area in the graph.

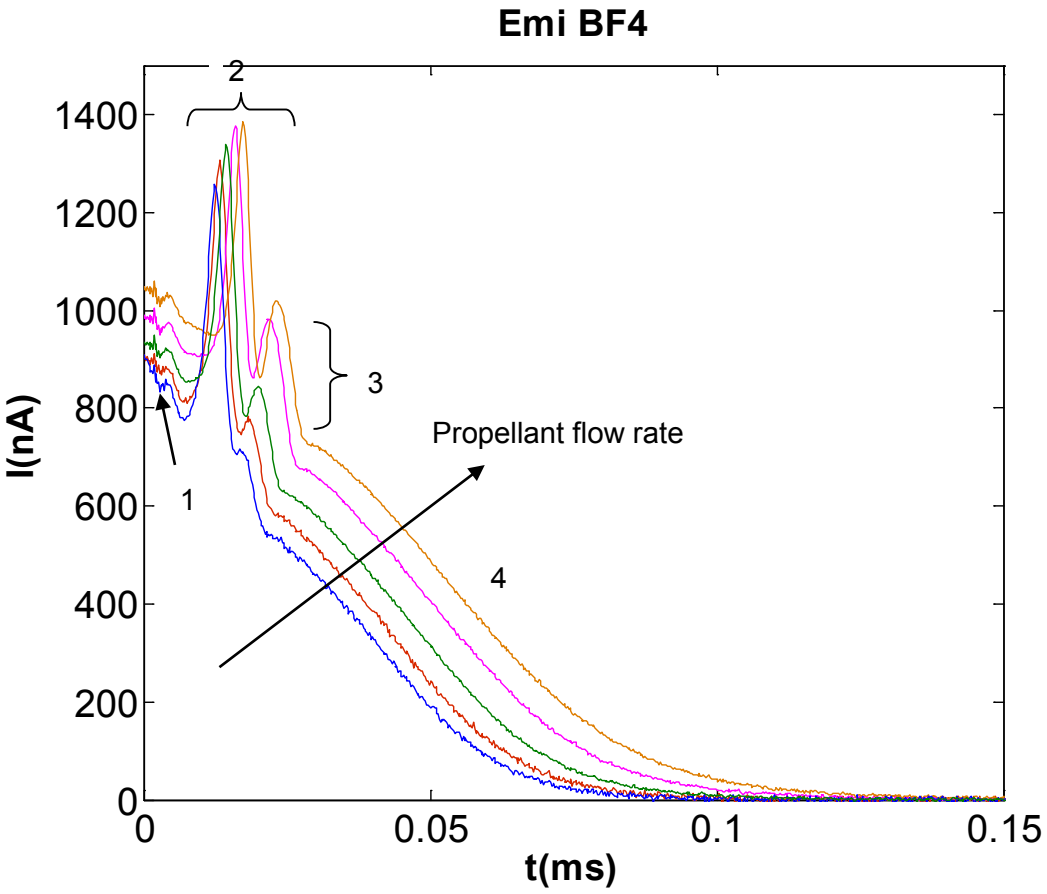

Figure 11. Time of Flight Spectra for solution EMI BF4 (for stable sprays)

3.6.1.4 EMI TF

Time of Flight spectra of solution EMI TF for various mass flow rates of the propellant is shown in Figure 12 . The needle voltage for this experiment is of $2047\ Volts$ and $L_{TOF} = 102.14\ mm$.

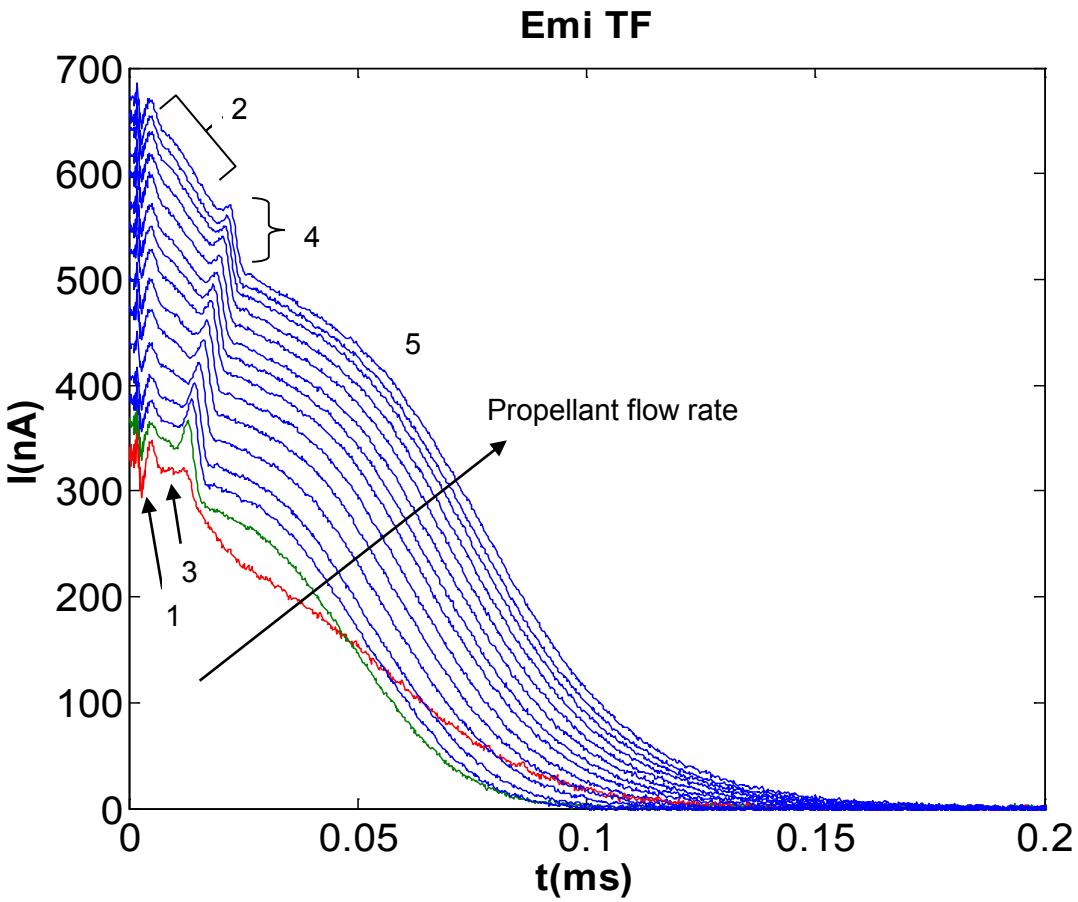

Figure 12. Time of Flight Spectra for solution EMI TF

It can be seen that the graph with $I \cong 350\ nA$, i.e the one with minimum flow rate, is quite different in comparison to the others. This might be because of the instability of the spray in that regime. Hence, this one will be discarded for all analyses that will be done for Emi TF. Now, let's continue with the analysis of the rest of the graphs.

There are mainly 5 different regions in the graph which are identified as this way.

- Region 1: Electronic Noise

- Region 2: This region is supposed to be created due to the inefficient voltage shorting. The width of this region goes on increasing while the flow rate increases.
- Region 3: This distortion is supposed to be due to Capacitive Coupling.
- Region 4: These are the ions as they show a sharp drop in the Current. Because of the voltage shorting error, the TOF goes on increasing with the flow rate. If the voltage shorting would be corrected, all the ions should have same TOF which would be similar to the TOF of the beam with $I \cong 360\, nA$ i.e. that one with minimum flow rate among the stable sprays, as the voltage shorting error is minimum here, which is approximately $0.014\, ms$. Hence, the specific charge of these ions is:

$$\frac{q}{m} = \frac{1}{2 \cdot V_{acc}} \left(\frac{L_{TOF}}{TOF}\right)^2 \cong \frac{1}{2 \cdot 2047} \left(\frac{102.14e-03}{0.014e-03}\right)^2 \cong 13000\, C/kg$$

- Region 5: These are the slow charge carrying entities or the main droplets. They cover a larger area due to a broader distribution of their Specific Charge. It can also be noted that the TOF associated with them increases while the current increases and it occupies a broader area in the graph.

3.6.1.5 TES

Time of Flight spectra of solution TES is shown in Figure 13 . The needle voltage for this experiment is of $1768\, Volts$ and $L_{TOF} = 102.14\, mm$. Graphs are drawn for various mass flow rates of the propellant.

It can be seen that the graph with $I \cong 220\, nA$, i.e the one with minimum flow rate is quite different in comparison to the others. This might be because of the instability of the spray in that regime. Hence, this one will be discarded for all analyses that will be done for TES. Now, let's continue with the analysis of the rest of the graphs. There are mainly 4 different regions in the graph which are identified as this way.

- Region 1: Electronic Noise
- Region 2: This region is supposed to be created due to the inefficient voltage shorting. The width of this region goes on increasing while the flow rate increases.

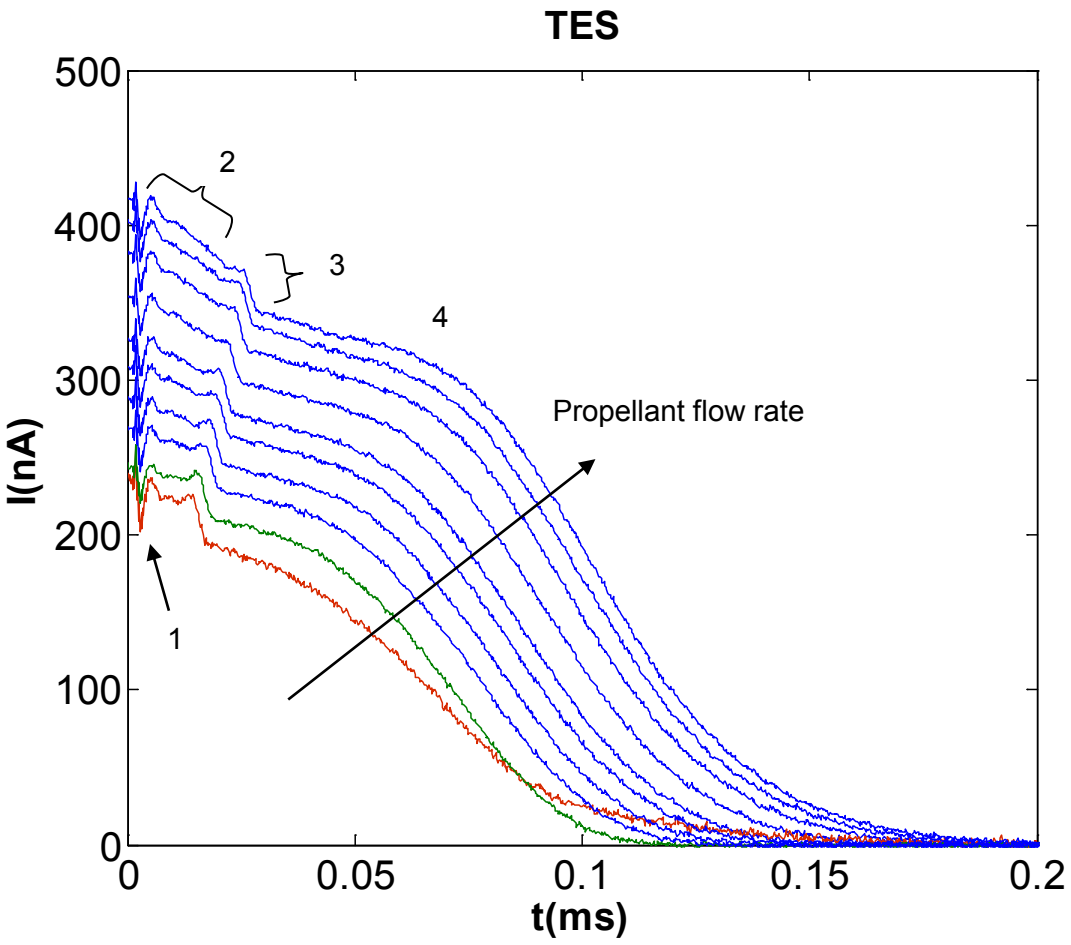

Figure 13. Time of Flight Spectra for solution TES

- Region 3: These are the ions as they show a sharp drop in the Current. Because of the voltage shorting error, the TOF goes on increasing with the flow rate. If the voltage shorting would be corrected, all the ions should have same TOF which would be similar to the TOF of the beam with $I \cong 250\, nA$ i.e. that one with minimum flow rate among the stable sprays, as the voltage shorting error is minimum here, which is approximately $0.017\, ms$. Hence, the specific charge of these ions is:

$$\frac{q}{m} = \frac{1}{2 \cdot V_{acc}} \left(\frac{L_{TOF}}{TOF}\right)^2 \cong \frac{1}{2 \cdot 1768} \left(\frac{102.14e-03}{0.017e-03}\right)^2 \cong 10200\ C/kg$$

- Region 4: These are the slow charge carrying entities or the main droplets. They cover a larger area due to a broader distribution of their Specific Charge. It can also be noted that the TOF associated with them increases while the current increases and it occupies a broader area in the graph.

3.6.1.6 Formamide 1 (50% Emi Im in Formamide)

Time of Flight spectra of solution Formamide 1 is shown in Figure 14. The needle voltage for this experiment is of $1598\ Volts$ and $L_{TOF} = 102.14\ mm$. Graphs are drawn for various mass flow rates of the propellant.

There are mainly 4 different regions in the graph which are identified as this way.

- Region 1: Electronic Noise
- Region 2: These are the ions as they show a sharp drop in the Current. These ions don't appear for smaller flow rates and only appear after $I > 400\ nA$. It can be seen that as the total current increases, the drop of the ions is sharper. The TOF of these ions if of approximately $0.007\ ms$. Hence, the specific charge of these ions is:

  $$\frac{q}{m} = \frac{1}{2 \cdot V_{acc}} \left(\frac{L_{TOF}}{TOF}\right)^2 \cong \frac{1}{2 \cdot 1598} \left(\frac{102.14e-03}{0.007e-03}\right)^2 \cong 66600\ C/kg$$

  It is hard to imagine how multiply charged droplets could be produced having such large specific charge, which furthermore is constant in a wide range of flow rates. These particles must be highly solvated ions.
- Region 3: This region is supposed to be created due to the inefficient voltage shorting. The width of this region goes on increasing while the flow rate increases.
- Region 4: These are the slow charge carrying entities or the main droplets. They cover a larger area due to a broader distribution of their Specific Charge. It can also be noted that

the TOF associated with them increases while the current increases and it occupies a broader area in the graph. It has to be noted that for $I > 1000nA$, the total current reaching the collector increases for a while and again starts decreasing (Region 5), this also must be an effect of inefficient voltage shorting.

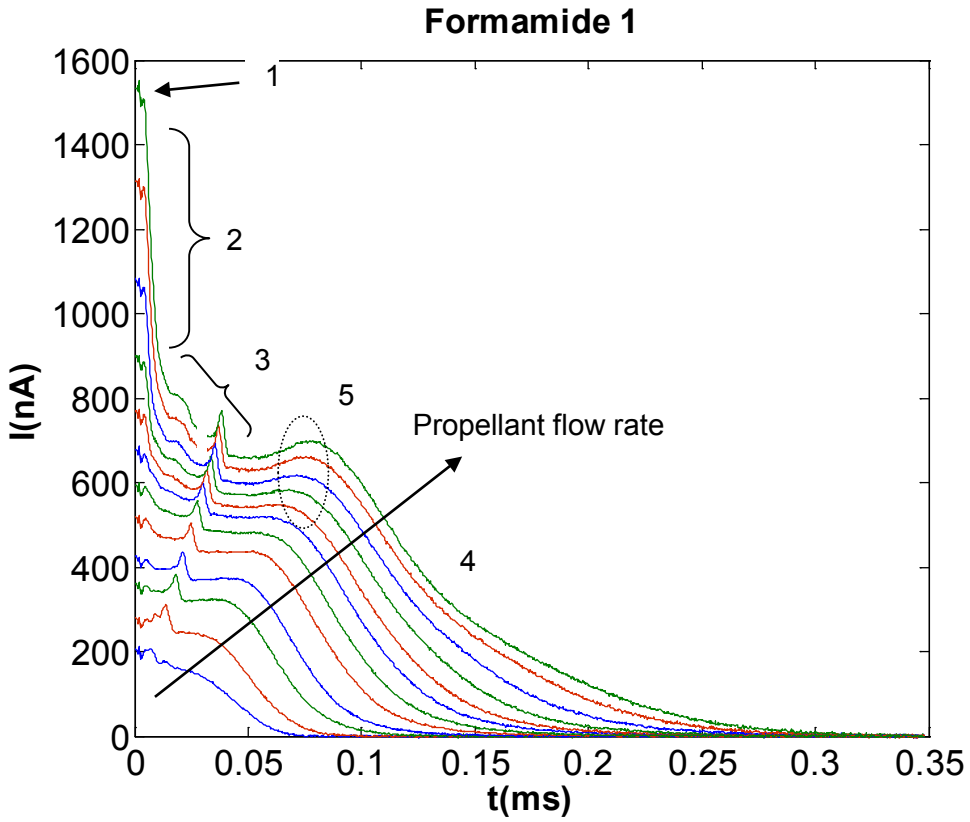

Figure 14. Time of Flight Spectra for solution Formamide 1

3.6.1.7 Formamide 2 (25% Emi Im in Formamide)

Time of Flight spectra of solution Formamide 2 is shown in Figure 15. The needle voltage for this experiment is of $1593\ Volts$ and $L_{TOF} = 102.14\ mm$. Graphs are drawn for various mass flow rates of the propellant.

There are mainly 4 different regions in the graph which are identified as this way.

- Region 1: Electronic Noise
- Region 2: These are the ions as they show a sharp drop in the Current. These ions don't appear for smaller flow rates and only appear after $I > 600\ nA$. It can be seen that as the total current increases, the drop of the ions is sharper. The TOF of these ions if of approximately $0.007\ ms$. Hence, the specific charge of these ions is:

$$\frac{q}{m} = \frac{1}{2 \cdot V_{acc}}\left(\frac{L_{TOF}}{TOF}\right)^2 \cong \frac{1}{2 \cdot 1593}\left(\frac{102.14e-03}{0.007e-03}\right)^2 \cong 66800\ C/kg$$

  As explained in the case of Formamide 1, these particles also must be highly solvated ions. Moreover, they have same TOF as in the case of Formamide 1 and also practically same Specific Charge, so we could also assume them to be same ions as in the case of Formamide 1.
- Region 3: This region is supposed to be created due to the inefficient voltage shorting. The width of this region goes on increasing while the flow rate increases.

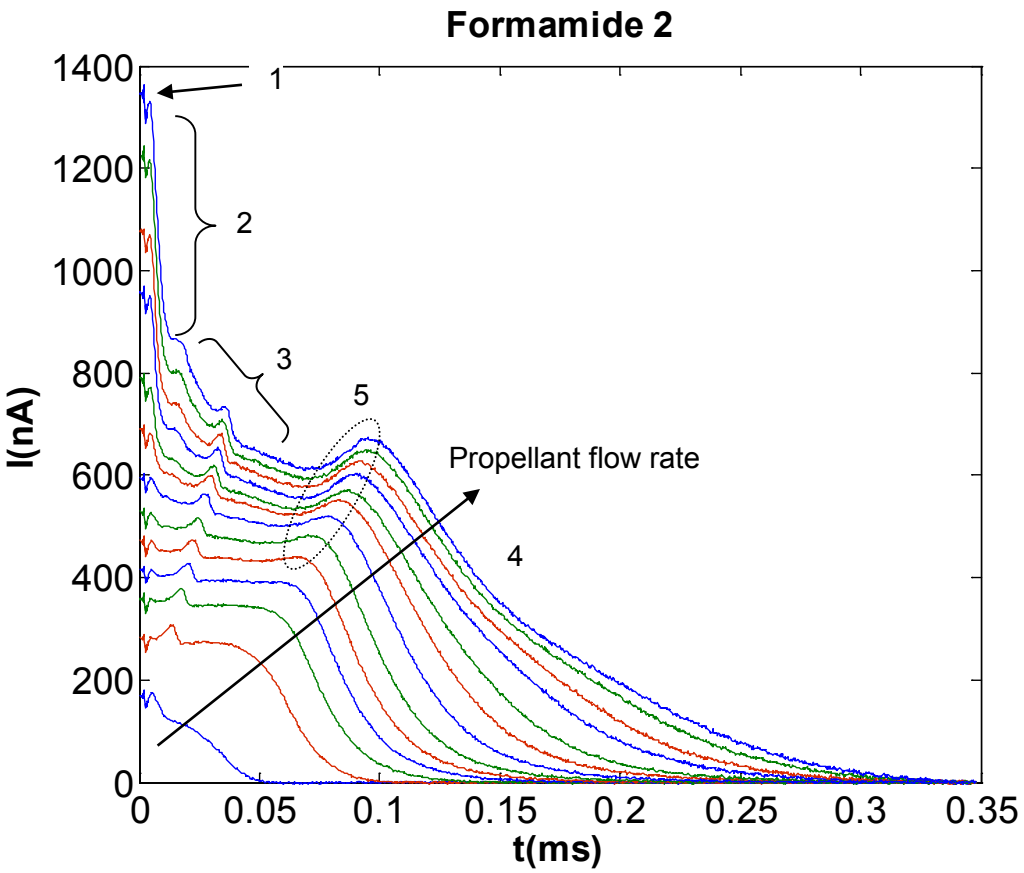

Figure 15. Time of Flight Spectra for solution Formamide 2

- Region 4: These are the slow charge carrying entities or the main droplets. They cover a larger area due to a broader distribution of their Specific Charge. It can also be noted that the TOF associated with them increases while the current increases and it occupies a broader area in the graph. It has to be noted that for $I > 400nA$, the total current reaching the collector increases for a while and again starts decreasing (Region 5), this also must be an effect of inefficient voltage shorting.

3.6.1.8 Formamide G (4% EAN in Formamide)

Time of Flight spectra of solution Formamide G is shown in Figure 16. The needle voltage for this experiment is of $1933\ Volts$ and $L_{TOF} = 102.14\ mm$. Graphs are drawn for various mass flow rates of the propellant.

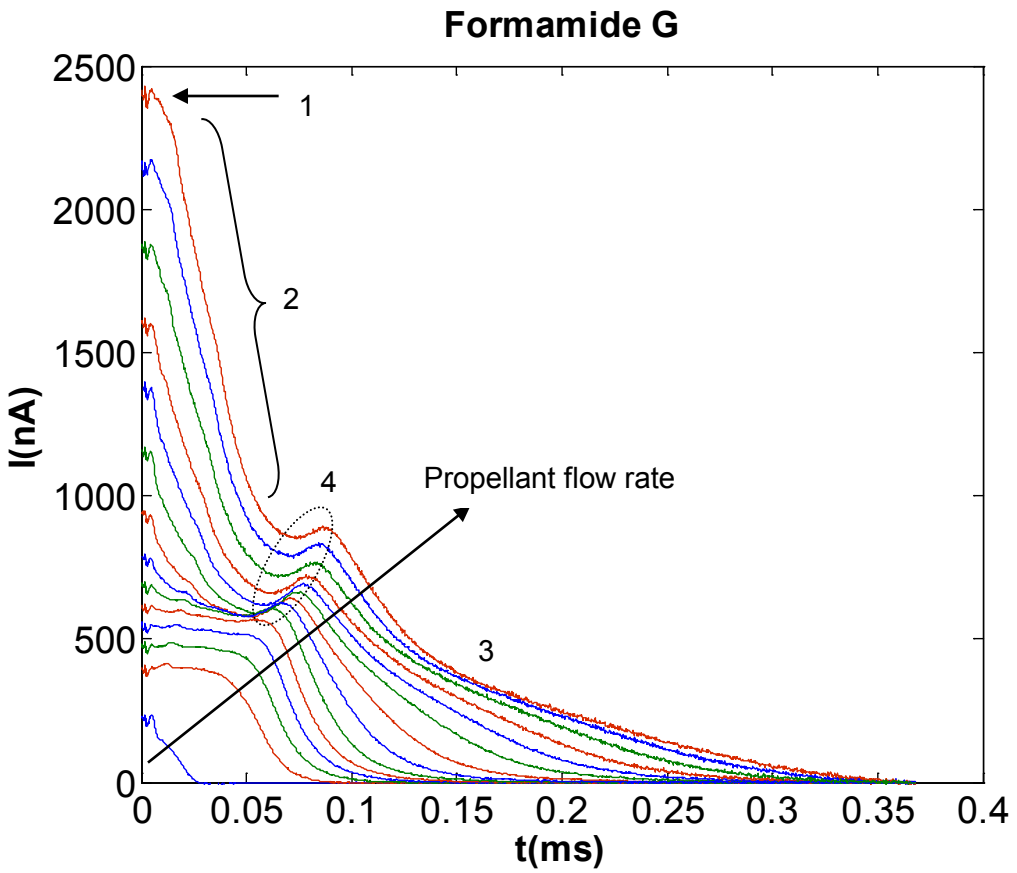

Figure 16. Time of Flight Spectra for solution Formamide G

There are mainly 4 different regions in the graph which are identified as this way.

- Region 1: Electronic Noise
- Region 2: If we see the graph with minimum flow rate ($I = 220\,nA$), there can be seen a clear drop corresponding to a possible ion. This has TOF of $0.0064\,ms$. Hence, the specific charge of these ions is:

$$\frac{q}{m} = \frac{1}{2 \cdot V_{acc}}\left(\frac{L_{TOF}}{TOF}\right)^2 \cong \frac{1}{2 \cdot 1933}\left(\frac{102.14e-03}{0.0064e-03}\right)^2 \cong 65880\ C/kg$$

  Now for higher flow rates, there can't be seen a clear distinction of whether the emission is an ion or a droplet. For $400\,nA \leq I \leq 800\,nA$, it can clearly be seen that there are no ions reaching the collector as the graph is almost horizontal. For $I > 800\,nA$, there starts to appear the drop but it is not as sharp as it was in case of $I \cong 220\,nA$. Hence, they must

be very tiny droplets with high charge carrying in them or ions that show up getting mixed with other droplets due to the inefficient voltage shorting.

- Region 3: These are the slow charge carrying entities or the main droplets. They cover a larger area due to a broader distribution of their Specific Charge. It can also be noted that the TOF associated with them increases while the current increases and it occupies a broader area in the graph. It has to be noted that for $I > 800nA$, the total current reaching the collector increases for a while and again starts decreasing (Region 4), this must be an effect of inefficient voltage shorting.

3.6.1.9 Formamide H (7% EAN in Formamide)

Time of Flight spectra of solution Formamide H is shown in Figure 17. The needle voltage for this experiment is of $1933\ Volts$ and $L_{TOF} = 102.14\ mm$. Graphs are drawn for various mass flow rates of the propellant.

There are mainly 4 different regions in the graph which are identified as:

- Region 1: Electronic Noise

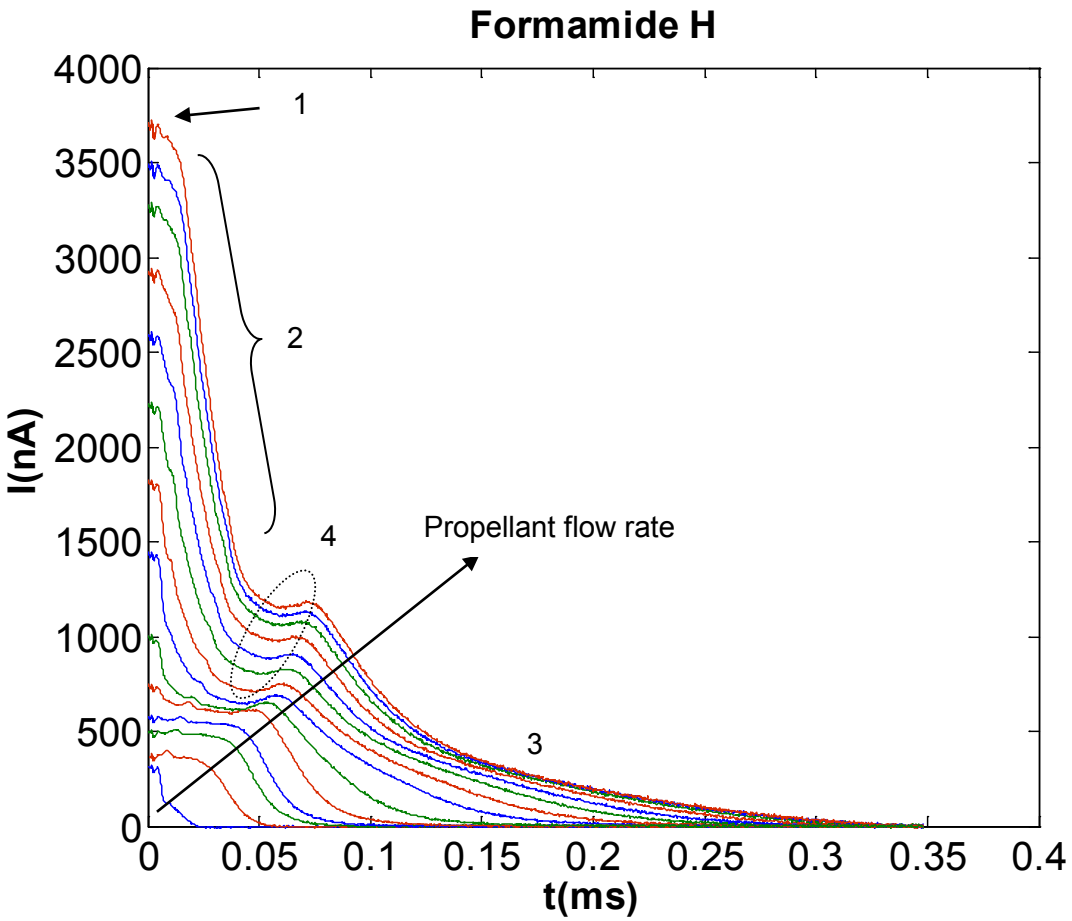

Figure 17. Time of Flight Spectra for solution Formamide H

- Region 2: If we see the graph with minimum flow rate ($I = 320\ nA$), there can be seen a clear drop corresponding to a possible ion. This has TOF of $0.0064\ ms$. Hence, the specific charge of these ions is:

$$\frac{q}{m} = \frac{1}{2 \cdot V_{acc}}\left(\frac{L_{TOF}}{TOF}\right)^2 \cong \frac{1}{2 \cdot 1933}\left(\frac{102.14e-03}{0.0064e-03}\right)^2 \cong 65880\ C/kg$$

Now for higher flow rates, there can't be seen a clear distinction of whether the emission is an ion or a droplet. For $400\ nA \leq I \leq 800\ nA$, it can clearly be seen that there are no ions reaching the collector as the graph is almost horizontal. For $I > 800\ nA$, there starts to appear the drop but it is not as sharp as it was in case of $I \cong 320\ nA$. Again, they must be very tiny droplets with high charge carrying in them or ions that show up getting mixed

with other droplets due to the inefficient voltage shorting as in case of Formamide G. Furthermore, they have the same specific charge and same TOF.

- Region 3: These are the slow charge carrying entities or the main droplets. They cover a larger area due to a broader distribution of their Specific Charge. It can also be noted that the TOF associated with them increases while the current increases and it occupies a broader area in the graph. It has to be noted that for $I > 800nA$, the total current reaching the collector increases for a while and again starts decreasing (Region 4), this must be an effect of inefficient voltage shorting.

3.6.1.10 Conclusions

Some important conclusions that can be drawn from the study of TOF graphs of these liquids are:

- In case of solutions formed by mixture of more than one liquid, some ions with very high specific charge appear called solvated ions.
- For high flow rates, sometimes the jet-breaking phenomenon gets transited from an axisymmetric or varicose instabilities to the lateral or kink instabilities, which has been seen in case of the solution Emi IM.
- Seeing the current values between Formamide 1 & 2 and Formamide G & H (the acceleration voltages were similar), it can be said that for a mixture including Formamide as principal ingredient, the lower the concentration of the second liquid, the higher is the total current produced by the spray.
- We have seen errors due to Electronic Noise and Inefficient Voltage shorting in almost every liquid.

3.6.2 Measurement of Thrust and Specific Impulse

Firstly, a graph of $\dot{m}$ (mass flow rate) with respect to ΔP (pressure difference between liquid bottle and atmosphere) is drawn for each liquid. The graph must be linear in order to assure that the experiment is correct.

Secondly, equations (5) and (6) of 3.1 is used to compute the thrust and mass flow rates of these electrosprays. Then the evolution of total accumulated thrust and mass flow rate for each liquid is calculated. To allow a proper comparison, the inverse of specific charge is taken as abscissa coordinate, rather than the TOF; this involves a straightforward change of variables from t_F to m/q Equation (4) of 3.1.

Afterwards, the corresponding graphs will be shown for each liquid. The code developed to calculate the accumulation of thrust and mass flow rate vs. m/q along with the code to draw the graphs is shown in Annex 7.3.3.6.

The acceleration voltage of each type of particle present in a given spray is taken to be the voltage of the electrospray needle. Assuming this, graphs of variation of thrust and specific impulse with respect to mass flow rate for a given liquid at a constant acceleration voltage is calculated. These graphs will also be presented later for each liquid. Furthermore, curves fitting the experimental data are offered to allow the extrapolation of T and Isp at different mass flow rate and acceleration voltage. The forms of the scaling laws given by equations (1) and (2) of 3.1 are used to model the data.

There exists an error estimating the thrust using the average specific charge of the colloids and the needle voltage as the acceleration voltage which is given by the following equation:

$$Thrust\ error\ (\%) = \left[\frac{\dot{m}\sqrt{2V_{acc}\left(\frac{I}{\dot{m}}\right)} - T}{T}\right] \cdot 100$$

Where $\dot{m}$ and T are the spray mass flow and thrust yielded by the TOF measurement. This parameter is also calculated for each liquid and the corresponding graphs will be shown later. Finally, using equation (8) of 3.1, the efficiency of the spray is calculated for each liquid.

3.6.2.1 Emi Im

Figure 18 shows the evolution of $\dot{m}$ (mass flow rate) with respect to ΔP (pressure difference between liquid bottle and atmosphere) for Emi Im. We see that the Correlation factor $R^2 = 0.9958 \cong 1$ which means the graph is almost linear.

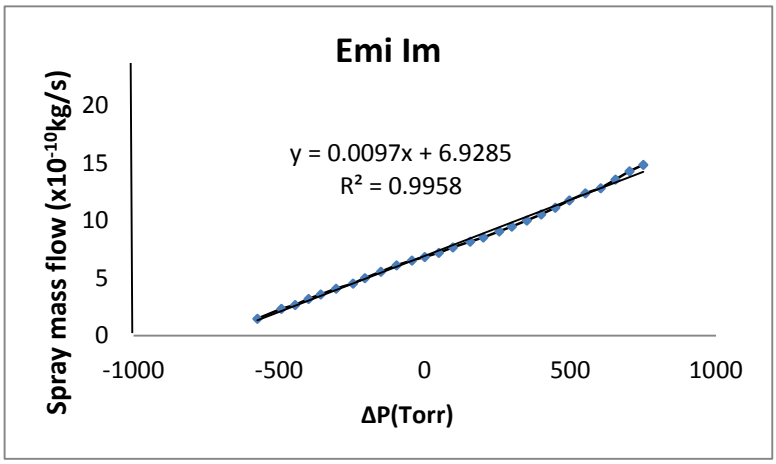

Figure 18. Mass flow rate vs. pressure difference for Emi Im

The evolution of total accumulated thrust and mass flow rate for several experimental runs obtained with Emi Im is shown in Figure 19 and Figure 20 and obviously, the thrust and mass flow rate associated with each spray will be the constant values reached at large m/q.

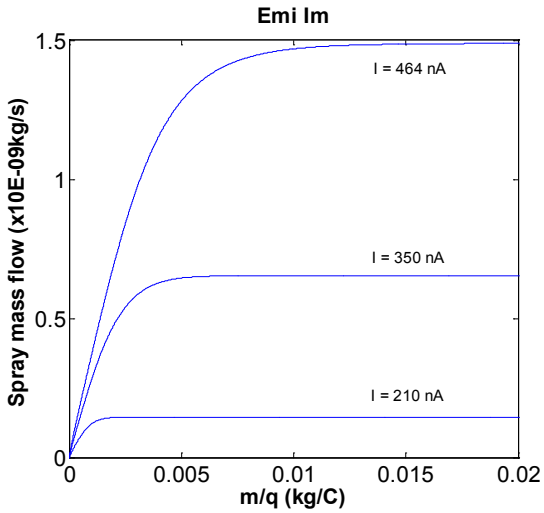

Figure 20. Beam mass flow for three Emi Im sprays

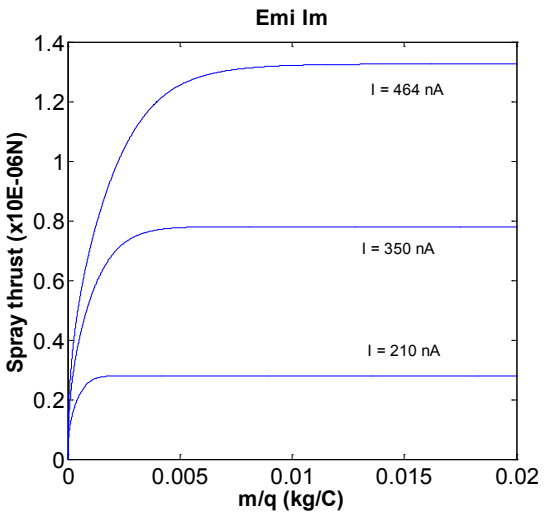

Figure 19. Thrust values rendered by TOF analysis for the sprays of Figure 20

Figure 22 and Figure 21 collect the specific impulses and thrusts of all the Emi Im sprays studied, at an acceleration voltage of 1628V. Although the lowest flow rate in these graphs is the minimum at which a stable cone jet could be set, flow rates larger than the largest shown are still possible.

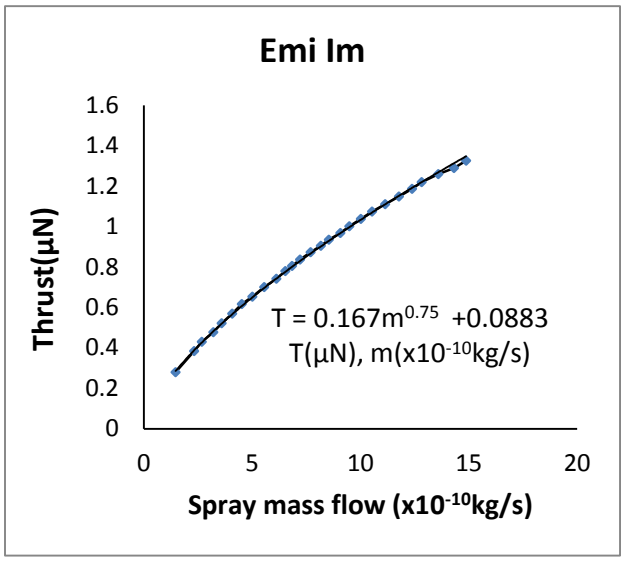

Figure 22. Thrust yielded by a single cone jet of Emi Im as a function of mass flow rate.

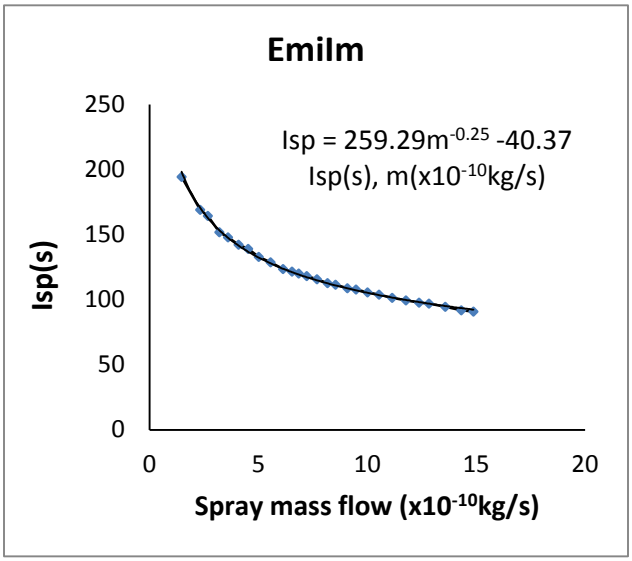

Figure 21. Specific impulse of Emi Im cone iets as a function of mass flow rate

Figure 23 shows the error involved in estimating the thrust. It is seen that the thrust computed by average values overestimates the measured value by 11% approximately, mainly because the voltage losses occurring in the electrospraying process are not included in the former.

The efficiency of Emi Im is shown in Figure 24 and its value is approximately 80%. Again, this 20% drop is mostly caused by voltage losses in the cone jet.

In Annex 7.3.4.1, all data required to build these graphs is presented.

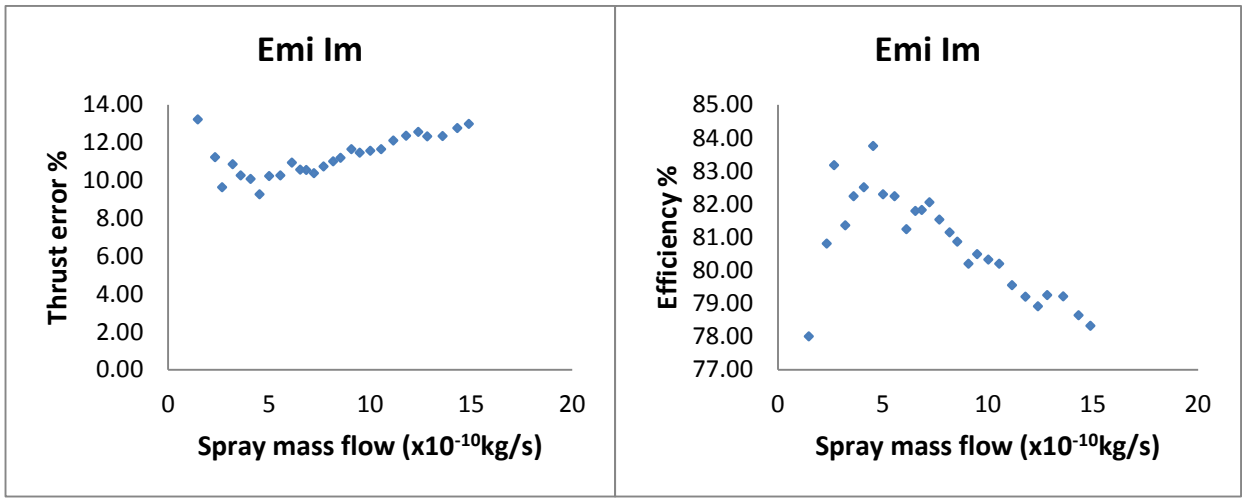

Figure 23. Error associated with using the average value of the specific charge to estimate spray thrust. The cone jets are those in Figure 21 and Figure 22.

Figure 24. Efficiency of Emi Im cone jets.

3.6.2.2 EAN

Figure 25 shows the evolution of $\dot{m}$ (mass flow rate) with respect to ΔP (pressure difference between liquid bottle and atmosphere) for EAN. We see that the Correlation factor $R^2 = 0.9981 \cong 1$ which means the graph is almost linear.

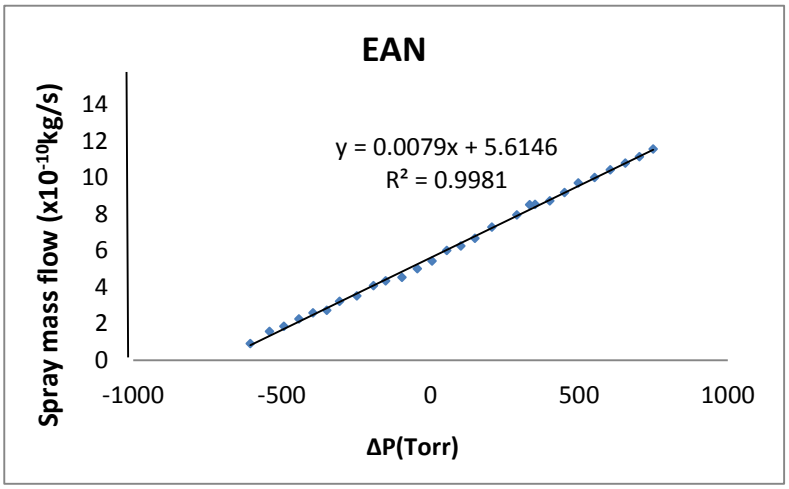

Figure 25. Mass flow rate vs. pressure difference for EAN

The evolution of total accumulated thrust and mass flow rate for several experimental runs obtained with EAN is shown in Figure 26 and Figure 27 and obviously, the thrust and mass flow rate associated with each spray will be the constant values reached at large m/q.

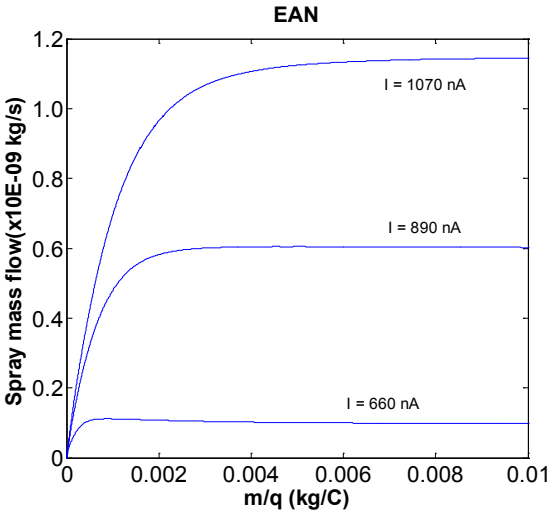

Figure 27. Beam mass flow for three EAN sprays

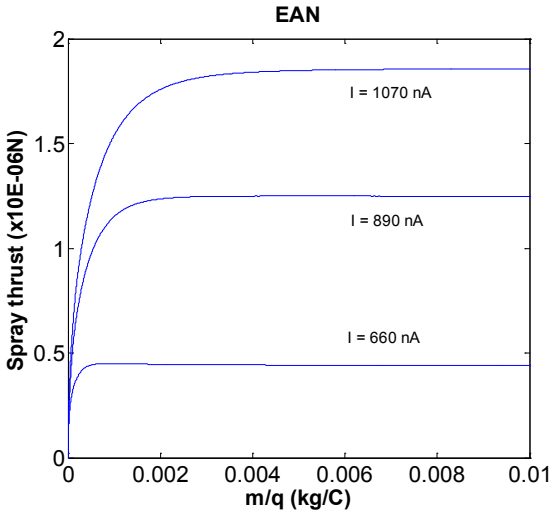

Figure 26. Thrust values rendered by TOF analysis for the sprays of Figure 27.

Figure 28 and Figure 29 collect the specific impulses and thrusts of all the EAN sprays studied, at an acceleration voltage of 1800V. Although the lowest flow rate in these graphs is the minimum at which a stable cone jet could be set, flow rates larger than the largest shown are still possible.

Figure 30 shows the error involved in estimating the thrust. It is seen that the thrust computed by average values overestimates the measured value by 8% - 12% approximately, mainly because the voltage losses occurring in the electrospraying process are not included in the former. It is to be noticed that this error tends slightly to increase with mass flow rate.

The efficiency of EAN is shown in Figure 31 and its average value is approximately 80%. Again, this 20% drop is mostly caused by voltage losses in the cone jet. Just opposite to the thrust error, the efficiency tends slightly to decrease with the mass flow rate.

In Annex 7.3.4.2, all data required to build these graphs is presented.

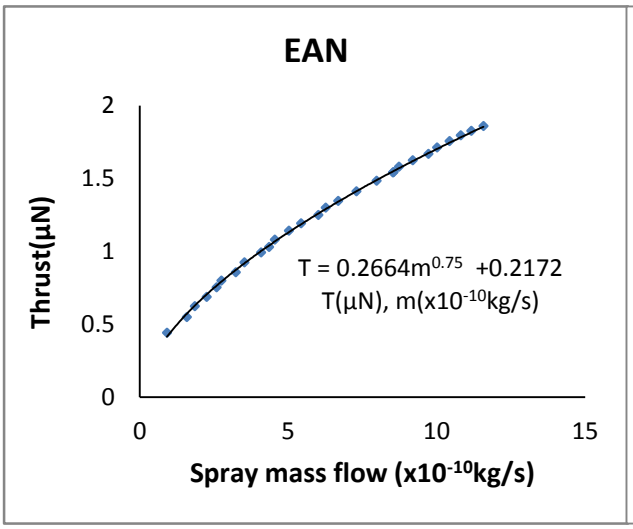

Figure 29. Thrust yielded by a single cone jet of EAN as a function of mass flow rate.

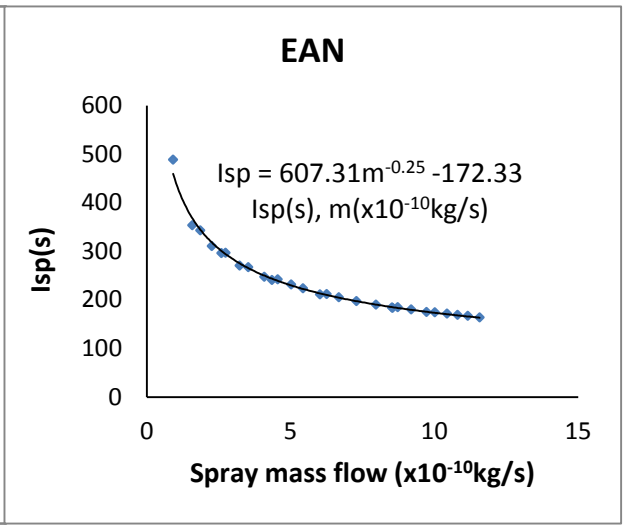

Figure 28. Specific impulse of EAN cone jets as a function of mass flow rate.

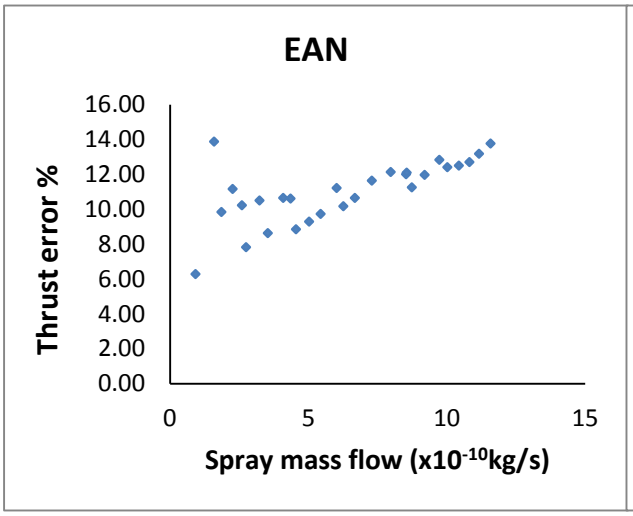

Figure 30. Error associated with using the average value of the specific charge to estimate spray thrust. The cone jets are those in Figure 28 and Figure 29

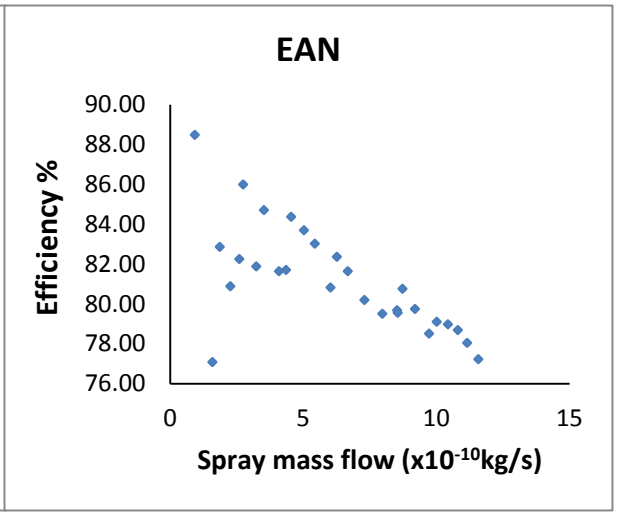

Figure 31. Efficiency of EAN cone jets.

3.6.2.3 Emi BF4

Figure 32 shows the evolution of $\dot{m}$ (mass flow rate) with respect to ΔP (pressure difference between liquid bottle and atmosphere) for Emi BF4. We see that the Correlation factor $R^2 = 0.9923 \cong 1$ which means the graph is almost linear.

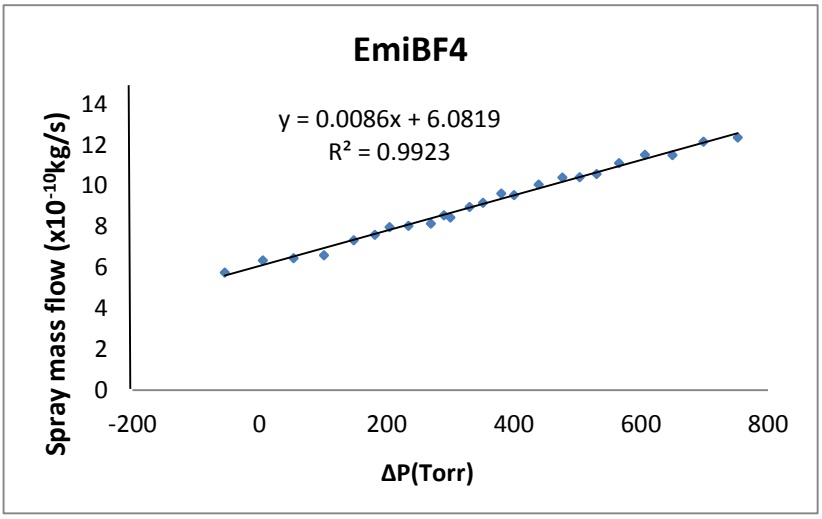

Figure 32.Mass flow rate vs. pressure difference for Emi BF4

The evolution of total accumulated thrust and mass flow rate for several experimental runs obtained with Emi BF4 is shown in Figure 33 and Figure 34 and obviously, the thrust and mass flow rate associated with each spray will be the constant values reached at large m/q.

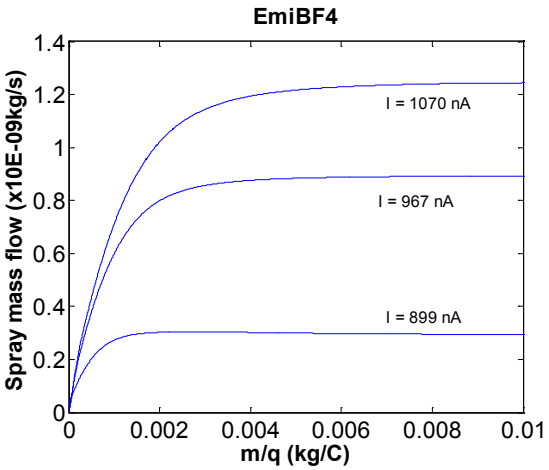

Figure 34. Beam mass flow for three Emi BF4 sprays

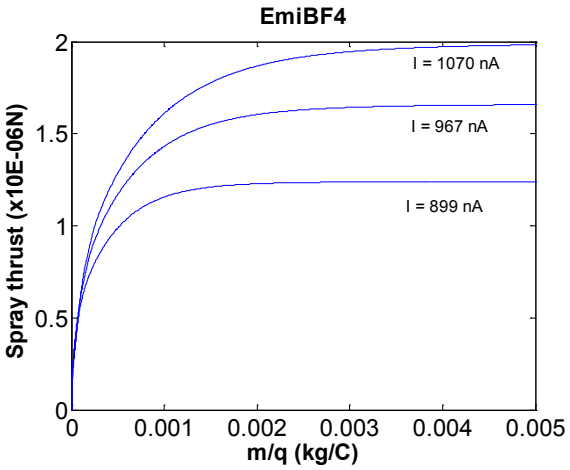

Figure 33.Thrust values rendered by TOF analysis for the sprays of Figure 33

Figure 35 and Figure 36 collect the thrusts and specific impulses of all the Emi BF4 sprays studied, at an acceleration voltage of 1917 V. Although the lowest flow rate in these graphs is the minimum at which a stable cone jet could be set, flow rates larger than the largest shown are still possible.

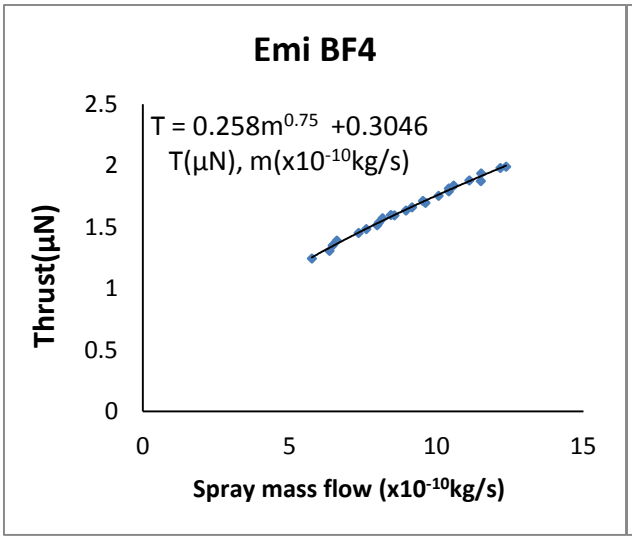

Figure 36. Thrust yielded by a single cone jet of Emi BF4 as a function of mass flow rate.

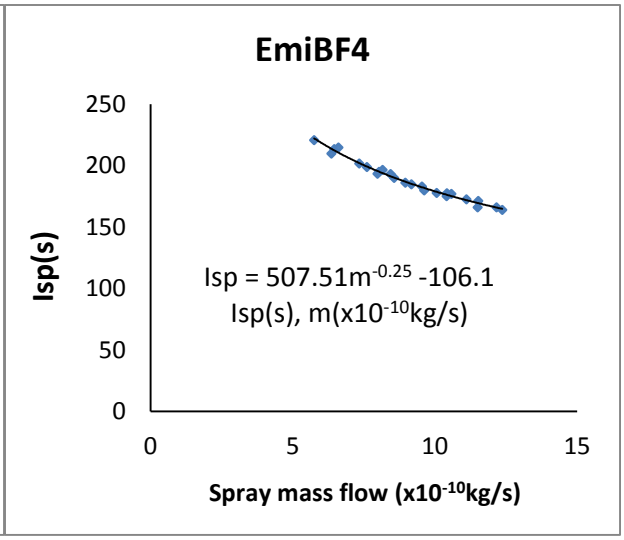

Figure 35. Specific impulse of Emi BF4 cone jets as a function of mass flow rate

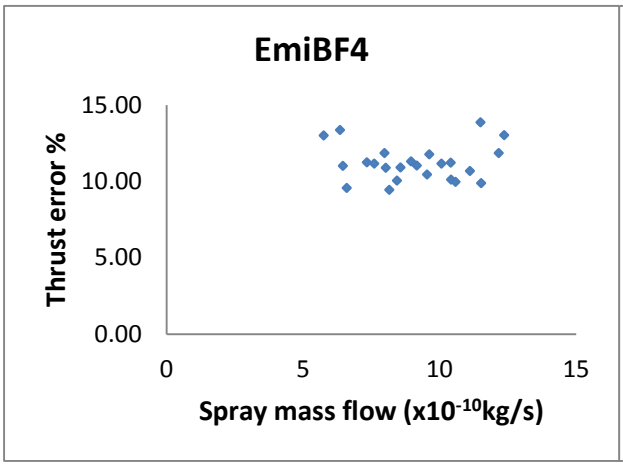

Figure 37. Error associated with using the average value of the specific charge to estimate spray thrust. The cone jets are those in Figure 36 and Figure 35.

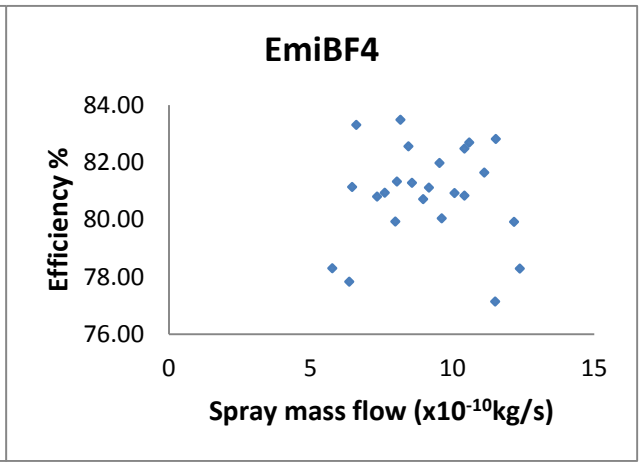

Figure 38. Efficiency of Emi BF4 cone jets.

Figure 37 shows the error involved in estimating the thrust. It is seen that the thrust computed by average values overestimates the measured value by 10% approximately, mainly because the voltage losses occurring in the electrospraying process are not included in the former.

The efficiency of Emi BF4 is shown in Figure 38 and its value is approximately 80%. Again, this 20% drop is mostly caused by voltage losses in the cone jet.

In Annex 7.3.4.3, all data required to build these graphs is presented.

3.6.2.4 Emi TF

Figure 39 shows the evolution of $\dot{m}$ (mass flow rate) with respect to ΔP (pressure difference between liquid bottle and atmosphere) for Emi TF. We see that the Correlation factor $R^2 = 0.9986 \cong 1$ which means the graph is almost linear.

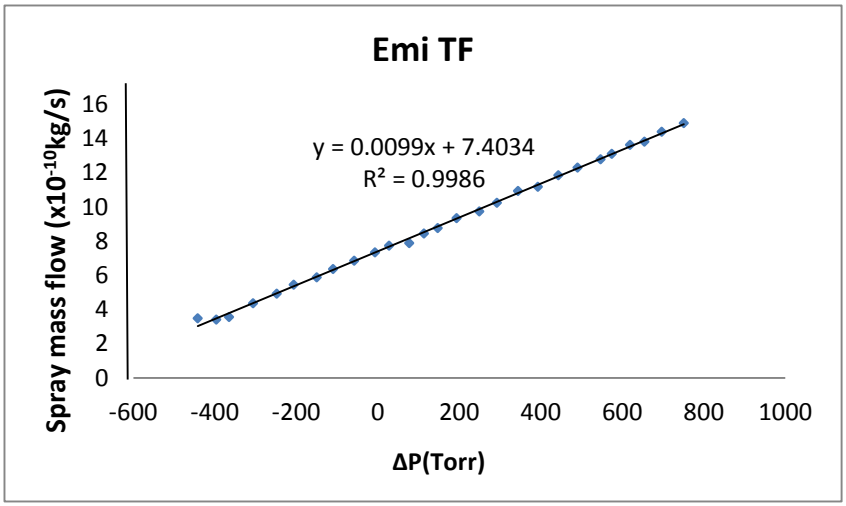

Figure 39. Mass flow rate vs. pressure difference for Emi TF

The evolution of total accumulated thrust and mass flow rate for several experimental runs obtained with Emi TF is shown in Figure 40 and Figure 41 and obviously, the thrust and mass flow rate associated with each spray will be the constant values reached at large m/q.

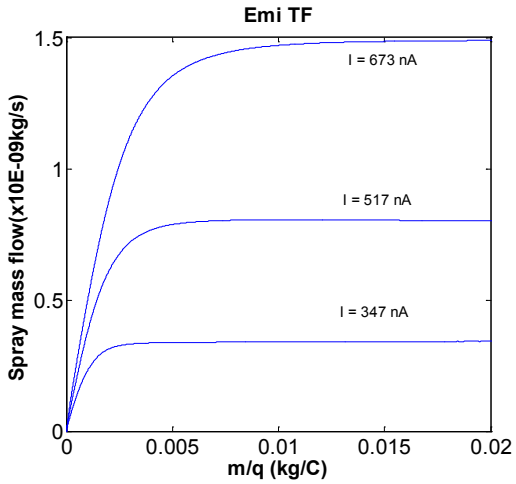

Figure 41. Beam mass flow for three Emi TF sprays

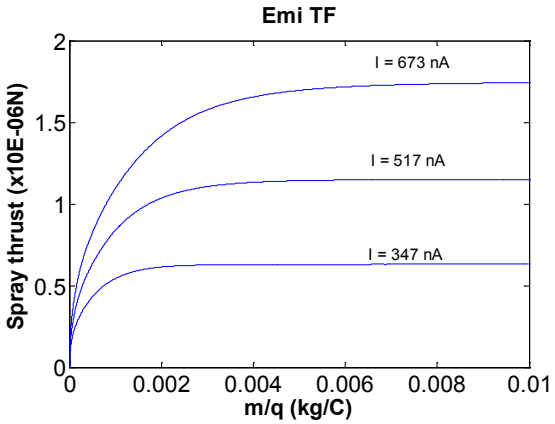

Figure 40.Thrust values rendered by TOF analysis for the sprays of Figure 41

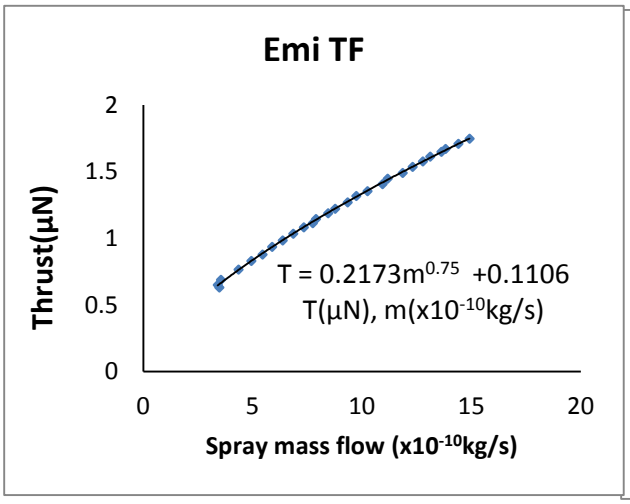

Figure 43. Thrust yielded by a single cone jet of Emi TF as a function of mass flow rate.

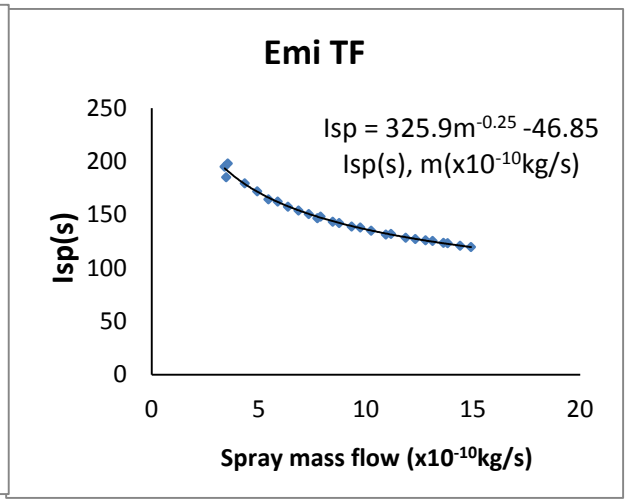

Figure 42. Specific impulse of Emi TF cone jets as a function of mass flow rate.

Figure 43 and Figure 42 collect the thrusts and specific impulses of all the Emi TF sprays studied, at an acceleration voltage of 2047 V. Although the lowest flow rate in these graphs is the minimum at which a stable cone jet could be set, flow rates larger than the largest shown are still possible.

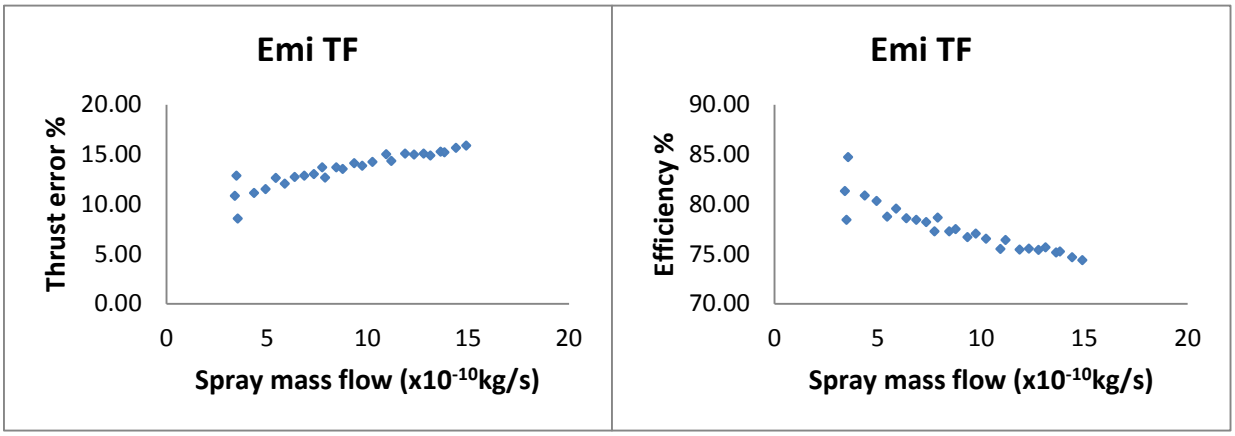

Figure 45. Error associated with using the average value of the specific charge to estimate spray thrust. The cone jets are those in Figure 43 and Figure 42

Figure 44. Efficiency of Emi TF cone jets.

Figure 45 shows the error involved in estimating the thrust. It is seen that the thrust computed by average values overestimates the measured value by 10%-15% approximately, mainly because the voltage losses occurring in the electrospraying process are not included in the former. It is to be noticed that this error tends slightly to increase with mass flow rate.

The efficiency of Emi TF is shown in Figure 44 and its average value is approximately 78%. Again, this 22% drop is mostly caused by voltage losses in the cone jet. Just opposite to the thrust error, the efficiency tends slightly to decrease with the mass flow rate going from 82%($\dot{m} = 4 \cdot 10^{-10}\ kg/s$) to 74%($\dot{m} = 15 \cdot 10^{-10}\ kg/s$). In Annex 7.3.4.4, all data required to build these graphs is presented.

3.6.2.5 TES

Figure 46 shows the evolution of $\dot{m}$ (mass flow rate) with respect to ΔP (pressure difference between liquid bottle and atmosphere) for TES. We see that the Correlation factor $R^2 = 0.9992 \cong 1$ which means the graph is almost linear.

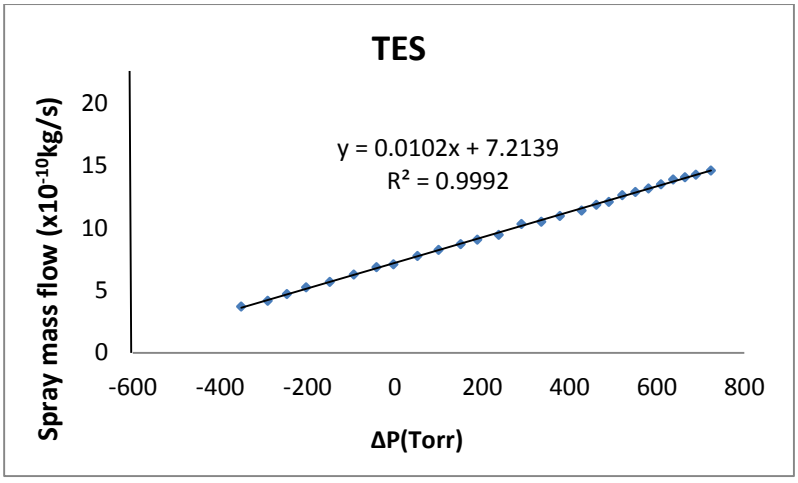

Figure 46. Mass flow rate vs. pressure difference for TES

The evolution of total accumulated thrust and mass flow rate for several experimental runs obtained with TES is shown in Figure 48 and Figure 47 and obviously, the thrust and mass flow rate associated with each spray will be the constant values reached at large m/q.

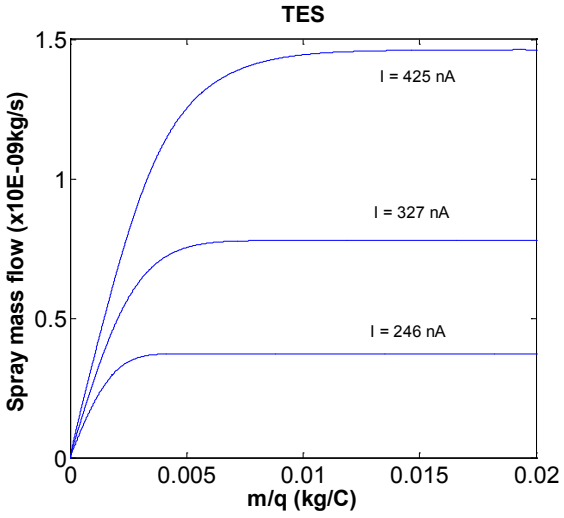

Figure 48. Beam mass flow for three TES sprays

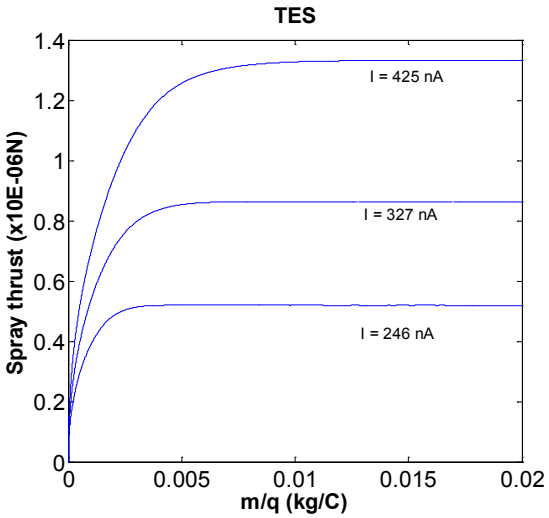

Figure 47. Thrust values rendered by TOF analysis for the sprays of Figure 48

Figure 49 and Figure 50 collect the specific impulses and thrusts of all the TES sprays studied, at an acceleration voltage of 1768 V. Although the lowest flow rate in these graphs is the minimum at which a stable cone jet could be set, flow rates larger than the largest shown are still possible.

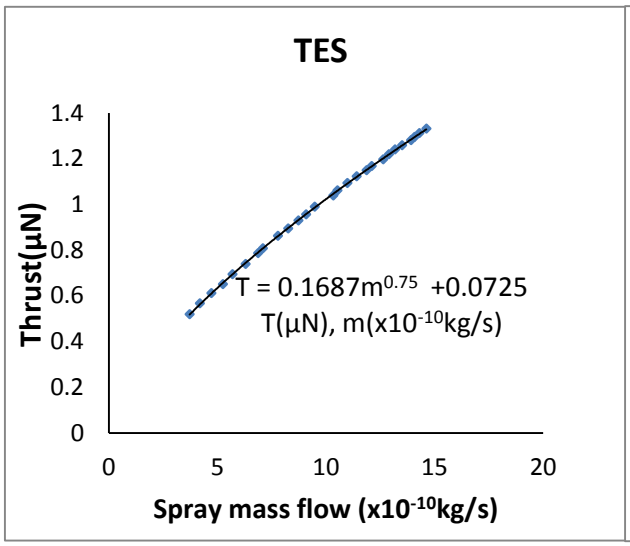

Figure 50. Thrust yielded by a single cone jet of TES as a function of mass flow rate.

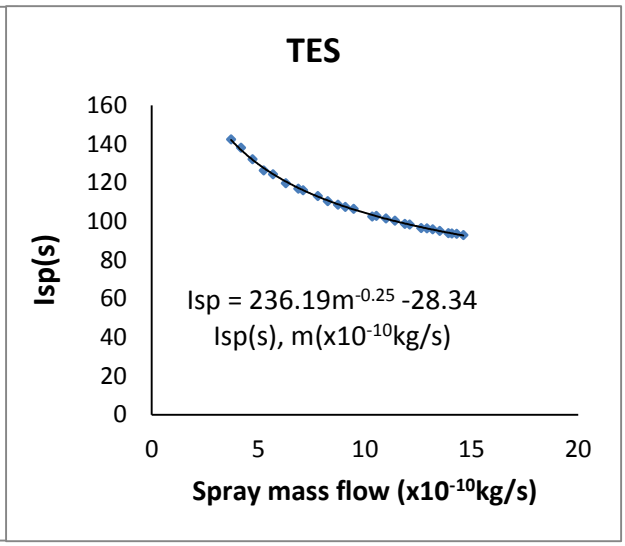

Figure 49. Specific impulse of TES cone jets as a function of mass flow rate

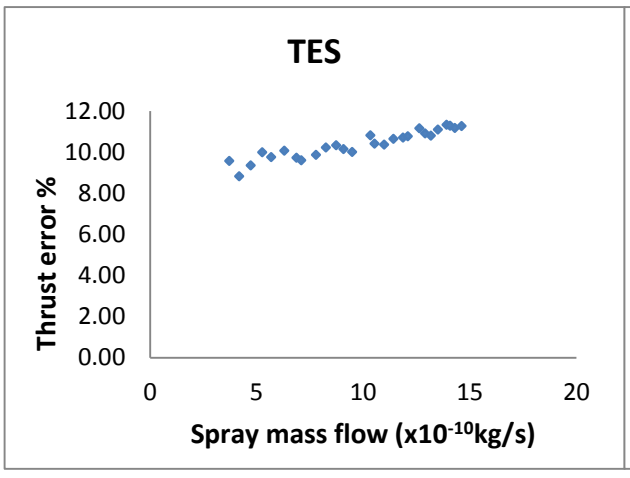

Figure 51. Error associated with using the average value of the specific charge to estimate spray thrust. The cone jets are those in Figure 49 and Figure 50

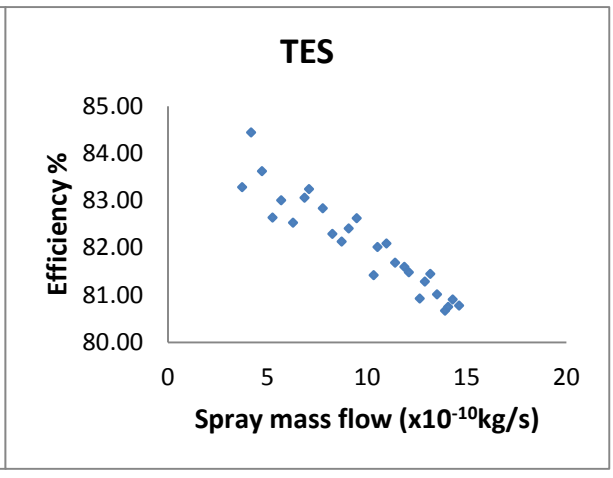

Figure 52. Efficiency of TES cone jets.

Figure 51 shows the error involved in estimating the thrust. It is seen that the thrust computed by average values overestimates the measured value by 10% approximately, mainly because the voltage losses occurring in the electrospraying process are not included in the former.

The efficiency of TES is shown in Figure 52 and its value varies from 84% for lower flow rates to 80% on higher flow rate. Again, this drop is mostly caused by voltage losses in the cone jet.

In Annex 7.3.4.5, all data required to build these graphs is presented.

3.6.2.6 Formamide 1 (50% Emi Im in Formamide)

Figure 53 shows the evolution of $\dot{m}$ (mass flow rate) with respect to ΔP (pressure difference between liquid bottle and atmosphere) for FORMAMIDE 1. We see that the Correlation factor $R^2 = 0.9993 \cong 1$ which means the graph is almost linear.

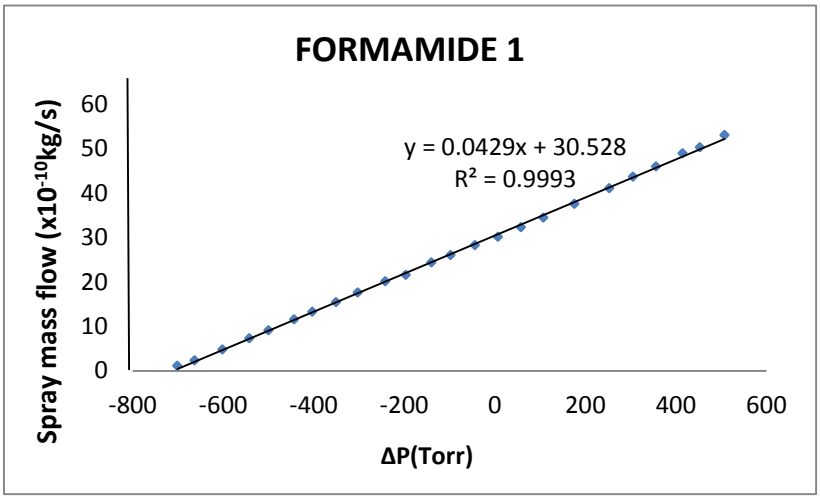

Figure 53. Mass flow rate vs. pressure difference for FORMAMIDE 1

The evolution of total accumulated thrust and mass flow rate for several experimental runs obtained with FORMAMIDE 1 is shown in Figure 54 and Figure 55 and obviously, the thrust and mass flow rate associated with each spray will be the constant values reached at large m/q.

Figure 57 and Figure 56 collect the thrusts and specific impulses of all the FORMAMIDE 1 sprays studied, at an acceleration voltage of 1598 V. Although the lowest flow rate in these graphs is the minimum at which a stable cone jet could be set, flow rates larger than the largest shown are still possible.

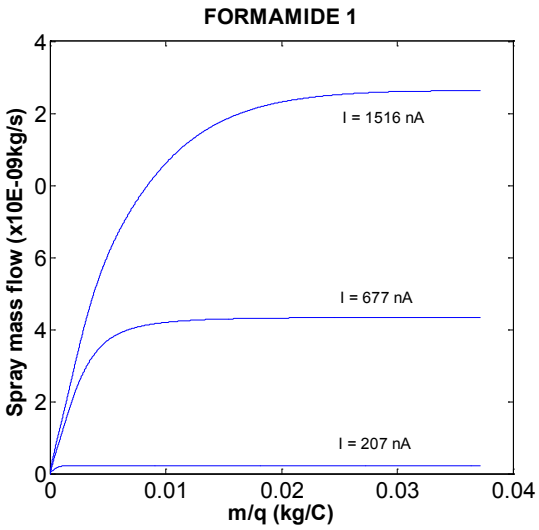

Figure 55. Beam mass flow for three FORMAMIDE 1 sprays

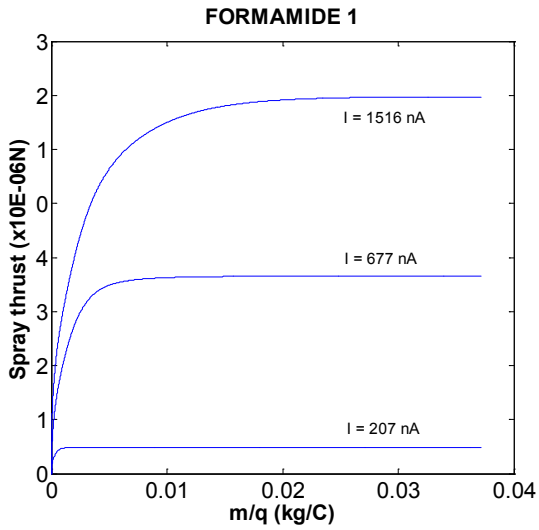

Figure 54. Thrust values rendered by TOF analysis for the sprays of Figure 55

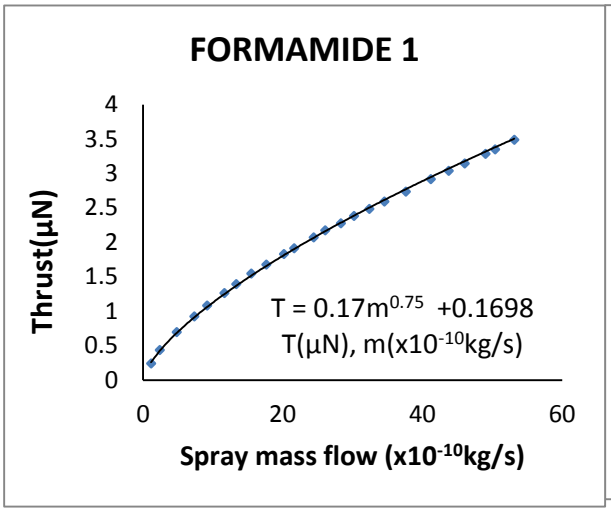

Figure 57. Thrust yielded by a single cone jet of FORMAMIDE 1 as a function of mass flow rate.

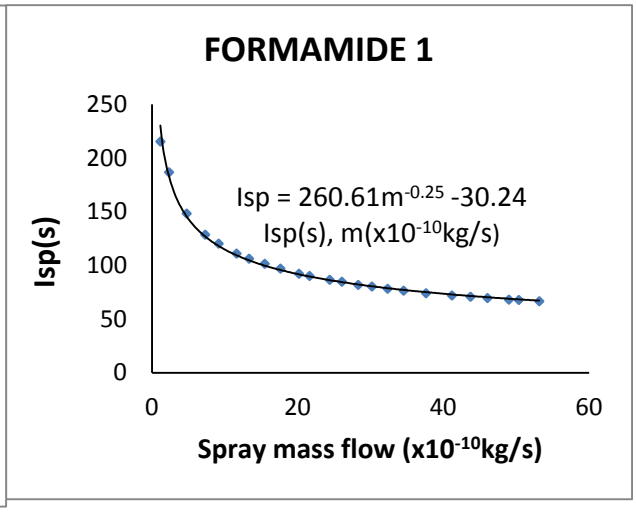

Figure 56. Specific impulse of FORMAMIDE 1 cone jets as a function of mass flow rate.

Figure 59 shows the error involved in estimating the thrust. It is seen that the thrust computed by average values overestimates the measured value by 6% - 45% depending on the mass flow rate. The error goes on increasing with the flow rate and now the reason is not only the voltage loss in cone jet. As seen in Figure 14 (TOF spectra of FORMAMIDE 1), the total fraction of current emitted in ionic form increases with the increase in flow rate. This implies that most of the mass

is emitted in the form of droplets, but their average specific charge in considerably lower than $I/\dot{m}$. Hence, the reduction in the thrust generated by the droplets cannot be compensated by the ions because of the minute mass flow of the latter. This is the reason for the high error.

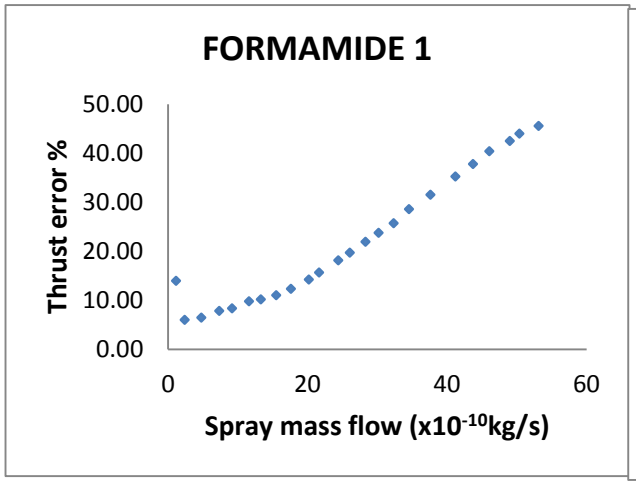

Figure 59. Error associated with using the average value of the specific charge to estimate spray thrust. The cone jets are those in Figure 57 and Figure 56.

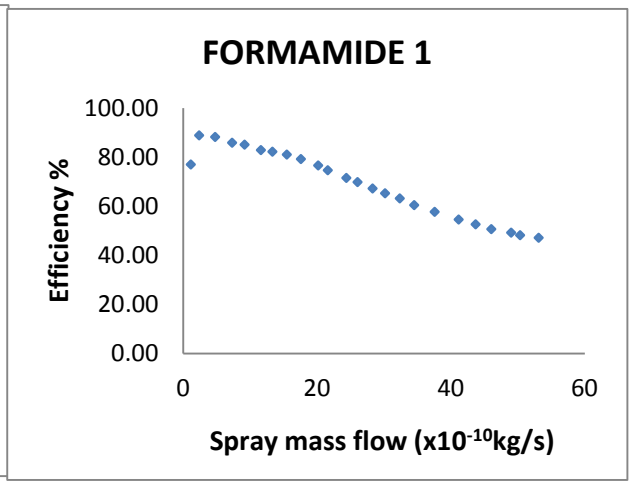

Figure 58. Efficiency of FORMAMIDE 1 cone jets.

The efficiency of FORMAMIDE 1 is shown in Figure 58. It also varies with mass flow rate as the thrust error but in an opposite manner. Its highest value is obtained for $\dot{m} = 2.37 \cdot 10^{-10} kg/s$ which is approximately 89% and its lowest value is obtained for $\dot{m} = 53.1 \cdot 10^{-10} kg/s$ which is approximately 47%. Here also, apart from the voltage loss in cone-jet, the reason is the important current fraction given by the ions as the extra thrust obtained from these ions does not compensate the power required to accelerate them.

In Annex 7.3.4.6, all data required to build these graphs is presented.

3.6.2.7 Formamide 2 (25% Emi Im in Formamide)

Figure 60 shows the evolution of $\dot{m}$ (mass flow rate) with respect to ΔP (pressure difference between liquid bottle and atmosphere) for FORMAMIDE 2. We see that the Correlation factor $R^2 = 0.9998 \cong 1$ which means the graph is almost linear.

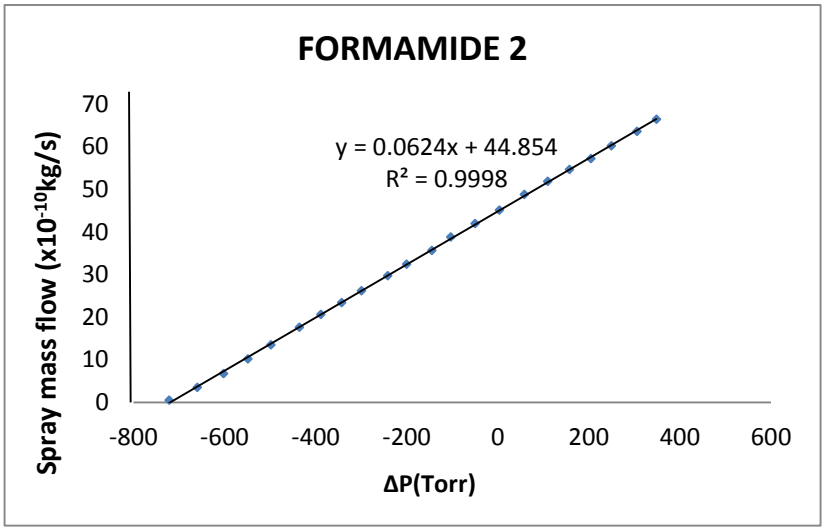

Figure 60. Mass flow rate vs. pressure difference for FORMAMIDE 2

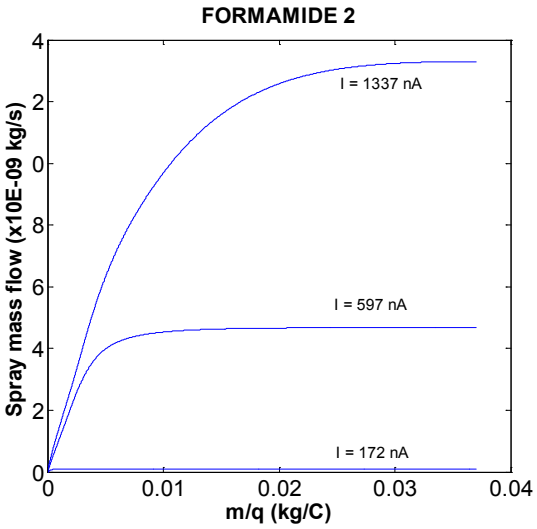

Figure 61. Beam mass flow for three FORMAMIDE 2 sprays

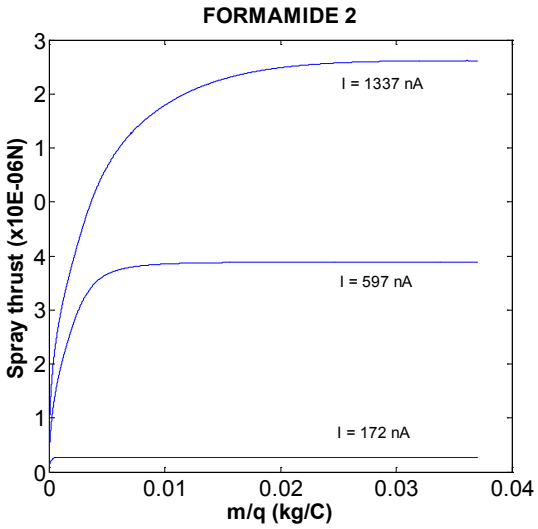

Figure 62. Thrust values rendered by TOF analysis for the sprays of Figure 61

The evolution of total accumulated thrust and mass flow rate for several experimental runs obtained with FORMAMIDE 2 is shown in Figure 62 and Figure 61 and obviously, the thrust and mass flow rate associated with each spray will be the constant values reached at large m/q.

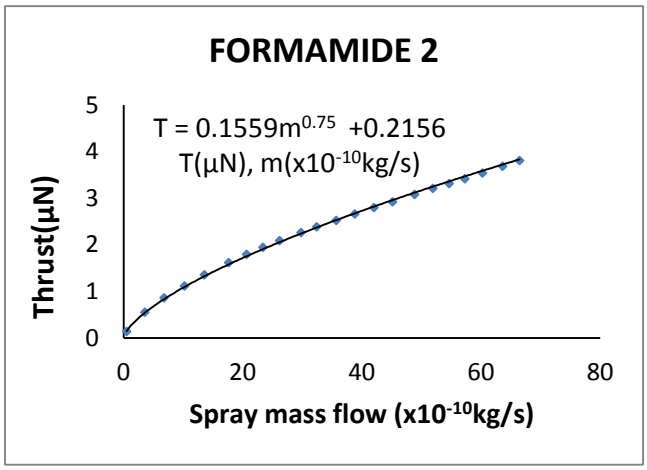

Figure 64. Thrust yielded by a single cone jet of FORMAMIDE 2 as a function of mass flow rate.

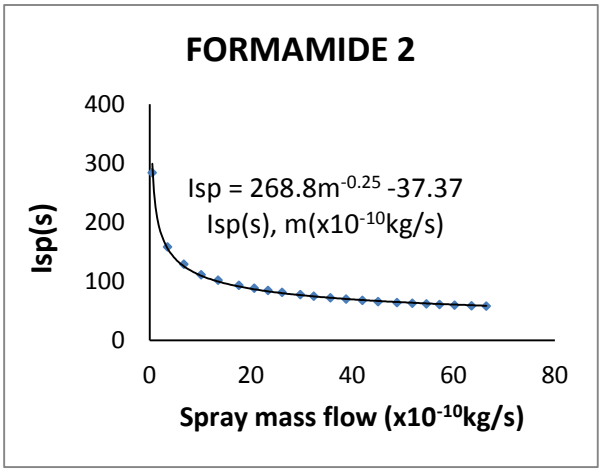

Figure 63. Specific impulse of FORMAMIDE 2 cone jets as a function of mass flow rate.

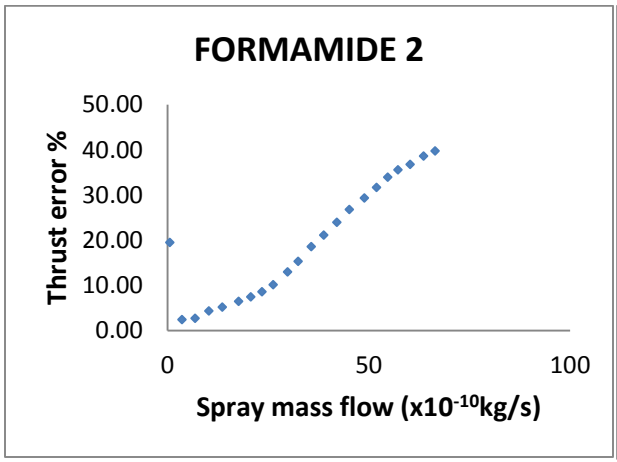

Figure 66. Error associated with using the average value of the specific charge to estimate spray thrust. The cone jets are those in Figure 64 and Figure 63.

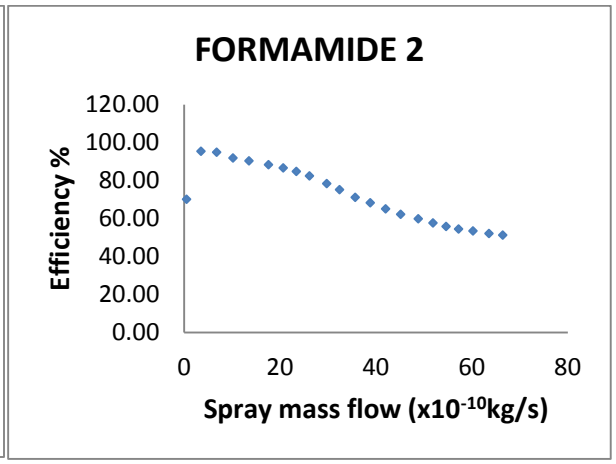

Figure 65. Efficiency of FORMAMIDE 2 cone iets.

Figure 64 and Figure 63 collect the thrusts and specific impulses of all the FORMAMIDE 2 sprays studied, at an acceleration voltage of 1593 V. Although the lowest flow rate in these graphs is the minimum at which a stable cone jet could be set, flow rates larger than the largest shown are still possible.

Figure 66 shows the error involved in estimating the thrust. It is seen that the thrust computed by average values overestimates the measured value by 2% - 40% depending on the mass flow rate. The error goes on increasing with the flow rate and now the reason is not only the voltage loss in cone jet. (We have discarded the value for the minimum flow rate (20%) as the spray might not have been truly stable yet by then). As seen in Figure 15 (TOF spectra of FORMAMIDE 2), the total fraction of current emitted in ionic form increases with the increase in flow rate. This implies that most of the mass is emitted in the form of droplets, but their average specific charge in considerably lower than $I/\dot{m}$. Hence, the reduction in the thrust generated by the droplets cannot be compensated by the ions because of the minute mass flow of the latter. This is the reason for the high error.

Furthermore, the ionic emission is not so pronounced till $I \cong 600\,nA \leftrightarrow \dot{m} \cong 23 \cdot 1E-10\,kg/s$ (Annex 7.3.4.7) and for higher current/flow rate it goes on increasing gradually. Now, we can see in Figure 66 that till $\dot{m} \cong 23 \cdot 1E-10\,kg/s$, the error is below 10% and later it increases. After this we can say even more firmly that the error has to see with the emission of ions.

The efficiency of FORMAMIDE 2 is shown in Figure 65. It also varies with mass flow rate as the thrust error but in an opposite manner. Its highest value is obtained for $\dot{m} = 3.55 \cdot 10^{-10} kg/s$ which is approximately 95% and its lowest value is obtained for $\dot{m} = 55.5 \cdot 10^{-10} kg/s$ which is approximately 51%. Also in this case, apart from the voltage loss in cone-jet, the reason is the important current fraction given by the ions as the extra thrust obtained from these ions does not compensate the power required to accelerate them.

In Annex 7.3.4.7, all data required to build these graphs is presented.

3.6.2.8 Formamide G (4% EAN in Formamide)

Figure 67 shows the evolution of $\dot{m}$ (mass flow rate) with respect to ΔP (pressure difference between liquid bottle and atmosphere) for FORMAMIDE G. We see that the Correlation factor $R^2 = 0.9989 \cong 1$ which means the graph is almost linear. As shown in Annex 7.3.4.8, for the first experiment, the efficiency obtained was of more than 100%. Hence, this curve will be discarded for the analysis.

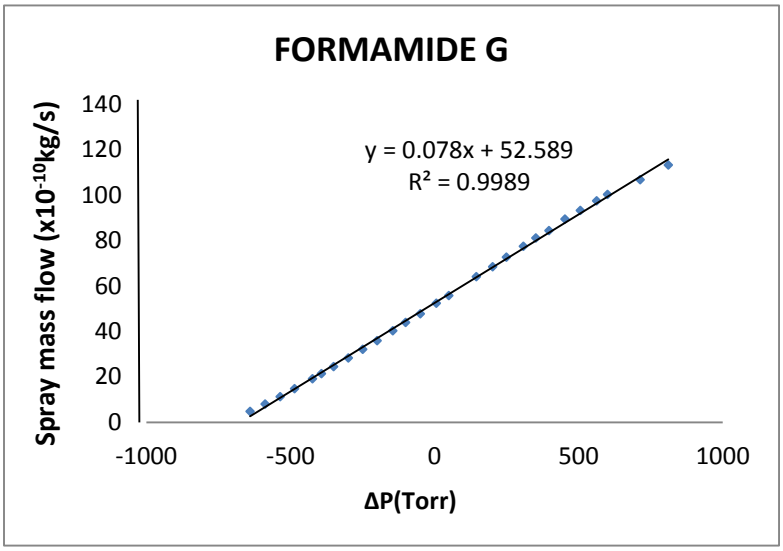

Figure 67. Mass flow rate vs. pressure difference for FORMAMIDE G

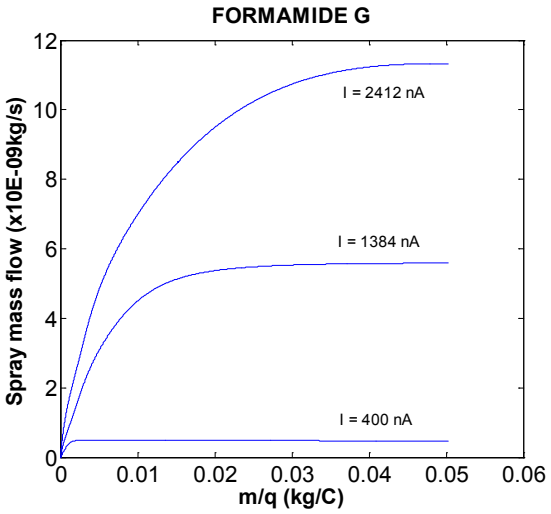

Figure 69. Beam mass flow for three FORMAMIDE G sprays

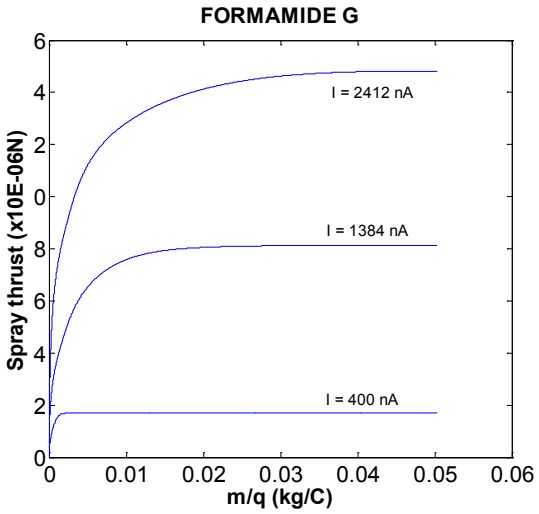

Figure 68. Thrust values rendered by TOF analysis for the sprays of Figure 69

The evolution of total accumulated thrust and mass flow rate for several experimental runs obtained with FORMAMIDE G is shown in Figure 68 and Figure 69 and obviously, the thrust and mass flow rate associated with each spray will be the constant values reached at large m/q.

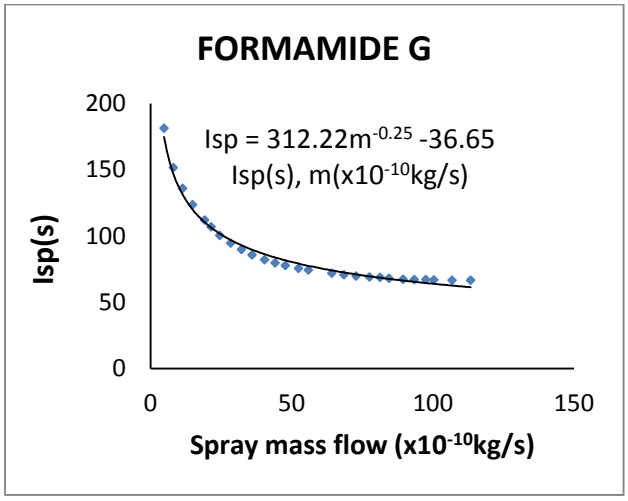

Figure 71. Thrust yielded by a single cone jet of FORMAMIDE G as a function of mass flow rate.

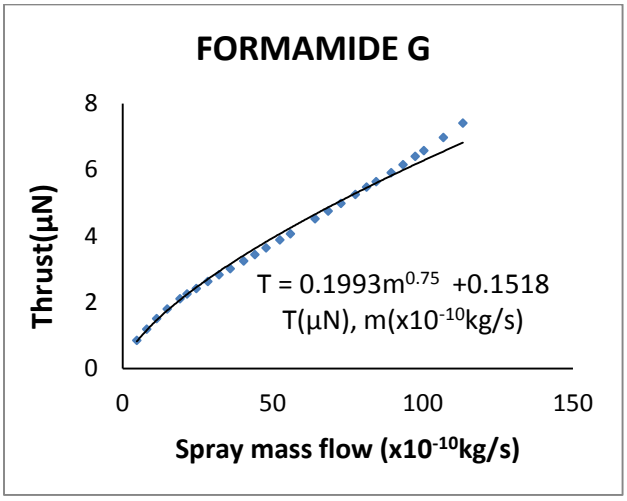

Figure 70. Specific impulse of FORMAMIDE G cone jets as a function of mass flow rate.

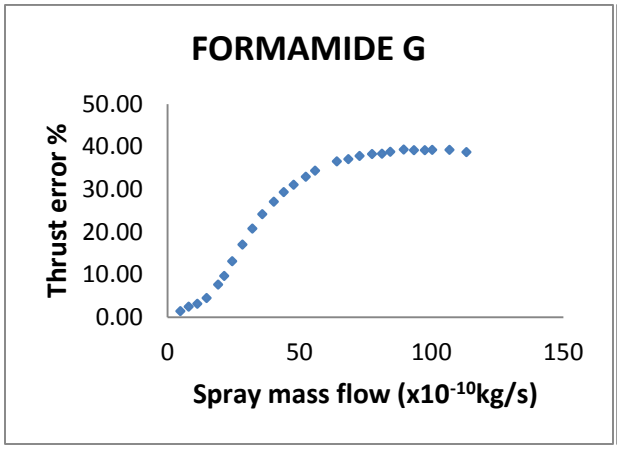

Figure 72. Error associated with using the average value of the specific charge to estimate spray thrust. The cone jets are those in Figure 71 and Figure 70.

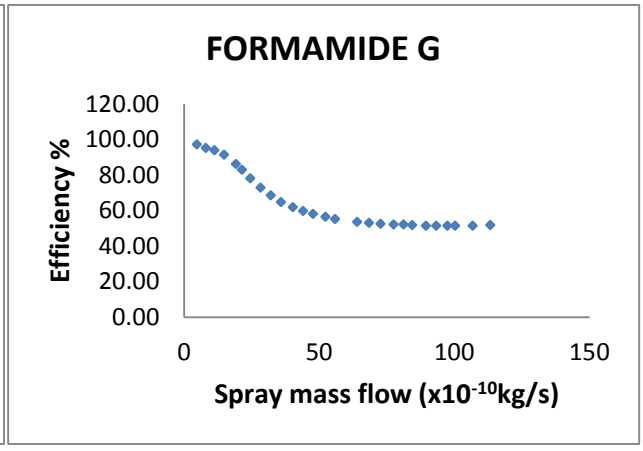

Figure 73. Efficiency of FORMAMIDE G cone jets.

Figure 70 and Figure 71 collect the thrusts and specific impulses of all the FORMAMIDE G sprays studied, at an acceleration voltage of 1933 V. Although the lowest flow rate in these graphs is the

minimum at which a stable cone jet could be set, flow rates larger than the largest shown are still possible.

Figure 72 shows the error involved in estimating the thrust. It is seen that the thrust computed by average values overestimates the measured value by 1% - 39% depending on the mass flow rate. In general, the error goes on increasing with the flow rate and the rate of increase is slow for smaller and higher flow rates $\dot{m} \leq 19.28E-10\ kg/s$ and $\dot{m} \geq 68.49E-10\ kg/s$. For $19.28E-10\ kg/s < \dot{m} < 68.49E-10\ kg/s$, the error increases rapidly with the flow rate. The reason of this high error is not only the voltage loss in cone jet. As seen in Figure 16 (TOF spectra of FORMAMIDE G), the total fraction of current emitted in ionic form increases with the increase in flow rate. This implies that most of the mass is emitted in the form of droplets, but their average specific charge in considerably lower than $I/\dot{m}$. Hence, the reduction in the thrust generated by the droplets cannot be compensated by the ions because of the minute mass flow of the latter. Again, if we analyze Figure 16, for $700\ nA \leq I \leq 1600\ nA\ \ i.e\ 19.12E-10\ kg/s \leq \dot{m} \leq 68.49E-10\ kg/s$ (Annex 7.3.4.8) there can be seen a sharp drop in the graph, hence the particles emitted must be ions. For $I < 700\ nA \leftrightarrow \dot{m} < 19.12E-10\ kg/s$, there is no sharp drop seen and hence we can say that no ions are produced. For $I > 1600\ nA\ \leftrightarrow \dot{m} > 68.49E-10\ kg/s$, the drop is not very sharp and hence these particles must be very tiny droplets with high charge carrying in them. All this assures us more that the error is due to the higher fraction of current emitted in ionic form.

The efficiency of FORMAMIDE G is shown in Figure 73. It also varies with mass flow rate as the thrust error but in an opposite manner. The explanation is the same as done in the case of Thrust error: there exists an important current fraction given by the ions and the extra thrust obtained from these ions does not compensate the power required to accelerate them.

In Annex 7.3.4.8, all data required to build these graphs is presented.

3.6.2.9 Formamide H (7% EAN in Formamide)

Figure 74 shows the evolution of $\dot{m}$ (mass flow rate) with respect to ΔP (pressure difference between liquid bottle and atmosphere) for FORMAMIDE H. We see that the Correlation factor $R^2 = 0.998 \cong 1$ which means the graph is almost linear. As shown in Annex 7.3.4.9, for the first two experiments, the efficiency obtained was of more than 100%. Hence, these two curves will be discarded for the analysis.

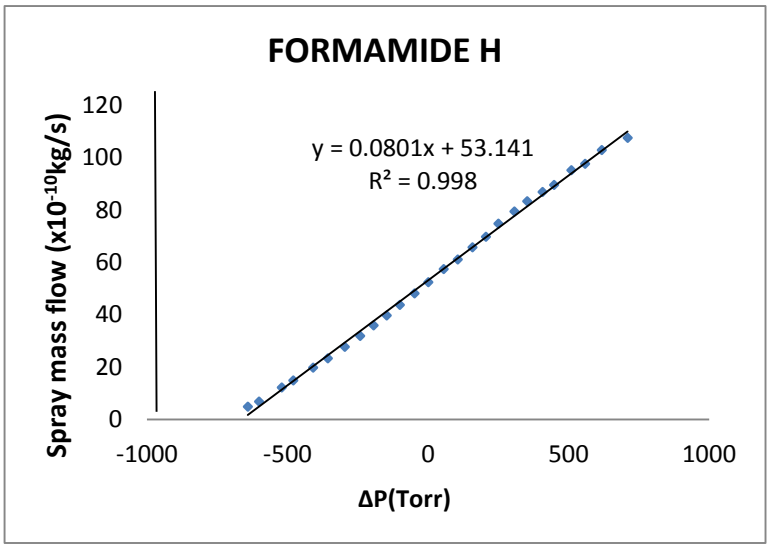

Figure 74. Mass flow rate vs. pressure difference for FORMAMIDE H

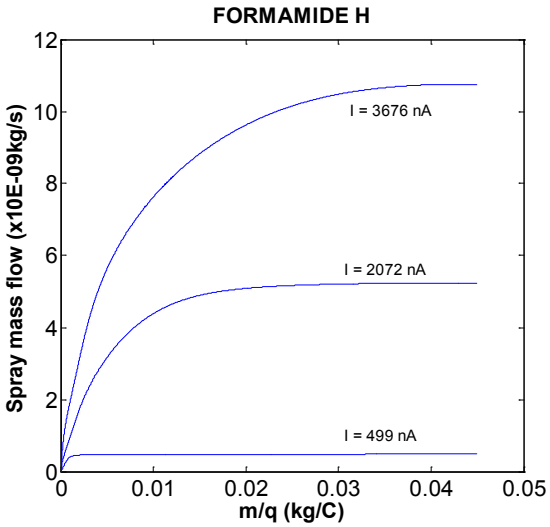

Figure 76. Beam mass flow for three FORMAMIDE H sprays

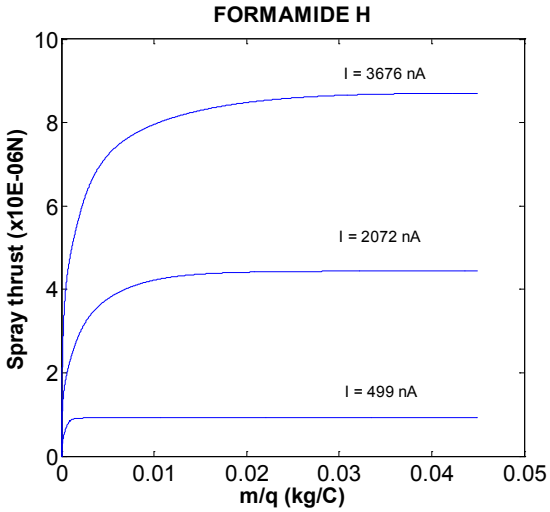

Figure 75. Thrust values rendered by TOF analysis for the sprays of Figure 76

The evolution of total accumulated thrust and mass flow rate for several experimental runs obtained with FORMAMIDE H is shown in Figure 75 and Figure 76 and obviously, the thrust and mass flow rate associated with each spray will be the constant values reached at large m/q.

Figure 78 and Figure 77 collect the thrusts and specific impulses of all the FORMAMIDE H sprays studied, at an acceleration voltage of 1933 V. Although the lowest flow rate in these graphs is the minimum at which a stable cone jet could be set, flow rates larger than the largest shown are still possible.

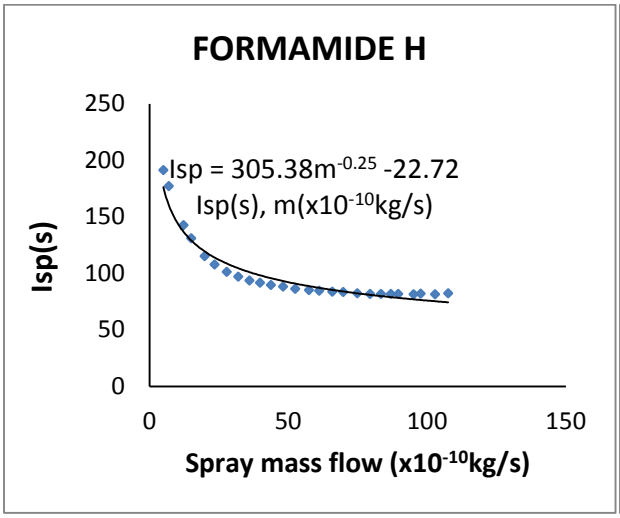

Figure 78. Thrust yielded by a single cone jet of FORMAMIDE H as a function of mass flow rate.

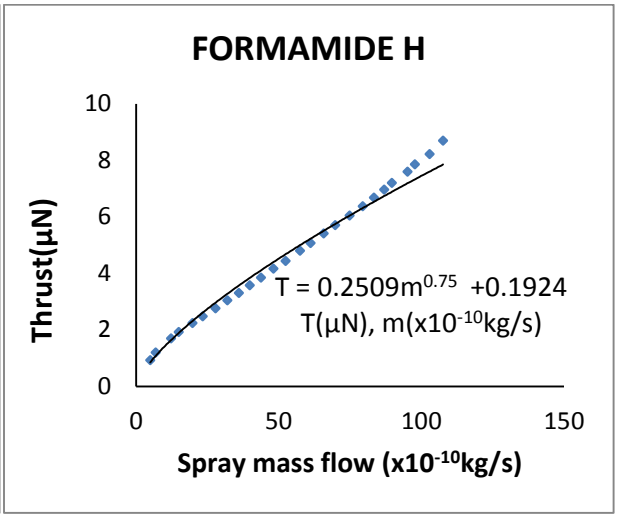

Figure 77. Specific impulse of FORMAMIDE H cone jets as a function of mass flow rate.

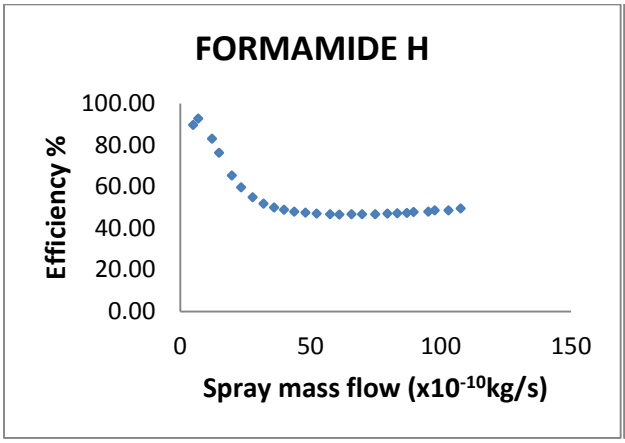

Figure 80. Error associated with using the average value of the specific charge to estimate spray thrust. The cone jets are those in Figure 77 and Figure 78.

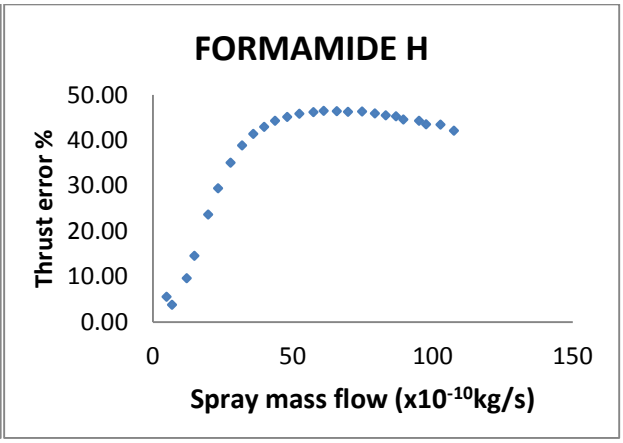

Figure 79. Efficiency of FORMAMIDE H cone jets.

Figure 80 shows the error involved in estimating the thrust. Now, according to Figure 17 (TOF spectra of FORMAMIDE H), forgetting about the first two spectra as explained earlier, for $I \leq 579\,nA \leftrightarrow \dot{m} \leq 6E-10\,kg/s$ (Annex 7.3.4.9), there is no ionic emission and hence the thrust error is the lowest (below 5%). Later, error goes on increasing with the flow rate for $\dot{m} \leq 40E-10\,kg/s$ and after this it remains almost constant in around 43%. This range of increasing error corresponds to $579\,nA \leq I \leq 1700\,nA$.

Again according to Figure 17, there can be seen sharp drops in the current beam for $579\,nA \leq I \leq 1700\,nA$, which means the current is emitted in form of ions and moreover, in this range, the fraction of ionic current increases with flow rate. Also, for $I \geq 1700\,nA$, there is droplet emission and not ionic emission which matches with the constant error seen in Figure 80.

In conclusion, the reason of this high error is not only the voltage loss in cone jet but also the emission of current in ionic form. The emission in ionic form implies that most of the mass is emitted in the form of droplets, but their average specific charge in considerably lower than $I/\dot{m}$. Hence, the reduction in the thrust generated by the droplets cannot be compensated by the ions because of the minute mass flow of the latter.

The efficiency of FORMAMIDE H is shown in Figure 79. It also varies with mass flow rate as the thrust error but in an opposite manner. The explanation is the same as done in the case of Thrust error: there exists an important current fraction given by the ions and the extra thrust obtained from these ions does not compensate the power required to accelerate them.

In Annex 7.3.4.9 all data required to build these graphs is presented.

3.6.3 Comparison of several propellants

Figure 81 collects the thrust values produced by a single electrospray emitter for different mass flow rate for all the propellants experimented. All the experiments were done for similar pressure difference between the vacuum tank and the liquid bottle but as seen in the figure above, only the liquids containing Formamide show higher mass flow rate than $20E-10\ kg/s$. The reason might be because the viscosity of Formamide is one order less than that of other liquids and hence the liquids containing Formamide (FORMAMIDE 1, 2, G & H) flow faster for similar Pressure differences.

A zoom is done in case of lower mass flow rates in order to identify better the curves present in this area which is shown in Figure 82.

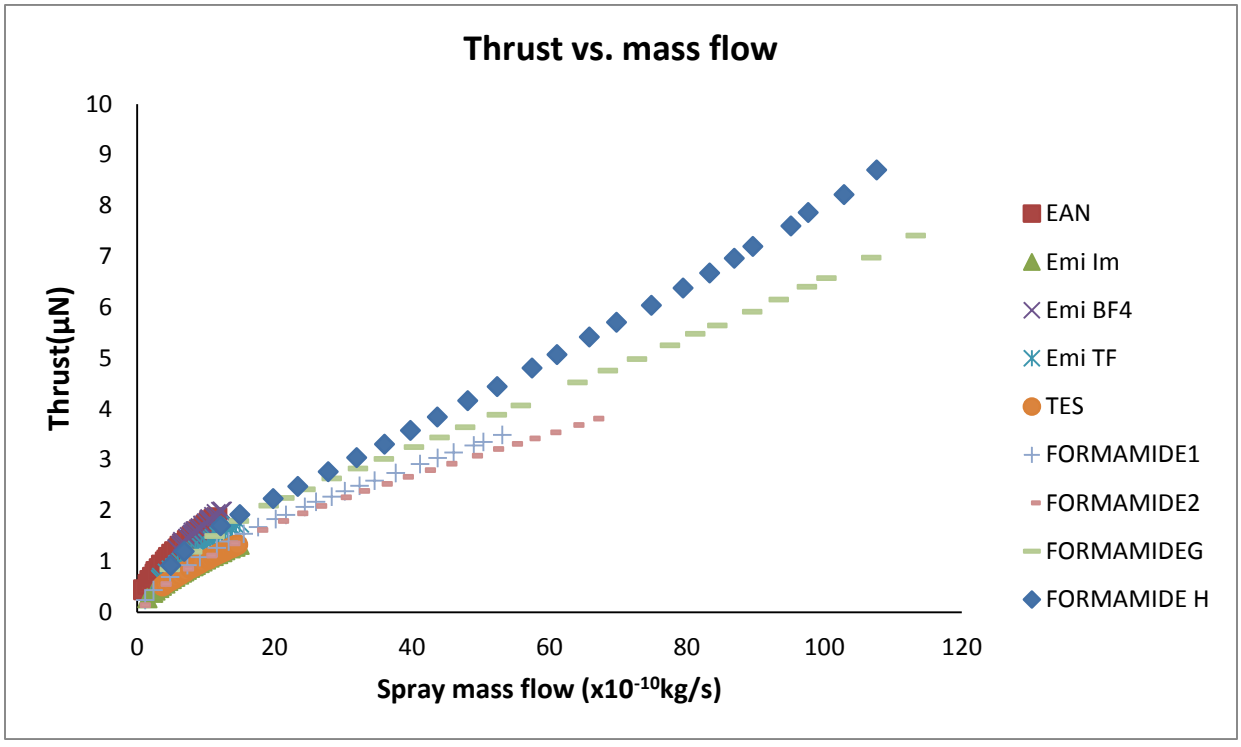

Figure 81. Thrust vs. mass flow rate for all the liquids analyzed

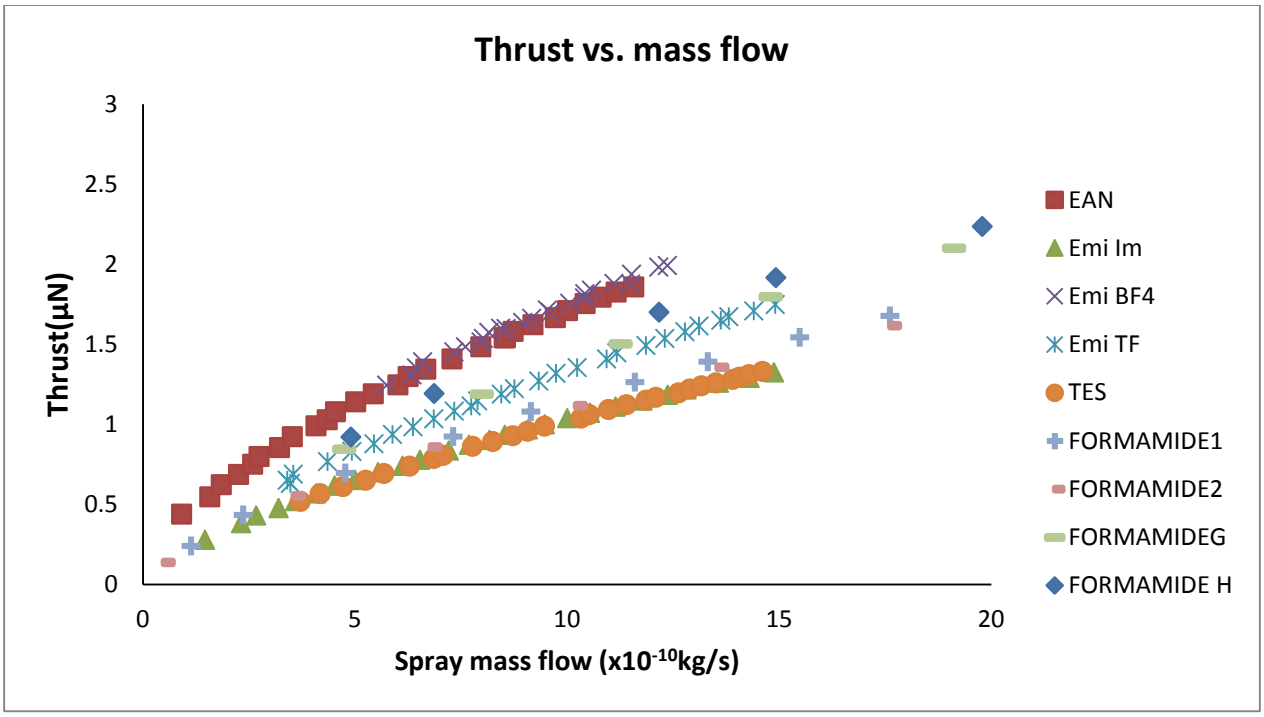

Figure 82. Thrust vs. mass flow rate for all the liquids analyzed (zoom for lower flow rates)

Maintaining the same pressure difference for all fluids, it is clear that the maximum thrust is obtained for FORMAMIDE G & H as seen in Figure 81. If we compare for the same range of mass flow, EAN and Emi BF4 are the liquids that give higher thrust values than others. Emi Im and TES are the ones that show lower thrust values.

Figure 83 collects the values of specific impulses for different mass flow rate for all the propellants experimented. A zoom is done in case of lower mass flow rates in order to identify better the curves present in this area which is shown in Figure 84.

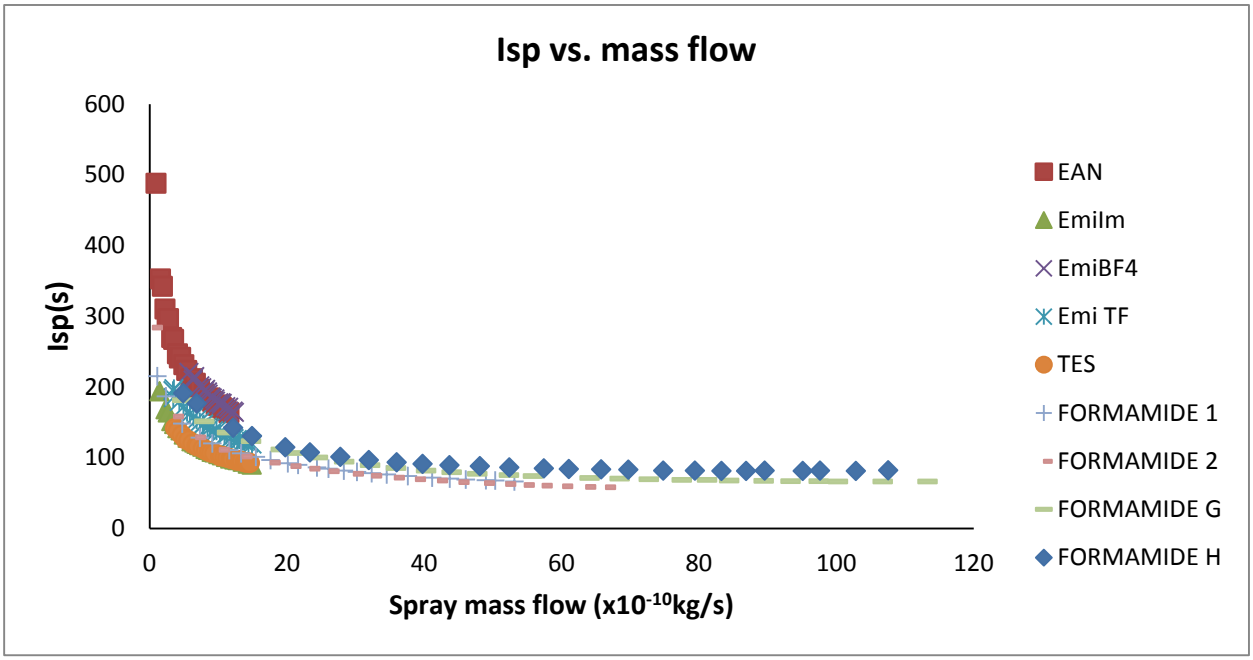

Figure 83. Specific impulse vs. mass flow rate for all the liquids analyzed

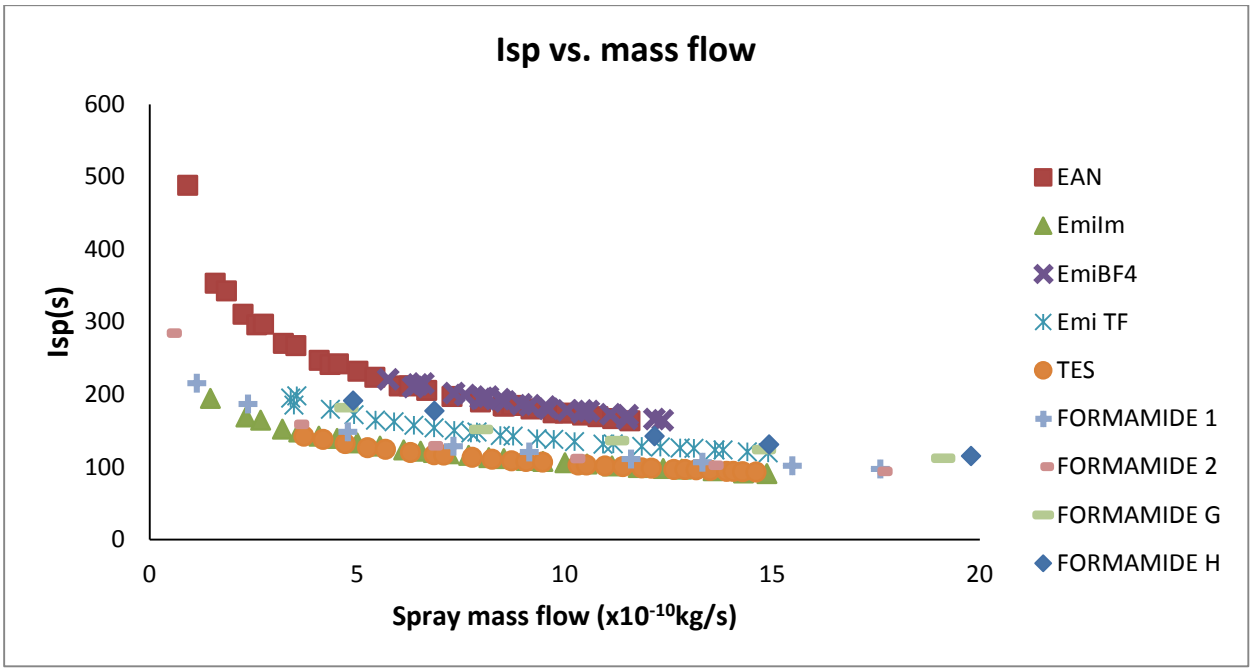

Figure 84. Specific impulse vs. mass flow rate for all the liquids analyzed (zoom for lower flow rates)

EAN and Emi BF4 are again the propellants with highest specific impulse for the range of mass flow where they can form stable cone-jets. For $6 \cdot 10^{-10} kg/s \leq \dot{m} \leq 11 \cdot 10^{-10} kg/s$, the specific impulse they provide varies from 220 s to 170 s decreasing with the flow rate. For lower flow rates, Emi BF4 cannot form stable cone jet (in the experimental setup we had) but EAN provides even higher specific impulses reaching till 500 s for flow rates of order of $10^{-11} kg/s$.

The liquids containing Formamide give Isp of nearly 200s for the case where we have stable cone-jet with minimum flow rate and it goes on decreasing gradually while we increase the flow rate. The rate of decrease decreases with the flow rate and eventually it gets stable giving values of around 80s-90s. Among them, FORMAMIDE G and FORMAMIDE H present higher values of specific impulses than FORMAMIDE 1 and FORMAMIDE 2.

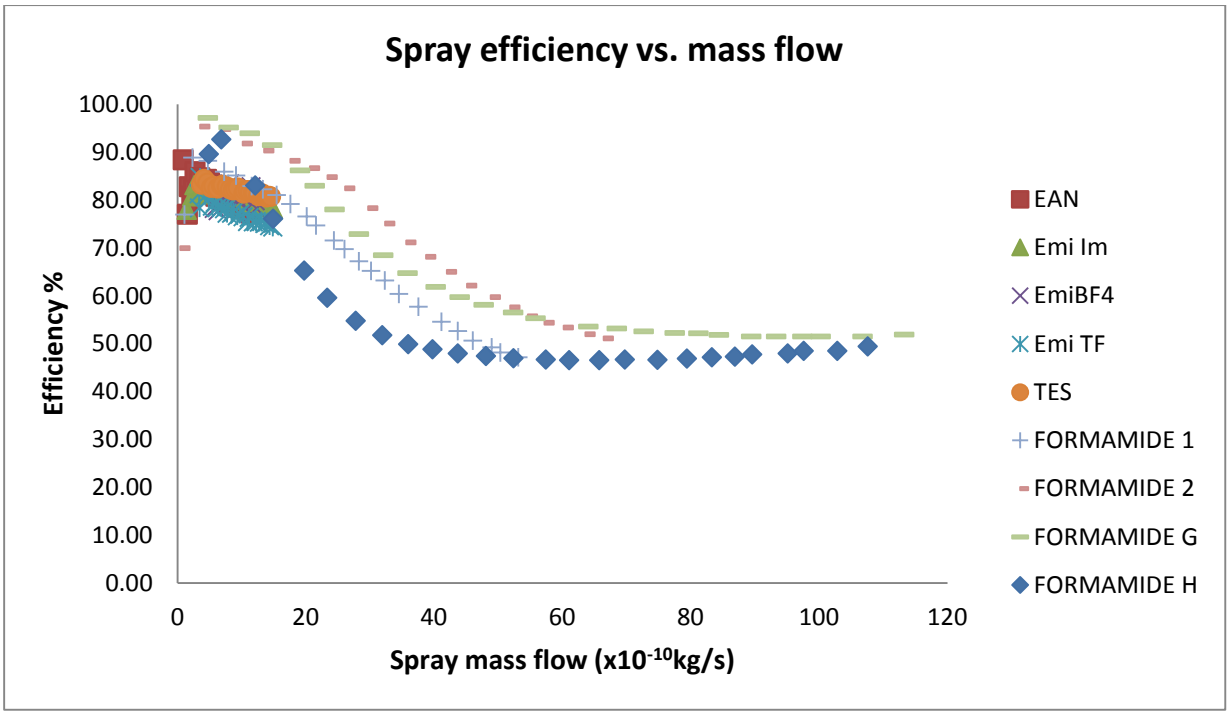

Figure 85. Spray efficiency vs. mass flow rate for all the liquids analyzed

The spray efficiency for various liquids with respect to flow rate is given in Figure 85. A zoom is done in case of lower mass flow rates in order to identify better the curves present in this area which is shown in Figure 86.

For liquid containing Formamide, efficiency goes on decreasing with an increase in the mass flow rate and for each of them, the curve is different. FORMAMIDE 2 has higher efficiency than FORMAMIDE 1 and FORMAMIDE G has higher efficiency than FORMAMIDE H. It makes sense because the lower the concentration of ionic liquid in Formamide, the lower will be the fraction of ionic current and hence efficiency is higher. For flow rates lower than $m \leq 20 \cdot 10^{-10} kg/s$, efficiency of FORMAMIDE 2 and FORMAMIDE G remains almost constant at around 90% whereas all other liquids present and efficiency of around 80%.

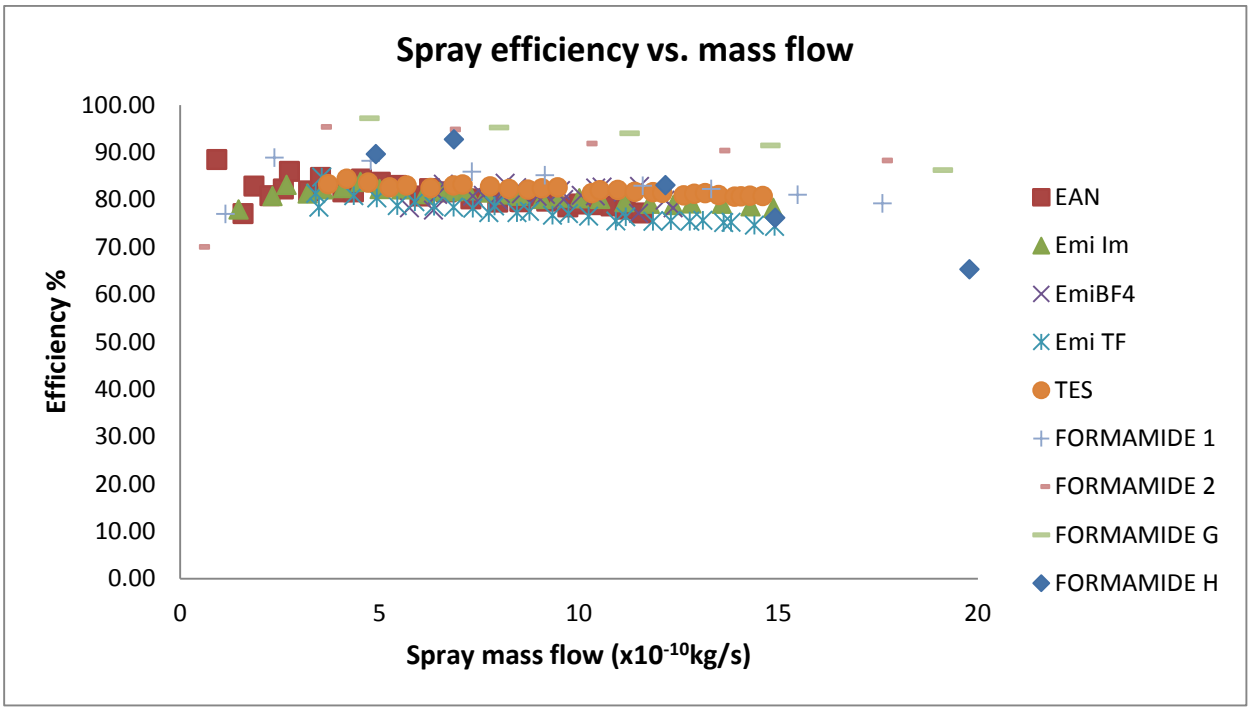

Figure 86.Spray efficiency vs. mass flow rate for all the liquids analyzed (zoom for lower flow rates)

4. ACS TEST IN CUBESAT

4.1 Theory

In this section, all the theoretical bases behind the proper functioning of the attitude control system will be explained.

4.1.1 Electrospray Formation

A high voltage difference between the emitter, where the propellant reaches by capillary action, and an extractor which is a few millimeters away from the emitter produces the electric field necessary for the spray formation. Table 4 lists the voltages to be applied to different parts of the thrusters for turning the spray on and off. As the satellite should be controlled remotely, we will have to develop a high voltage current and a high voltage switch to change the voltage of the internal extractor through Wi-Fi. Both of these concepts will be explained separately.

Table 4. Voltages to be applied to the emitter and the extractors for turning ON/OFF the electrospray

Component	Voltages for Spray ON	Voltages for Spray OFF
Emitter	High Voltage	High Voltage
Internal Extractor	Ground	High Voltage
External Extractor	Ground	Ground

4.1.1.1 High Voltage Production

A Ni-Cd 7.2V rechargeable battery will be used as the primary power supply for the satellite. We need to produce the voltages required for all the components of the satellite using this battery. As it will be explained later in the subtopic of 'Testing', the spray formation occurs when the voltage at the emitter is between 2360V and 2580V. To obtain these high voltages, we will use a high voltage converter. We use the Q101 model of EMCO with a power consumption of 0.5W and maximum output voltage of 10KV.

In order to find out what input voltage we should apply to obtain a desired output voltage, a measurement is done with a High voltage Probe. Table 5 gives the corresponding conversion values.

Table 5. Input-Output voltages and corresponding current values for the high voltage converter

Vin(V)	Vout(V)	Current (With Fluke Probe Load) (mA)	Current(without Load) (mA)
0.536	1070	5.65	2.98
0.697	1500	8.83	4.97
0.891	2000	12.9	7.58
1.089	2500	17.15	10.36
1.290	3000	21.50	13.30
1.490	3500	26.23	16.26
1.695	4000	30.69	19.37

To avoid electrical breakdown, the high voltage system inside the satellite shouldn't be turned on before it is already in a complete vacuum. Hence, this system has to be controlled remotely using the Arduino controller.

One of the ways to do this is to use one of the digital output pins of the Arduino which works at 5V to provide input power to the high voltage converter. We will run the emitter at 2500V, so according to Table 5, the input voltage required is of 1.089 V which could be obtained using a voltage divider. However, there is another requirement to be fulfilled: the power required to run the high voltage converter. As stated earlier, the power in the circuit has to be more than 0.5W to ensure the proper functioning of the EMCO high voltage converter. According to Arduino specifications given in its website, the current given by the Arduino is 40 mA. So the power available from its digital output is: $P = V * I = 5 * (40 * 1e - 03) = 0.2W$. Hence the EMCO power converter can't run through the Arduino. So, the power for the Arduino should come from the battery.

As we need to remotely control the high voltage supply and powering directly from Arduino won't work, we need to introduce a transistor in the circuit which could be powered by the Arduino. One option could be using a MOSFET.

The metal-oxide-semiconductor field-effect transistor (MOSFET) is a type of transistor with three separate terminals: source(S), gate (G) and drain (D). Depending on the voltage difference at G-S, D-S will be conducting or not. For our application, we use an IRFBG30 MOSFET. 'S' will be grounded and 'G' will be connected to one of the digital outputs of the Arduino. Hence, when the digital output will be ON, the voltage difference between G and S will be 5 V, thus connecting D-S. On the other hand, when the digital output will be OFF, the voltage difference between G and S will be zero and hence disconnecting D-S.

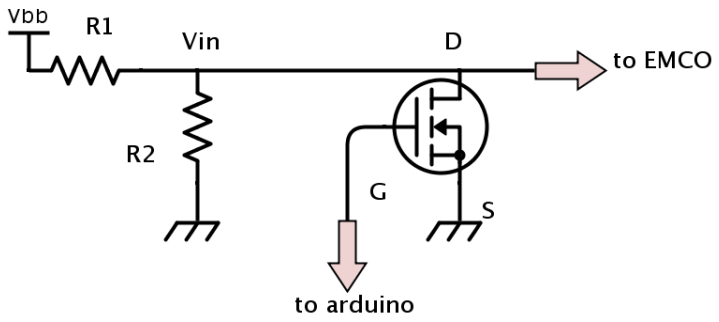

Figure 87. Circuit to power and control remotely the high voltage converter

Figure 87 shows the schematic of the circuit that controls the high voltage generation. V_{bb} is the battery voltage: $V_{bb} \cong 7.2\,V$ and V_{in} is the input voltage required to produce 2500 V through the EMCO high voltage converter. According to Table 5, $V_{in} = 1.089\,V$.

When the Arduino signal is ON, i.e. G-S = 5V: D-S is connected which means $V_{in} = 0\,V$, thus high voltage formation doesn't occur.

When the Arduino signal is OFF: $V_{in} = \frac{R2}{R1+R2} * V_{bb}. As\ V_{in} = 1.089V\ and\ V_{bb} = 7.2V \rightarrow \frac{R_2}{R_1+R_2} = 0.15125 \rightarrow R_1 = 5.61 * R_2$. We should also make sure that the power available in the circuit is enough to power the high voltage converter. . For the circuit designed above, $P = \frac{V_{bb}^2}{R} = \frac{V_{bb}^2}{R_1+R_2}$.

As $P \geq 0.5\ W\ and\ V_{bb} = 7.5V$, $R_1 + R_2 \leq \frac{7.2^2}{0.5} \rightarrow\ R_1 + R_2 \leq 103.68\Omega$.

Even though the theory gives the above results, in practice, the combination of all the resistances completing the conditions $R_1 + R_2 \leq 103.68\Omega\ and\ R_1 = 5.61 * R_2$ don't give the output voltage as 2500 V. Hence, we've had to try different combinations of resistances in a hit and trial method to find out the correct combination. The resistances that will give a 2500 V output are $\boldsymbol{R_1} = \mathbf{107}\ \Omega\ and\ \boldsymbol{R_2} = \mathbf{25}\ \Omega$.

Another thing we should take into account is that the voltage given by the battery is not a 7.2 V constant voltage. We've found out by testing it that most of the time the voltage given is higher than 7.2 V. A fully charged battery gives 8.02 V which decreases with its use. So, the output voltage from the high voltage converter is not always going to be constant. As stated earlier, the spray formation starts from 2360 V so even if the voltage given by the battery decreases, the spray will still be formed but the thrust given by the thrusters will show a small variation.

4.1.1.2 High Voltage Switch

In this section, we try to develop a circuit to change the voltage applied to the internal extractor remotely so that we could turn ON/OFF individual thrusters.

The ideal would be to switch the inner extractor between ground and the voltage at which the emitter works (2500 V) so that either there is no electric field or there is one necessary for the spray formation. As it was expensive to design such a switch, we are going to use a MOSFET which can switch up to 1000V. The internal extractor will be switched between 0V and a high voltage such that the voltage difference with the emitter won't be enough for spray formation. As

explained earlier, the minimum voltage for spray formation is 2360V, so the switching voltage should be higher than 2500-2360 = 140 Volts.

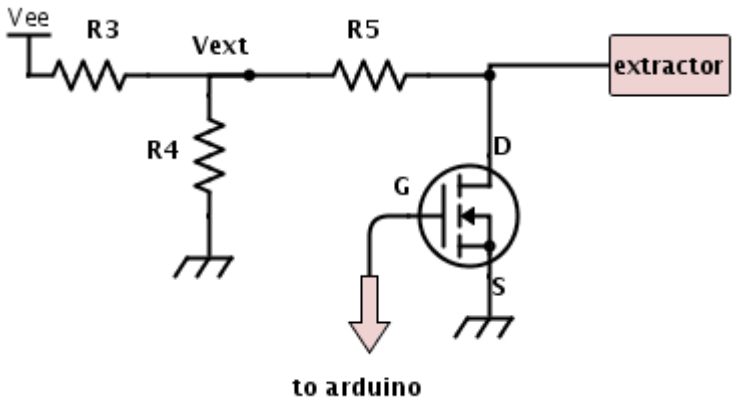

Figure 88. Schematic of the high-voltage switch

Figure 88 shows the schematic of the high-voltage switch that will be used to turn the electrospray ON/OFF remotely. V_{ee} is the emitter voltage: 2500 Volts.

When the Arduino signal is ON, i.e. G-S = 5V: The extractor is grounded and hence the voltage difference between the emitter and the extractor is good enough to form a spray. In this case, we want R5>>R4 such that there will be no current flow towards R5.

When the Arduino signal is OFF: The extractor is at V_{ext} which is given by $V_{ext} = \frac{R4}{R3+R4} * V_{ee}$. We will choose high resistances so that low current is passed in the circuit. After doing various combinations, the chosen values of the resistances are: $\boldsymbol{R_3 = 35\,M\Omega, R_4 = 20\,M\Omega}\ and\ \boldsymbol{R_5 = 100\,M\Omega}$. Hence, $V_{ext} = \frac{20}{20+35} * 2500 = 909.09\,V$.

4.1.2 Capillary Action

A passive propellant feeding is used in the thruster where the propellant travels from the tank to the emitter tip using Capillary action. In this section, we will find out the compatibility of this phenomenon in our experiment. The height a liquid can travel using capillary action is given by:

$$h = \frac{2\gamma cos\theta}{\rho g r}$$

where $h = height\ moved\ by\ the\ liquid$

$\gamma = surface\ tension\ of\ the\ liquid$

$\theta = angle\ of\ contact$

$\rho = density\ of\ the\ liquid$

$g = acceleration\ due\ to\ gravity$

$r = internal\ diameter\ of\ the\ emitter$

For our case, the propellant we will use is Emi-Im (1-ethyl-3-methylimidazolium bis (trifluoro-methylsulfonyl) imide / $C_8H_{15}F_6N_3O_4S_2[C_6H_{11}N_2]^+[N(SO_2CF_3)_2]^-$) as the propellant. For this liquid, $\gamma = 0.0349\frac{N}{m} and\ \rho = 1520\frac{kg}{m^3}$ [10]. The emitter we are using has an internal diameter of $r = 0.0035in = 8.89X10^{-05}\ m$. The angle of contact for the surface Emi-Im is $\theta = 27.2°$ [11]. With the value of acceleration due to gravity, $g = 9.81\ ms^{-2}$, the height we obtain is h = 4.68 cm. The satellite is a 10cm cube and the maximum vertical distance between the liquid surface and the emitter is not more than 2 cm. Hence, the capillary action is good to feed the propellant for our system.

4.1.3 Thruster configuration

A three-axis control is to be done for a complete attitude control of a satellite. As the satellite rotates around its center of gravity, a minimum of 6 thrusters (2 in each direction) is required. Some possible designs could be placing one thruster in each six corners of the cube, placing them in the middle of a side and not in the corner, placing more than one thruster in a corner in different axes, etc. Among various possibilities of distribution of thrusters, we have chosen to place three thrusters (one in each direction) in a corner of the cube and the other three in its diametrically opposite corner as shown in Figure 89. As we need to fit the microcontroller, electronics, etc. to run the sprays through wireless connection inside the cube, we have opted for this configuration as it will occupy less space.

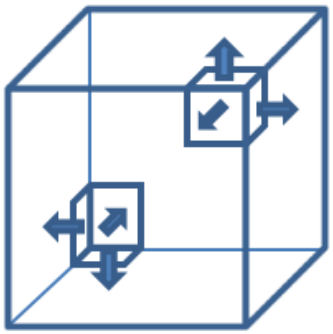

Figure 89. Positioning of thrusters in the cube (each arrow represents an electrospray thruster).

4.1.4 Measurement of Current in the Circuit

Measuring how much current is flowing in the circuit could be a way to find out if the thrusters are working or not. One of the many ways to do this could be by introducing a voltage follower somewhere in the circuit and relate the voltage seen with the current flowing in the circuit. Figure 90 shows a basic voltage follower circuit.

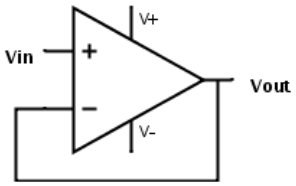

Figure 90. A voltage follower

For our case, the EMCO high voltage converter is supplying power to all the emitters/extractors. Hence, if we connect a resistor to a part of the circuit, the voltage drop in this resistor would be related to the current flowing in the circuit. We could also introduce a capacitor in parallel to the resistor which could help to decrease the oscillation in the current flowing in that circuit.

A LMC662CN op-amp could be used for our operations. As the voltage needed to run this MOSFET could be derived from our primary power supply: the battery, it is the best option for us.

The voltage is read by analog input in the Arduino. Arduino converts the voltage received (from 0 to 5 Volts) to numbers between 0 and 1023 in a linear scale. Given this, the minimum voltage that can be read through the Arduino is equal to $\frac{5}{1023} = 4.887\ mV$. Hence the voltage drop in the resistor should be higher than this one.

As it will be seen in the part of testing, the current generated when one electrospray thruster is functioning is ≈ 600 nA. Therefore, the resistance that should be used is $R_6 \geq \frac{4.887\ mV}{600\ nA} = 8145\ \Omega$. In simpler words, if 600 nA current passes through the circuit, the value seen in the LabView program that processes the data from Arduino will increase from its initial value by 1. We should use a resistance higher than this to be able to see if the thrusters are working. If we choose $R_6 = 200\ k\Omega$, for each 25 nA of current increase in the circuit, the value seen will be increased by 1. So for 600 nA, the value will be increased by 24. The advantage of choosing a higher resistance is that there will be no confusion in whether the increase in value is because of the thrusters or because of some electronic noise. So, we will choose $\boldsymbol{R_6 = 200\ k\Omega}$. Figure 91 shows a scheme of the current measuring circuit. The capacitor C1 is not obligatory to be introduced in the circuit. For our case, we have chosen it to be of capacitance $0.01\ \mu F$. R_6 is introduced between the HV return port of the high voltage converter and ground.

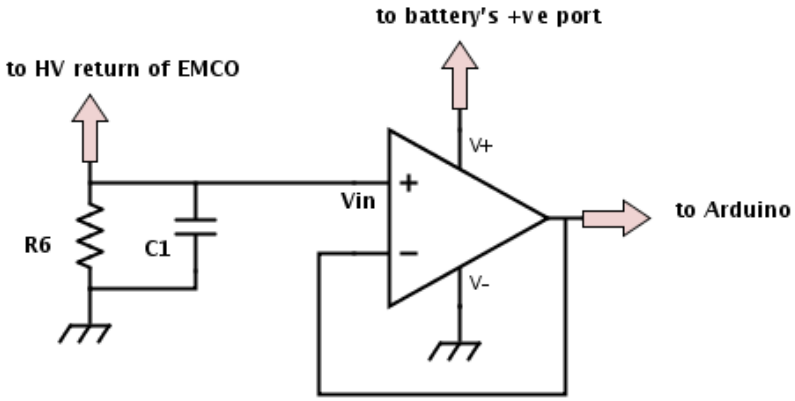

Figure 91.Schematic of the current measuring circuit

4.1.5 Wire

Once the satellite is built, it has to be hung using a wire and placed inside the vacuum chamber to test the thrusters. This wire has to support the weight of the satellite and be simultaneously able to turn enough to be visible by the naked eye due to the force given by the thrusters which is of order of few micronewtons.

By Hooke's law,

$$\sigma = E\epsilon \; with \; \sigma = \frac{F}{A} = \frac{mg}{A} \; and \; \epsilon = \frac{\Delta l}{l} \rightarrow \frac{mg}{A} = E\frac{\Delta l}{l} \qquad (9)$$

Where

$$E = Young's \; Modulus$$

$$A = cross \; sectional \; area \; of \; the \; wire$$

$$m = mass \; of \; the \; satellite$$

$$l = length \; of \; the \; wire$$

$$\Delta l = increase \; in \; length \; when \; the \; force \; is \; applied$$

From the above equation, to handle a certain weight with a thinner wire, the Young's modulus is expected to be as large as possible. According to [12], tungsten is the material with the highest young's modulus ~ 400 GPa, so we will use a tungsten wire to hang the satellite.

Again, according to [12], the angle turned per unit length by a cylindrical rod because of torsional forced applied is given by

$$\theta' = \frac{M_T}{GI_o} \qquad (10)$$

where

$$\theta' = angle\ turned\ per\ unit\ length$$

$$M_T = Torsor\ moment\ applied\ in\ the\ two\ ends\ of\ the\ wire$$

$$G = Modulus\ of\ rigidity\ of\ the\ material\ (Shear\ modulus)$$

$$I_o = \frac{\pi R^4}{2}\ with\ R = radius\ of\ the\ wire$$

Proceeding with the assumption that the wire acts as a cylindrical rod, we want the angle turned per unit length to be bigger so that it is easier to visualize the movement of the satellite. This implies that the radius of the wire has to be as small as possible.

After assembling the whole satellite, its mass was measured as $m = 0.73\ kg$. According to [12], $\frac{\Delta l}{l} \cong 1\%$ for Tungsten. Substituting these values in equation (9),

$$\frac{mg}{A} = E\frac{\Delta l}{l} \rightarrow A = \frac{mg}{E\frac{\Delta l}{l}} = \frac{0.73 * 9.81}{400 * 10^9 * 0.01} = 1.79E-09\ m^2 \rightarrow R = 2.39E-05m = 9.4E-04\ in$$

It means that the minimum radius of the wire that supports the weight of the satellite is $R = 9.4E-04\ in$. Even though theoretically any radius larger than this should support the satellite, in the practice other factors like 'how you attach the wire to the satellite', etc. have a direct relation to if

the weight can be supported or not. Hence, we will buy wires of various radii and test them to see if they handle the satellite's weight.

Along with this, we will calculate the angle turned by each of these wires to find out which of these will work for us. According to equation (10), $\theta' = \frac{M_T}{GI_o}$, so total angle turned $\theta = \frac{M_T}{GI_o} * l$. As explained in thruster configuration in 4.1.3, there will be 3 thrusters, each in two diametrically opposite corners of the cube. For testing, we will only use four of these six thrusters as a pair of thrusters will be in the direction of the hanging wire.

As shown in Figure 92, the torsional moment created in the wire due to the two thrusters in any direction is given by

$$M_T = T * l + T * (l + l') = T(2l + l')$$

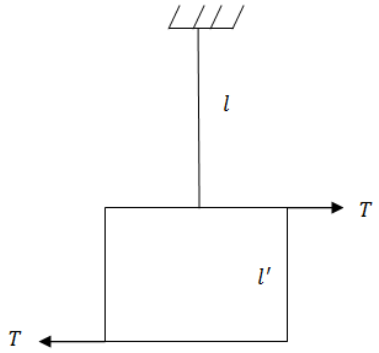

Figure 92. Calculation of Moment generated by thrusters in a direction

Hence, the total angle turned will be:

$$\theta = \frac{T(2l + l') * l}{G * \frac{\pi R^4}{2}}$$

For the experiment, length of wires used was $l = 22cm$ and the vertical distance between the two thrusters $l' = 7\ cm$. Also, Shear modulus for tungsten is$(G) = 161\ GPa$ [12]. As it will be presented later in 4.3.3.3, the Thrust obtained by an electrospray thruster working at similar conditions to the one in the satellite, $T = 1.4\ \mu N = 1.4E - 06\ N$. Table 6 presents the total angle turned by wires of various radii that could be used to hang the satellite.

Table 6. Angle turned by wires of various radii

Radius of the wire(in)	Radius of the wire(m)	Angle turned (rad)	Angle turned (degrees)
0.0005	1.27E-05	23.876	1367.99
0.001	2.54E-05	1.492	95.49
0.0015	**3.81E-05**	**0.295**	**16.90**
0.002	5.08E-05	0.093	5.32
0.0025	6.35E-05	0.038	2.18
0.005	1.27E-04	2.388E-03	0.14
0.01	2.54E-04	1.492E-04	8.54E-03
0.02	5.08E-04	9.32E-06	5.34E-04

When a force is applied in the hanging satellite, it starts to oscillate and after a long time it comes to rest at certain angle. It is very hard to differentiate this angle when it is less than 10 degrees. There were logistic problems while we were hanging the satellite using the first two wires (radius 0.0005in and radius 0.001 in) as a small turn applied to them easily broke them. So we've decided to conduct the experiment with the wire with radius 0.0015 in.

4.1.6 Electronic Circuit

Figure 93 presents the scheme of the whole electronic circuit designed for the project. As it can be seen, the circuit is designed only for four thrusters.

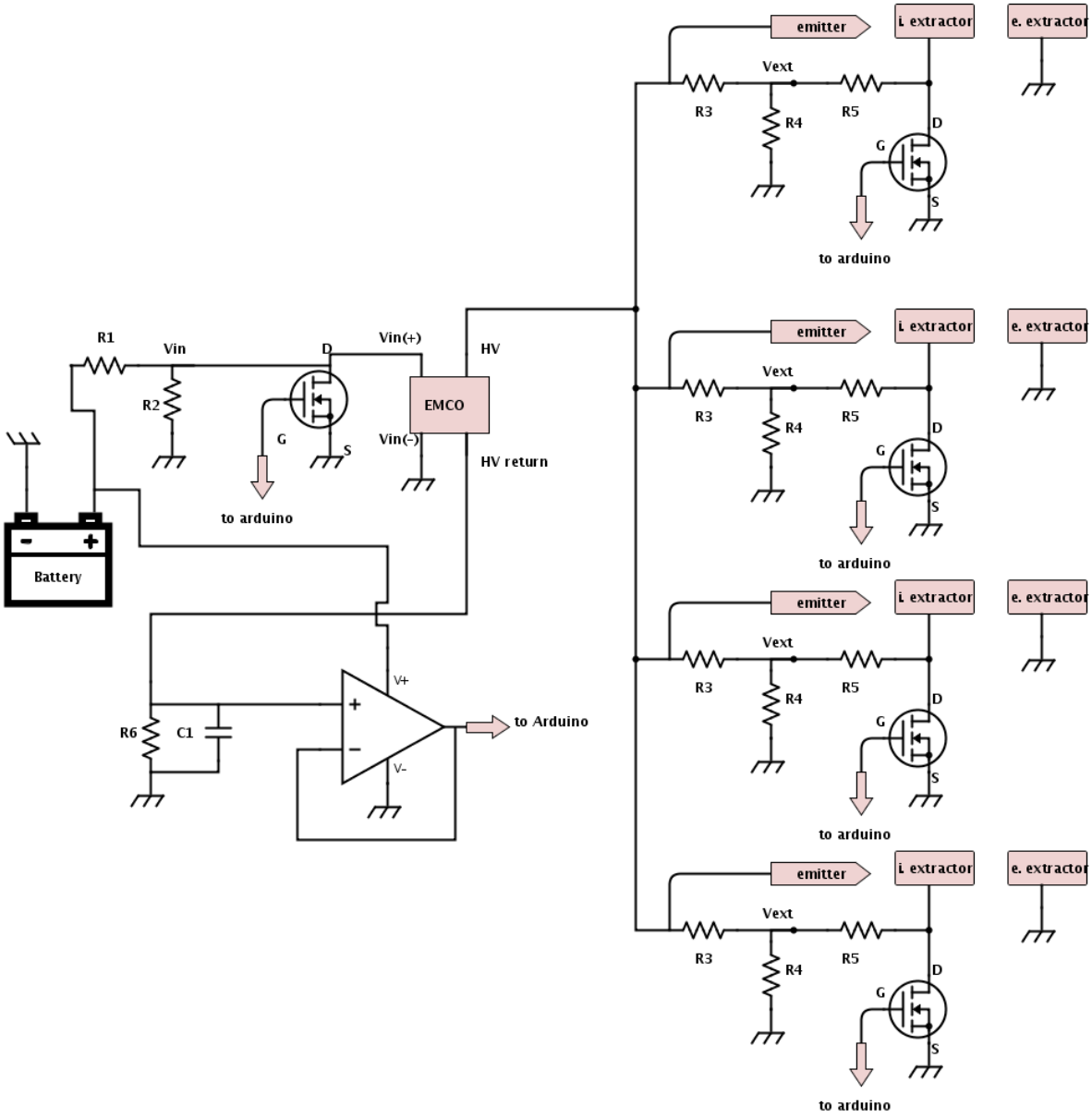

Figure 93. Scheme of the full electronic circuit designed for the ACS testing of the CubeSat

4.2 Design

4.2.1 Machines Used

All the parts of the satellite have been made from primary materials using different machines in the machine shop. A short description of the important ones is given hereafter:

- Lathe

A lathe is a machine tool which rotates the workpiece on its axis to perform various operations like cutting, sanding, drilling, facing, etc. This tool has been used with parts that are cylindrical and the objects to be created are symmetric with respect to the machine's axis of rotation. We've used the Sherline 4400 Lathe available at the Electric Propulsion Laboratory, UCI.

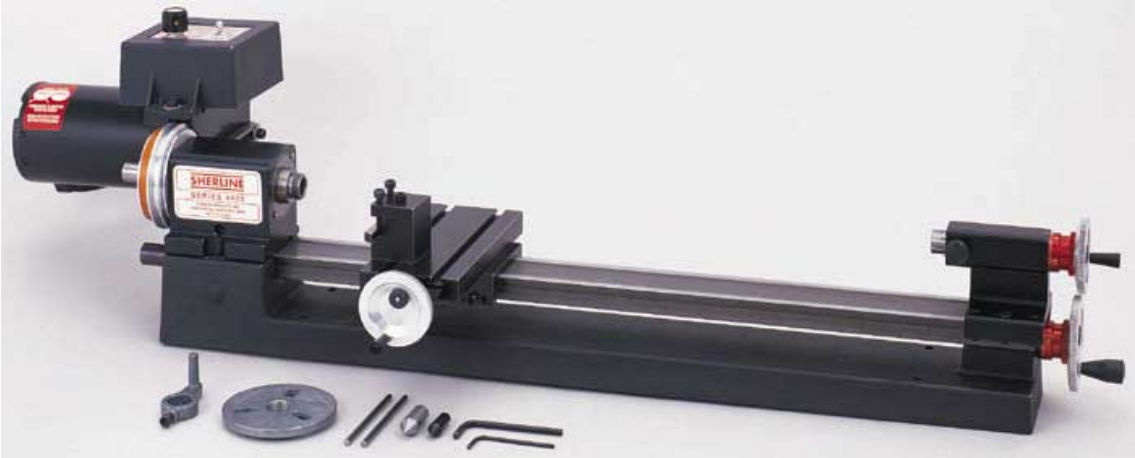

Figure 94. Lathe used for fabrication of certain parts of Satellite

- CNC Milling Machine

Unlike Lathe, in milling machine, the cutting devices rotate and the work-piece remains still. Thus, it is used to make holes in work-pieces that are not circular, remove material from certain parts of the work-piece which are not necessarily symmetric with respect to the axis of the device, etc. The milling machine we have used is a CNC (Computerized Numeric Control) Milling machine from the Machine Shop at Engineering Gateway, UCI.

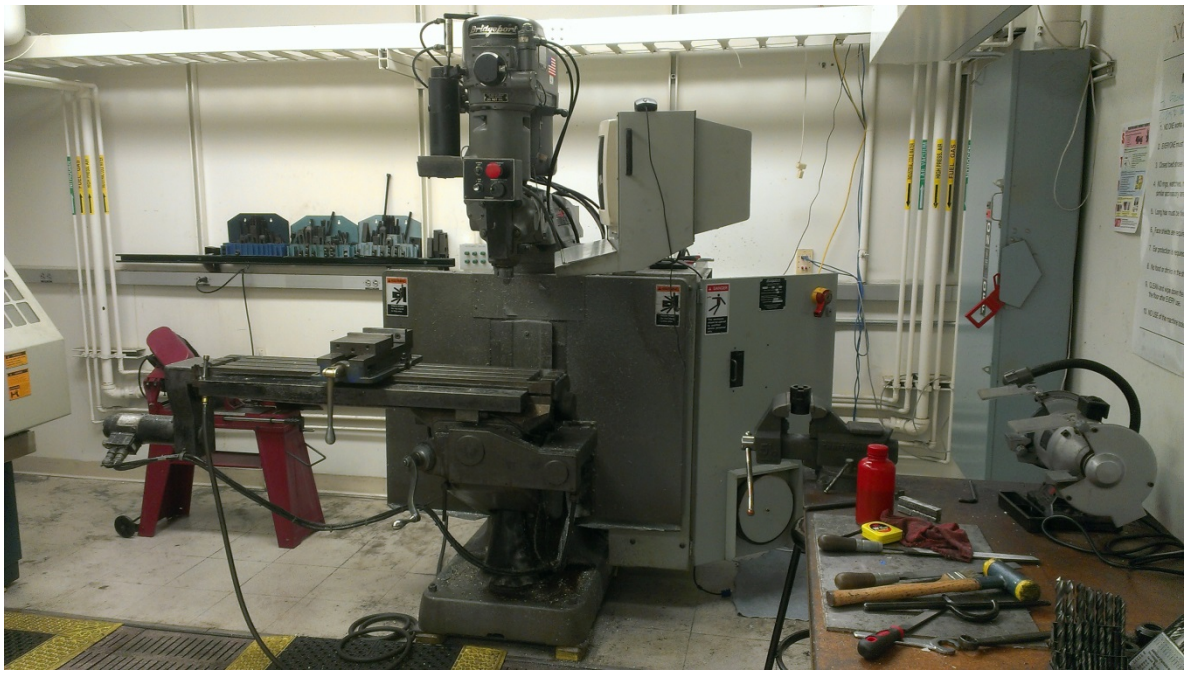

Figure 95. CNC Milling machine used for fabrication of certain parts of Satellite

4.2.2 Satellite Parts

Different parts of the Satellite designed for its Attitude Control are explained individually along with their process of fabrication, Solidworks images and real images.

4.2.2.1 External Cube

The cube gives the external structure to the satellite and also a base to assemble all the internal components. It is made up of 6 aluminum panels attached to each other by corner braces. 4-40 threaded screws and bolts are used to attach the panels and the corner braces. For the top panel, two metallic cubes are used to attach it to other panels instead. Properties of each component that build up the satellite are given in Table 7. The panels are of different sizes because the external dimensions of the satellite can't exceed 3.937 in /10 cm. The small corner braces are used in the sides where the thruster cubes are being placed. Figure 96 - Figure 99 give different images of the Cube.

Table 7. Properties of the components that build up the satellite's external cube

Components	Material	Number	Size (in inches)	Machines Used
Panel	Aluminum	2	3.937x3.937x0.063	CNC
Panel	Aluminum	2	3.937x3.812x0.063	CNC
Panel	Aluminum	2	3.812x3.812x0.063	CNC
Corner Braces	Stainless Steel	2	3.812x0.5x0.5	CNC
Corner Braces	Stainless Steel	6	2x0.5x0.5	CNC
Metallic Cube	Aluminum	2	0.394x0.394x0.394	CNC
Cap Screw 4-40 thread	Stainless Steel	24	Ø0.183x0.5	-
Hexagonal bolt 4-40 thread	Stainless Steel	24	Ø0.188x0.063	-

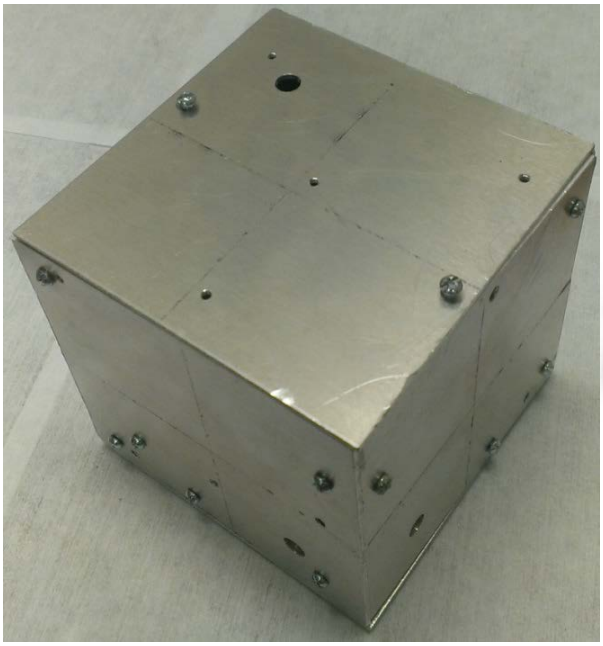

Figure 97. Real image of the cube

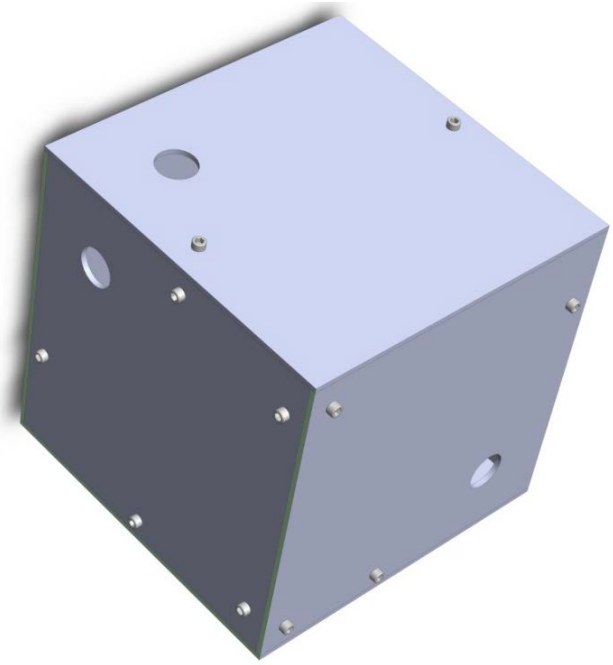

Figure 96. 3-D Model of Cube made in Solidworks

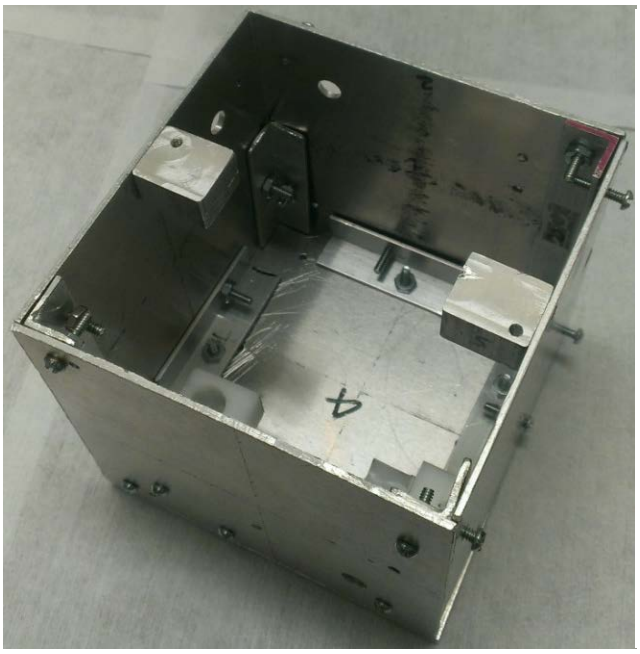

Figure 99. Internal view of Cube

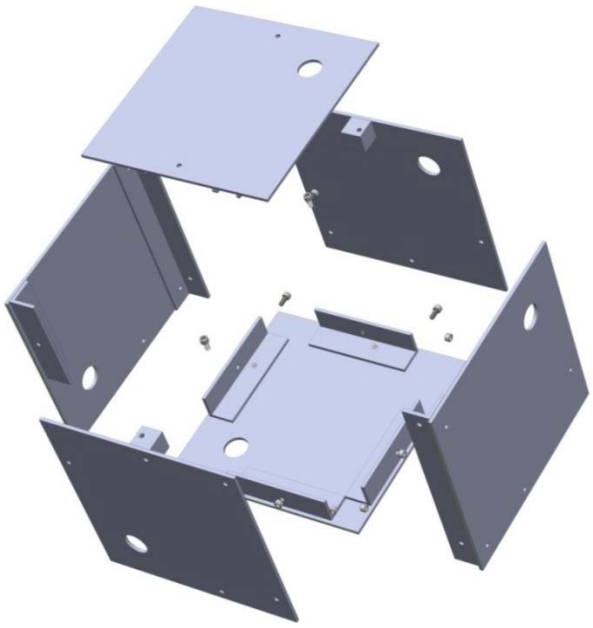

Figure 98. Exploded view of the cube showing the corner brackets and metallic cubes

4.2.2.2 Thruster Cube

As explained earlier, we have chosen to place three thrusters in any two diametrically opposite corners of the cube. To place these three thrusters in an efficient way, we will create a small cube which will hold these three thrusters. Each thruster in made up of an emitter, an internal extractor, an external extractor and the base where all of these are mounted. These three components after fabrication are presented in Figure 100-Figure 102.

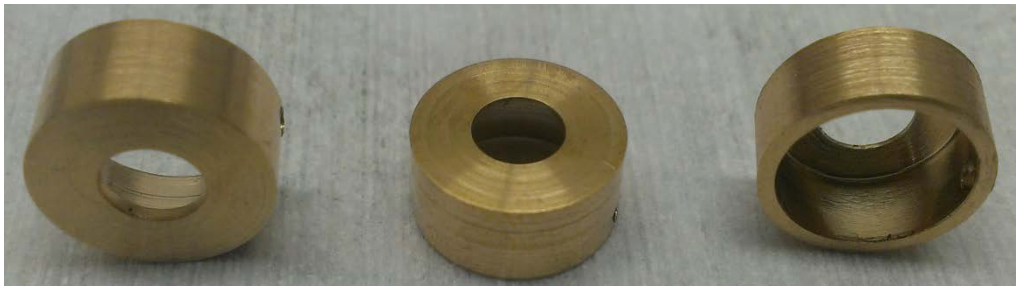

Figure 100. Different views of external extractor

Figure 101. Different views of a thruster's base

Figure 102. Different views of internal extractor

Putting these three components (extractors and the base), we obtain a thruster head as shown in Figure 104. An exploded model of different components of a thruster is shown in Figure 103. Three of these thruster heads are fitted into a cube: the thruster cube, whose 3-D models and images are presented in Figure 105 - Figure 106 and the properties of each component that build up the thruster cube is given in Table 8. Figure 148 gives the detailed drawing of these parts and distance between its elements.

Figure 103. A thruster head

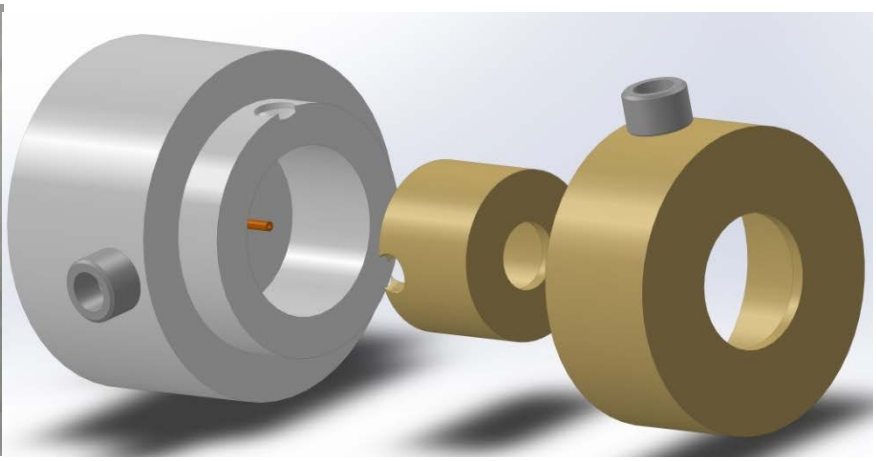

Figure 104. Exploded view of different parts of a thruster.

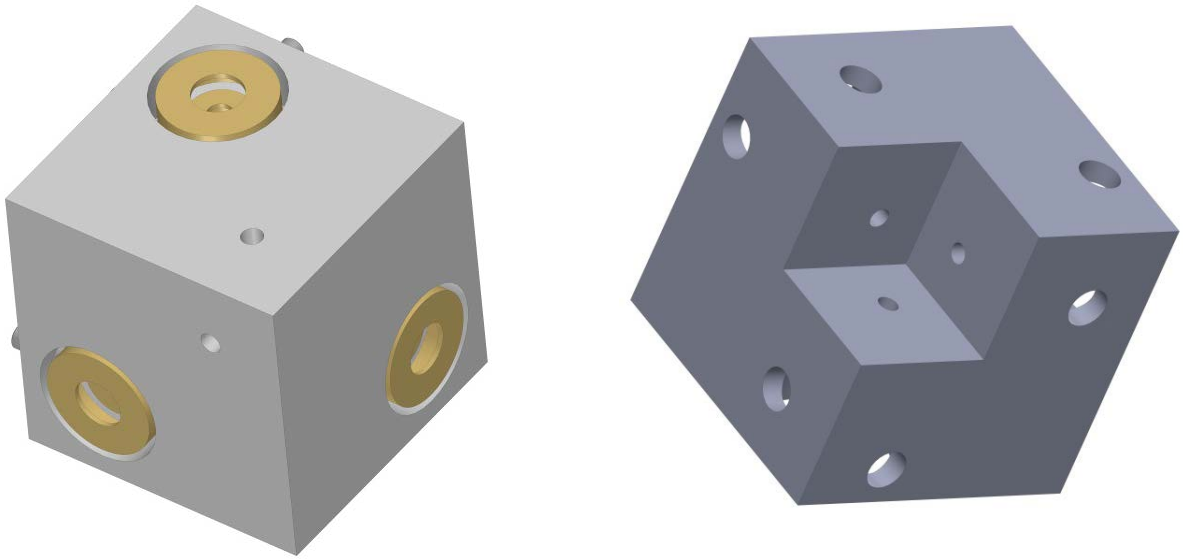

Figure 105. 3-D model of the thruster cube's base

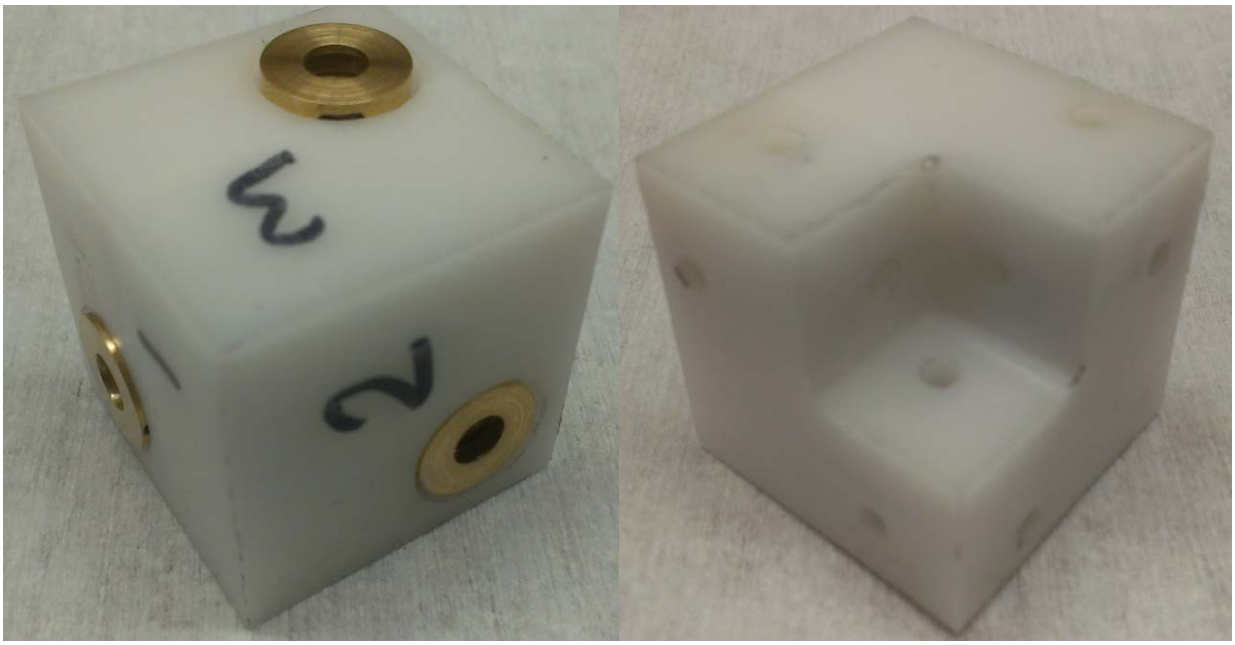

Figure 106. Real image of the thruster cube

Table 8. Properties of the components that build up the thruster cube

Components	Material	Number	Size (in inches)	Machines Used
Internal Extractor	Brass	3	Ø0.25x0.18	Lathe
External Extractor	Brass	3	Ø0.45x0.2	Lathe
Base	Teflon	3	Ø0.51x0.36	Lathe
Cube	Teflon	1	1.18x1.18x1.18	CNC
Cap Screw 0-80 thread	Stainless Steel	6	Ø0.096x0.5	-
Emitter	Stainless Steel	3	Ø0.014x2	Lathe

4.2.2.3 Wire Controller

The distance between the emitter-tip and the internal extractor has to be controlled to ensure a proper electrospray formation. Once we place the emitter in the proper position, we fix the position using screws as shown in Figure 107. We see only two emitters in the real image because only four thrusters are used in testing. The properties of the different components that make up the wire controller are given in Table 9.

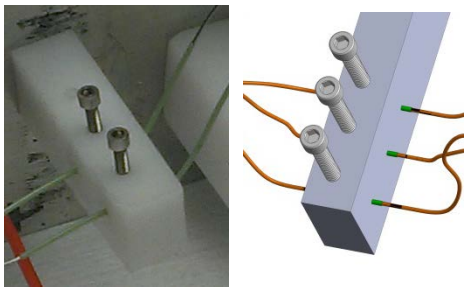

Figure 107. 3-D model and real image of the wire controller

Table 9. Properties of the components that build up the wire controller

Components	Material	Number	Size (in inches)	Machines Used
Controller Base	Teflon	1	1.18x0.39x0.2	CNC
Cap Screw 0-80 thread	Stainless Steel	3	Ø0.096x0.5	-

4.2.2.4 Propellant Feeding System

The propellant tank is attached to the Satellite Cube through a tank holder. Because the satellite will be hanging through the wire, we must make sure that the tank remains vertical to avoid spilling any propellant. Figure 108 presents images of the system and Table 10 gives the properties of different components of the feeding system.

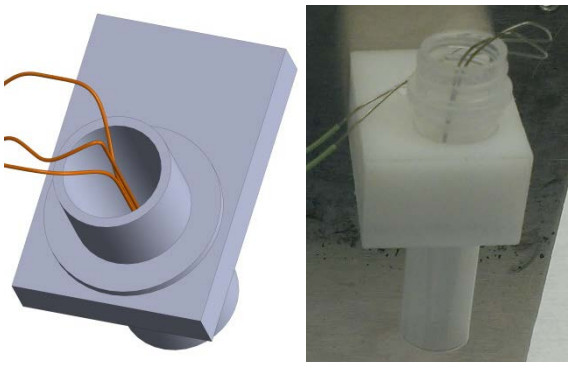

Figure 108. 3-D model and real image of the propellant feeding system

Table 10. Properties of the components that build up the propellant feeding system

Components	Material	Number	Size (in inches)	Machines Used
Propellant tank	Plastic	1	Ø0.71x1.18	-
Tank holder	Teflon	1	1.18x0.79x0.2	CNC
Cap Screw 4-40 thread	Stainless Steel	1	Ø0.183x0.5	-

Figure 109 and Figure 110 show an image and a 3-D model of an electrospray thruster system with three thrusters.

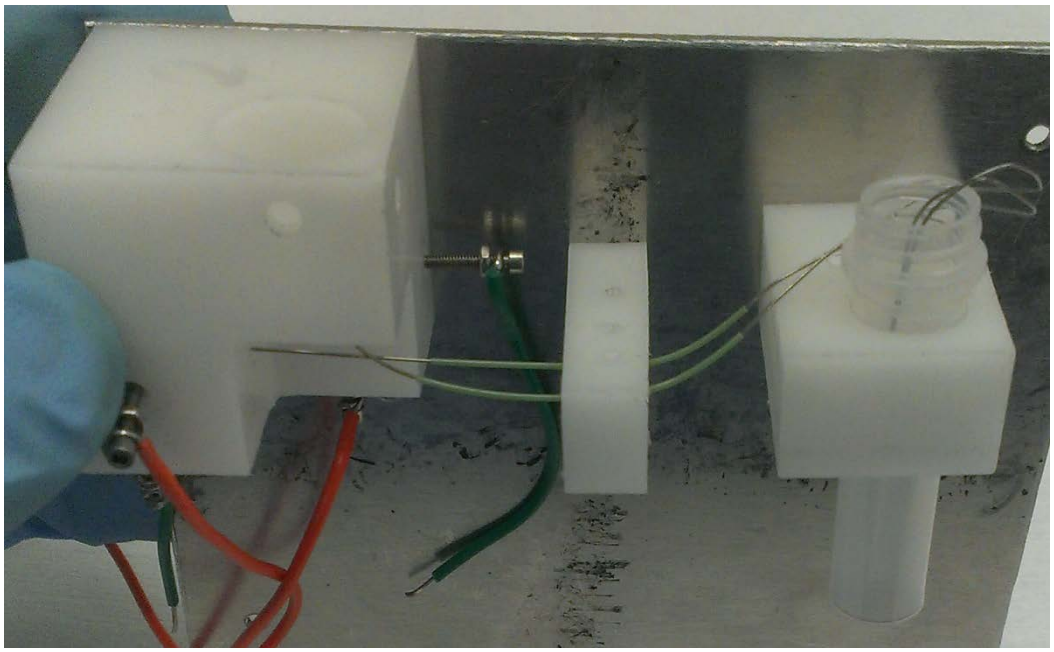

Figure 109. Image of an electrospray thruster system (thruster cube, propellant feeding system and wire controller)

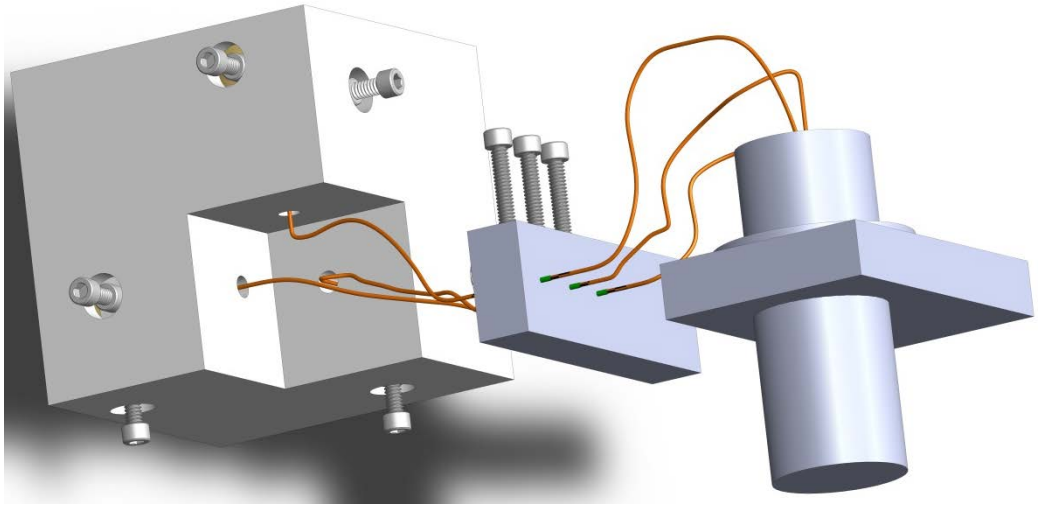

Figure 110. 3-D model of an electrospray thruster system in Solidworks

4.2.3 Electronic Circuit

The circuit in Figure 93 was designed using a breadboard and all the necessary electronic components. Images of the board built are presented in Figure 111 - Figure 112. As is apparent in the image below, the EMCO high voltage converter and the accelerometer are attached to the board for simplicity.

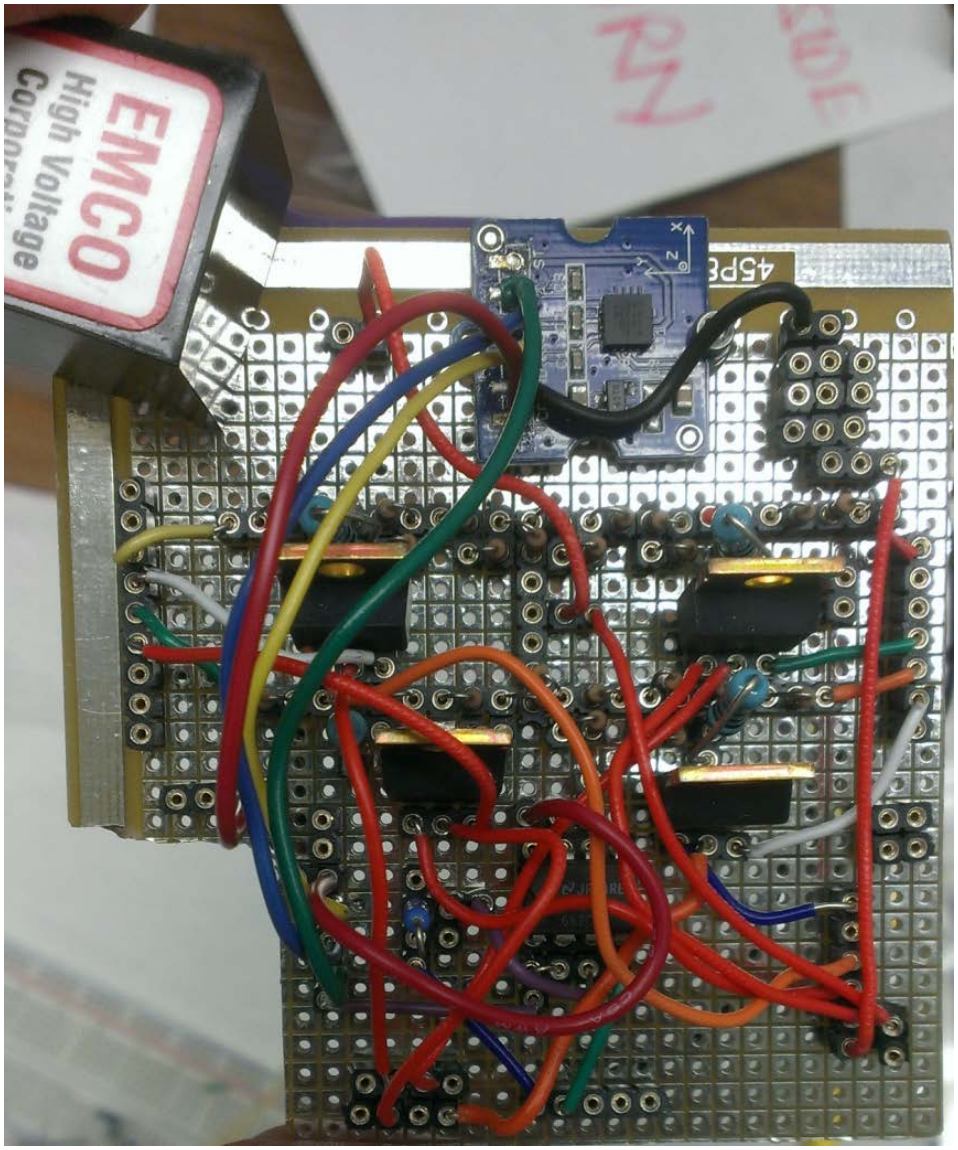

Figure 111. Front-view of the complete electronic board

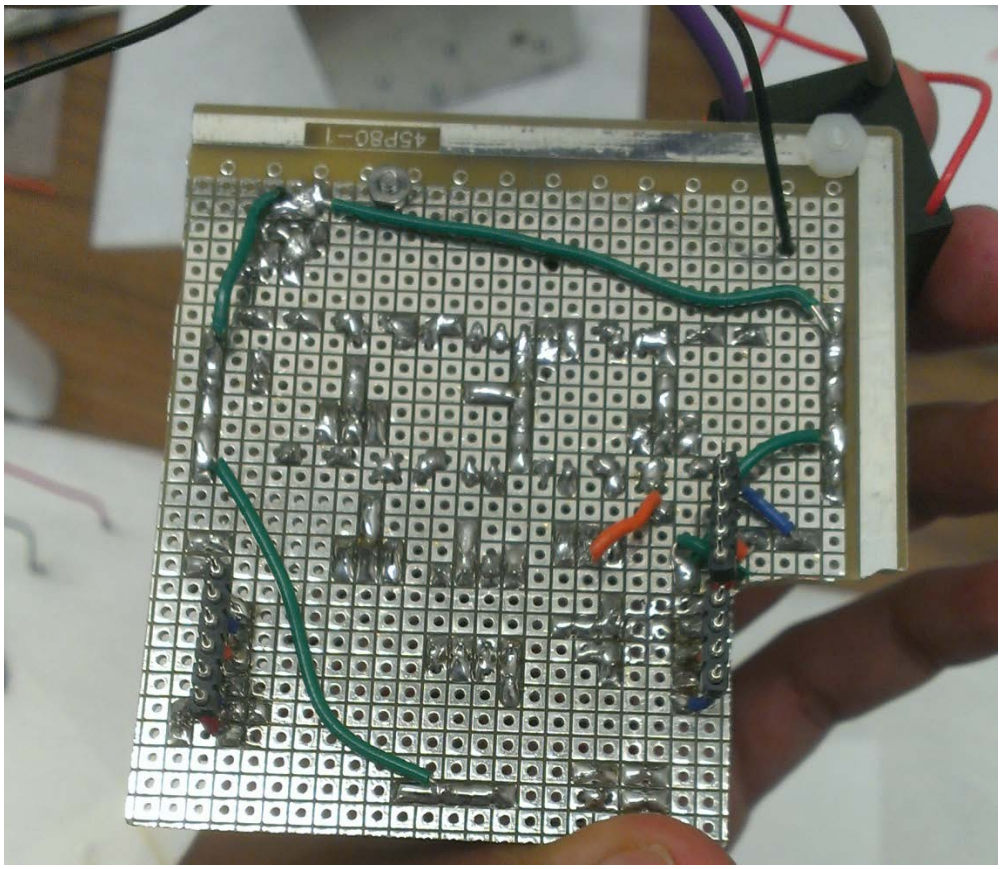

Figure 112. Rear-view of the complete electronic board

4.2.4 Wireless Communication

The satellite is remotely controlled and operated by an Arduino controller used concurrently with a program designed in LabView. Arduino Uno was selected as the microcontroller and Arduino WiFi Shield was used for wireless communication. The specifications of the Arduino and the WiFi Shield are found in the website of Arduino.

The basic wireless communication was designed by an undergraduate researcher at The Electric Propulsion Laboratory at the University of California-Irvine. For this section, his design has been changed in accordance to the necessities of the satellite's control.

- Arduino

The Arduino has various output and input pins which transfer analog and digital data. We will use four analog input pins to receive information from both the accelerometer and the voltage follower, which gives the total current in the circuit. A digital output pin will be used to turn ON/OFF the high voltage producing circuit. As explained in 4.1.1.1, this pin has to be ON to turn OFF the high voltage production and vice versa. So, as can be seen in the Arduino code in Annex 7.1, this pin will be left on HIGH even when the power supply will be off to ensure that no unexpected high voltage formation occurs. Four other digital output pins will be used to switch ON/OFF the four thrusters.

- LabView Code

For WiFi communication, UDP protocol is used because of its simplicity and faster speed of transmission in comparison to TCP protocol even though there is less guarantee of data delivery at all times. The front panel and the block diagram are shown in Figure 113 - Figure 114. The ports used for the communication, the local port used by the LabView to start connection with the Arduino, and the Arduino IP Address is presented in the left top left of the block diagram. The UDP Loop performs a UDP Write and UDP Read function in a series which is repeated according to the time given in the clock. The states of the pins are linked together into a string by the 'Format into String' function whose output is simplified and presented on the corresponding graphs/ output window. The data is saved in a format convertible to .txt form which would later be read and analyzed.

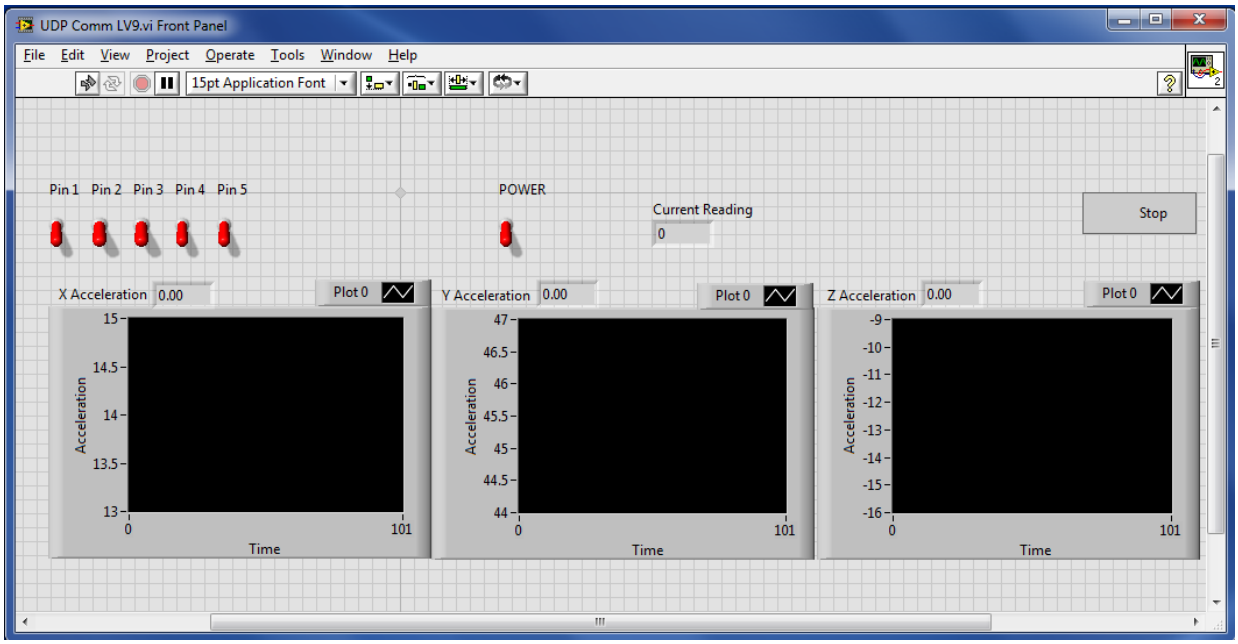

Figure 113. Front panel of the program in LabView used in wireless control of satellite

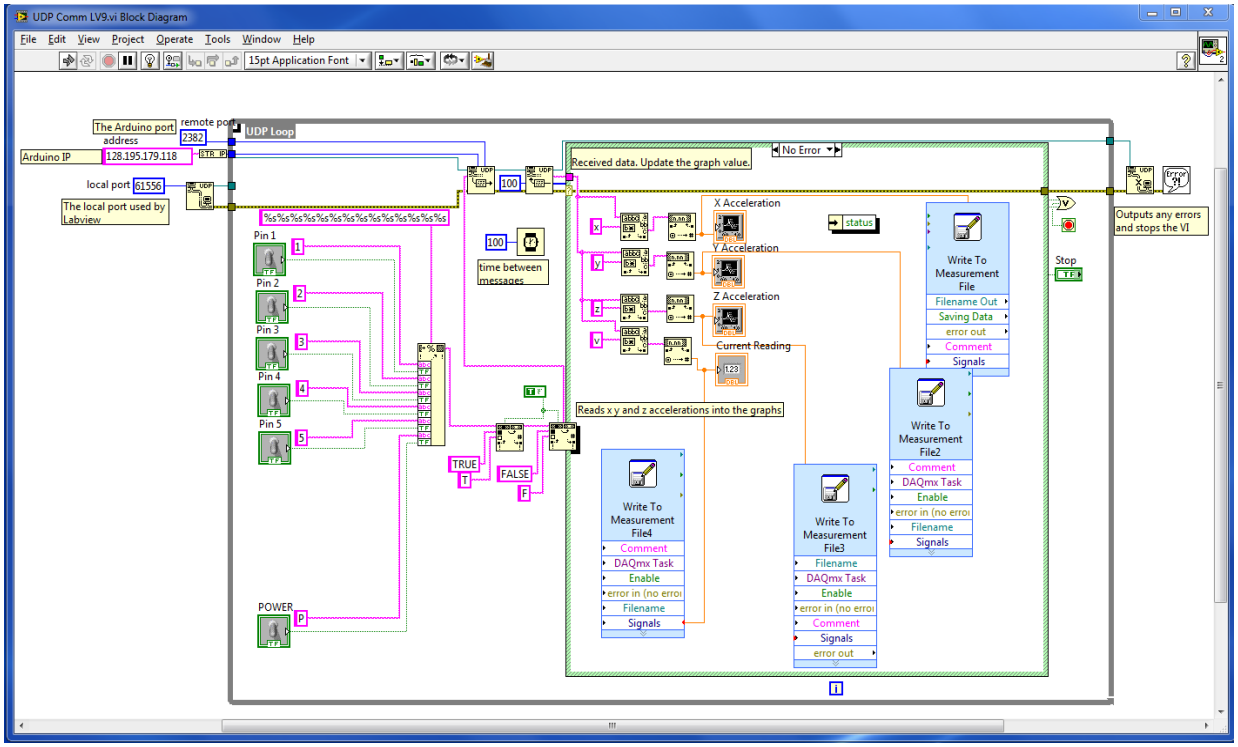

Figure 114. Block diagram of the program in LabView used in wireless control of satellite

4.2.5 Assembly

The satellite's thruster systems, the wireless transmission system, and the electronic board have been designed separately and have to be assembled inside the Cube along with the battery which gives power to the system. Several unforeseen problems occur while putting everything together and sometimes the design has to be changed to ensure the compatibility of a system with another. In this section, all the steps done to assemble the satellite are explained.

4.2.5.1 Arduino-Electronic Board

Pins from different points in the electronic board have to be connected to the Arduino microcontroller to send and receive information from the user through the LabView program. All these points are taken to a certain area of the board, and wires from these points are welded to SIP socket strips so that they can make a perfect fit into the Arduino. Figure 115 shows how the Arduino and the electronic board are assembled.

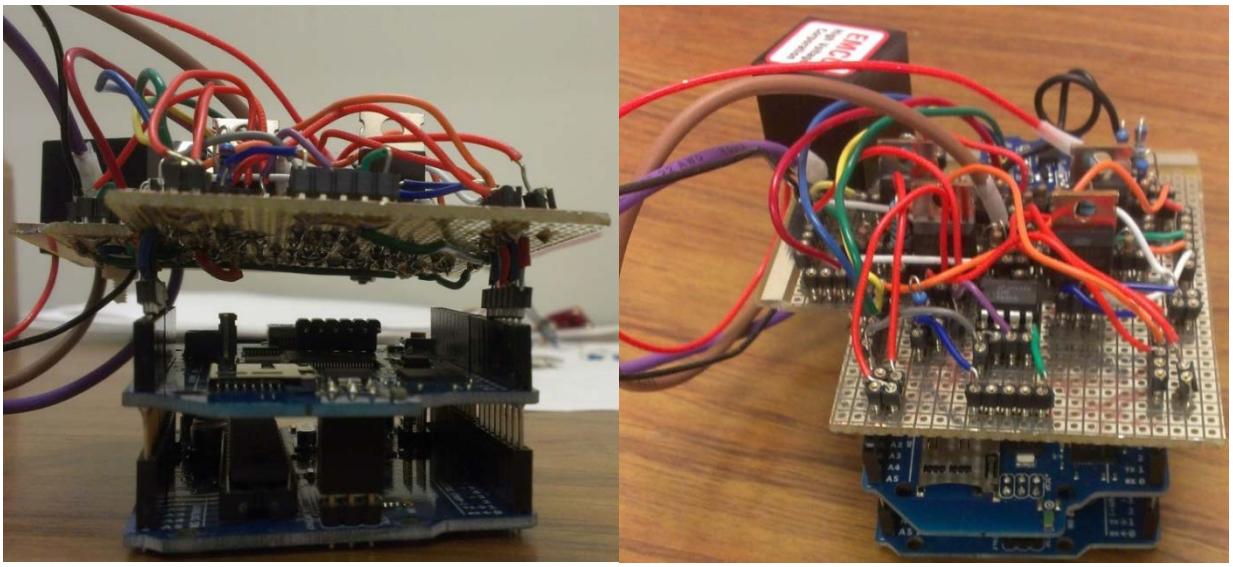

Figure 115. Arduino-Electronic board assembly

4.2.5.2 Thruster Systems

First, the components of a thruster system have to be attached to the corresponding panels and later the aluminum panels and the corner brackets have to be joined using screws to assemble the cube with the two thruster systems. Before starting the assembly procedure, all the components must be washed in acetone. Figure 116 - Figure 120 show steps to assemble the two thruster systems.

Figure 116. Components of the thruster systems before assembling them

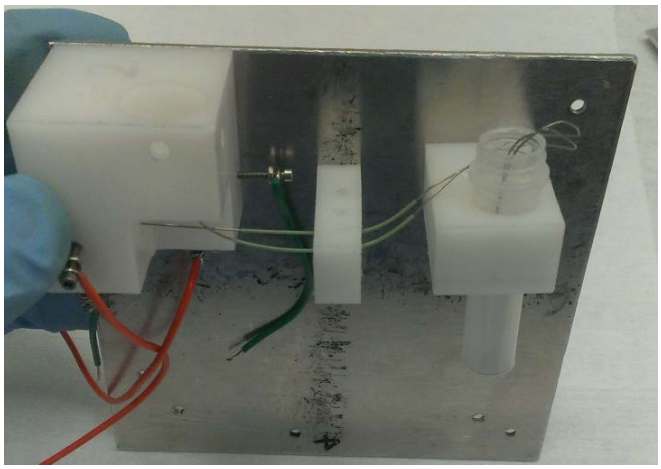

Figure 117. Thruster System I

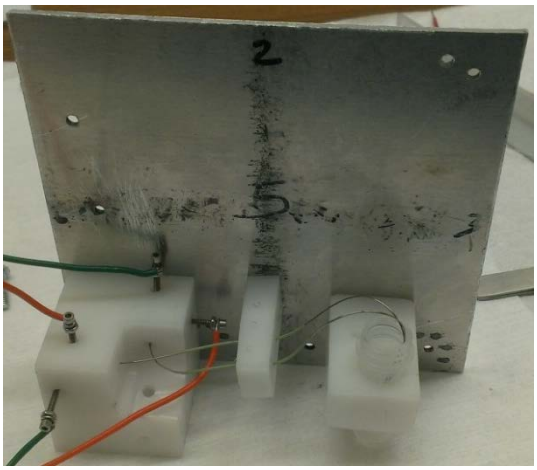

Figure 118. Thruster System II

Figure 119. Assembling the external cube

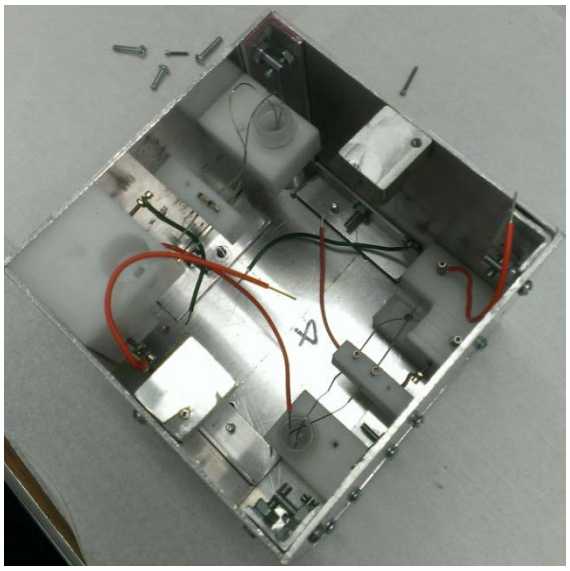

Figure 120. Two thruster systems assembled in the external cube

4.2.5.3 Thruster Systems - Electronics

The whole system of electronic components (Arduino+ WiFi shield, Electronic board, Battery) has to be inserted inside the Cube with the thruster system. Several placement issues had to be dealt with to obtain a perfect fit in the cube. One of the most important issues required that the high voltage areas of the satellite were sufficiently isolated from the ground and the microcontroller. Figure 121 - Figure 122 show different images of the satellite during this assembly.

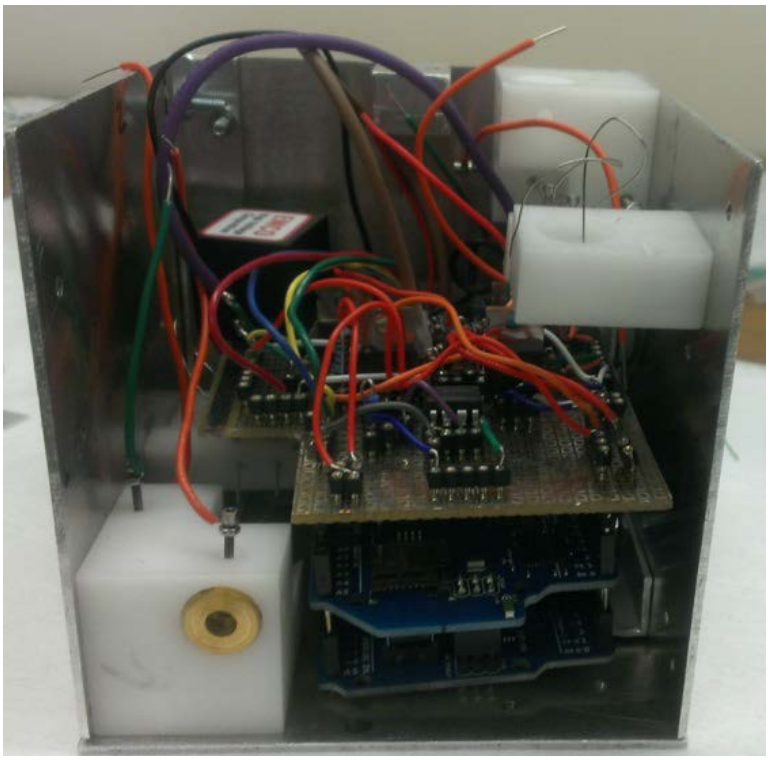

Figure 121. Arduino and the WiFi Shield assembled inside the cube with the two thruster systems

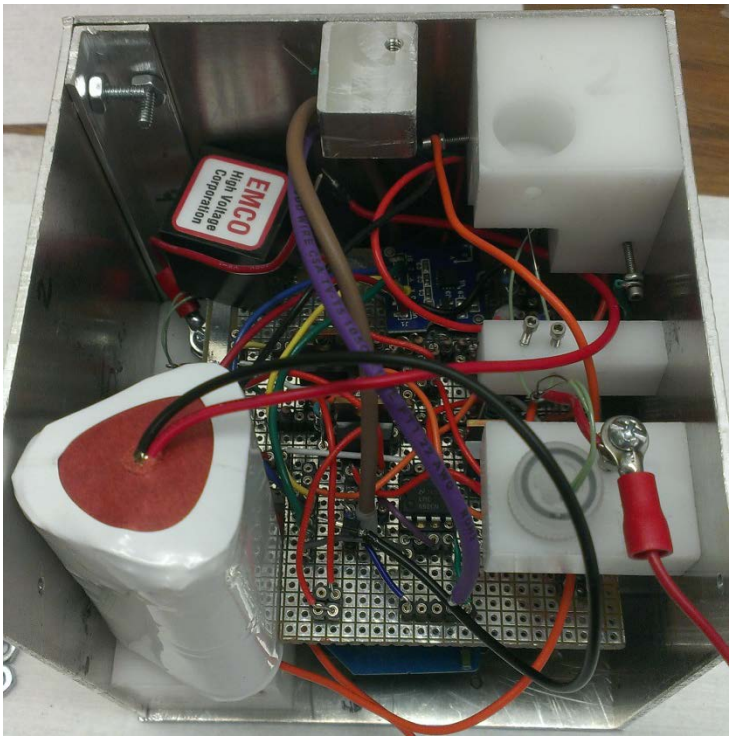

Figure 122. All components of the satellite assembled together

4.3 Tests

4.3.1 Battery-Vacuum Compatibility

Because the satellite has to be tested in a vacuum, it is necessary to ensure the battery functions properly and can therefore be used as a primary power supply in a vacuum. When the battery is working, some gases are produced inside the battery as a result of the chemical reactions occurring. During the experiment, the satellite is in a vacuum but these gases are produced in atmospheric pressure, so, if the battery's walls cannot handle this pressure difference, an explosion can occur. To see if this actually happens in our case, we will perform the battery-vacuum compatibility test.

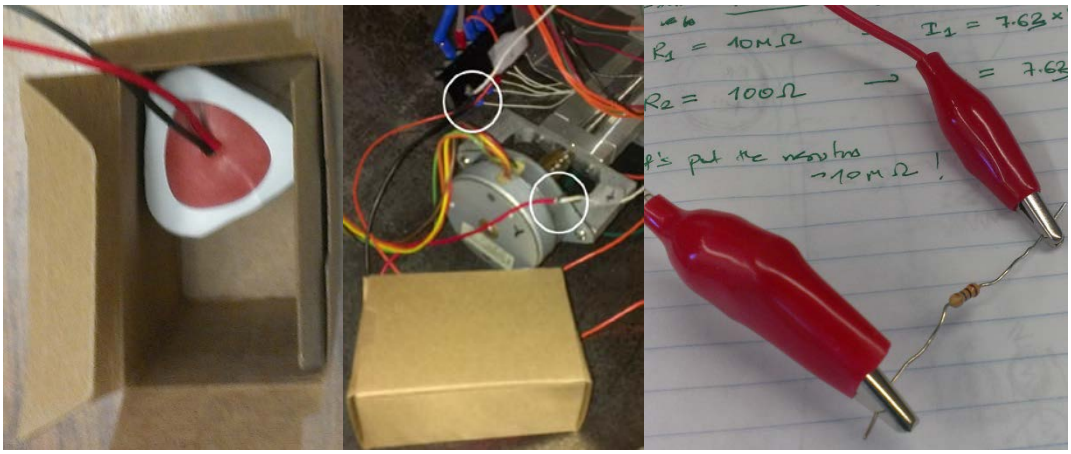

Figure 123. Images taken while testing battery-vacuum compatibility

First, we must put a battery inside a box, insert it inside the vacuum chamber and connect the anode and the cathode to wires that reach the outside of the vacuum chamber. Figure 123 shows various images of the connections made. Secondly, the chamber will be put into a complete vacuum and the voltage difference in the battery and current flowing in the circuit will be measured repeatedly. Finally, various resistances with different values will be introduced between the wires connecting to the anode and the cathode, which induces a current flow in the circuit, which means there is chemical reaction going on inside the battery. Change in voltage of the battery and current

in the circuit will be measured at different times for a couple of hours. After which we can conclude if the battery is compatible in a vacuum or not.

The voltage difference between the two terminals of the battery is measured while the chamber is being taken to vacuum. The testing was done on the 29th September 2014 in the afternoon and the external temperature of the lab was 22°C. Table 11 shows the voltage difference measured for various pressures and Table 12 shows the voltage difference and current measured for various resistances introduced in between the two terminals of the battery. The pressure given is relative to the atmospheric pressure at the Electric Propulsion Laboratory during that time.

Table 11. Voltage difference between the two terminals of the battery at different Pressures

Relative Pressure (atm)	Voltage Difference(V)
0	7.62
-100	7.62
-300	7.62
-500	7.62
-742.8	7.62

Table 12. Voltage difference and current in the circuit for different resistors introduced between the terminals

Resistance	Voltage difference measured	Current in the circuit (Amperes)
100 Ω	7.62	7.62E-02
10 kΩ	7.62	7.62E-04
1 MΩ	7.62	7.62E-06
10 MΩ	7.62	7.62E-07

The battery was left inside the vacuum for almost two hours and it was working correctly given the same voltage difference. Also, no abnormalities in its surfaces was seen when it was removed from the vacuum. Hence, we reached the conclusion that the NiCd battery that will be used for the ACS control test of the Satellite using Electrospray thruster is vacuum compatible.

4.3.2 Wireless Signal Transfer

Because the Arduino will be inside the cube, which is made of aluminum, and the satellite will be inside a metallic vacuum chamber, there might be a chance that the wireless signals from the router won't reach the satellite. To find out if this was a problem, we connected a LED which could be turned ON/OFF by sending wireless signals from the LabView program. It was apparent that the signals were travelling properly through the vacuum chamber and satellite's external wall. The setup is shown in Figure 124.

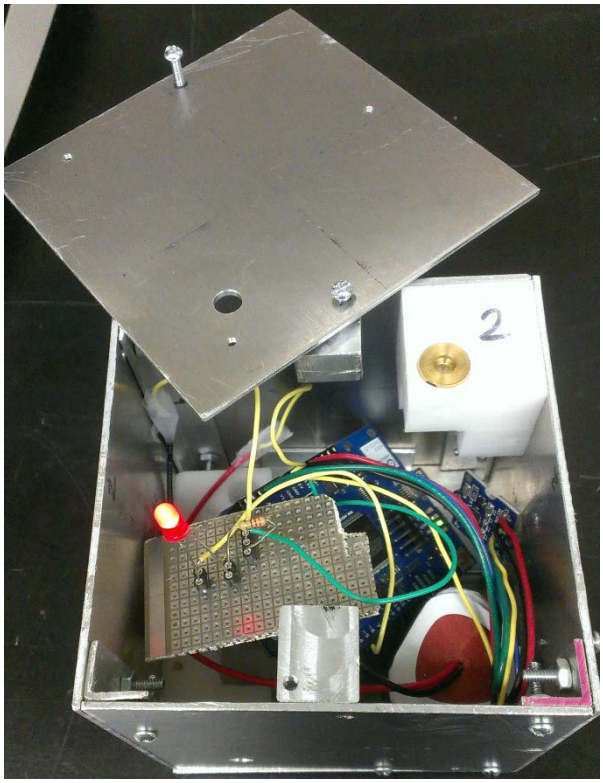

Figure 124. Setup to verify wireless signal transfer.

4.3.3 Passive Feeding

This experiment is to ensure if the thruster design is able to form a stable electrospray through a passive propellant feeding. We will also find out the range of the voltage difference where this spray will be formed. This information will be used in designing the final electronic circuit.

4.3.3.1 Experimental Setup

Figure 125 shows the experimental setup built for the passive propellant feeding test. The design tested is the one presented in Figure 104 which will also be used in the satellite. The emitter used is a silica emitter of internal diameter 200 μm. Emi-Im (1-ethyl-3-methyl imidazolium) was the

propellant chosen. The two extractors are screwed in and wires are connected in them which are taken out of the vacuum chamber to make appropriate connections.

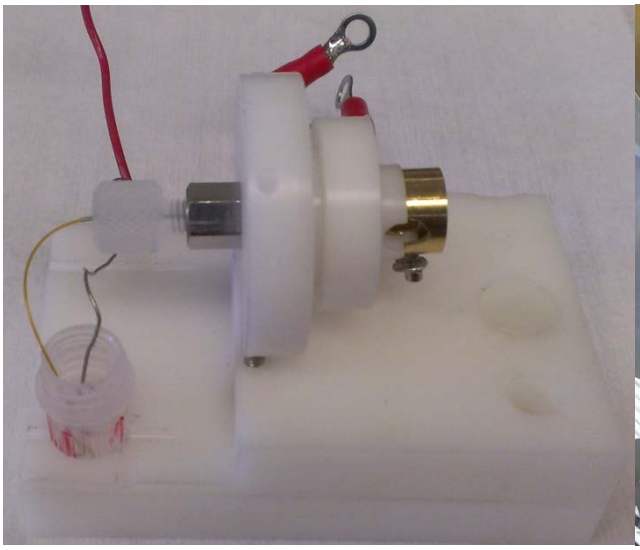

Figure 126. Setup to test passive propellant feeding

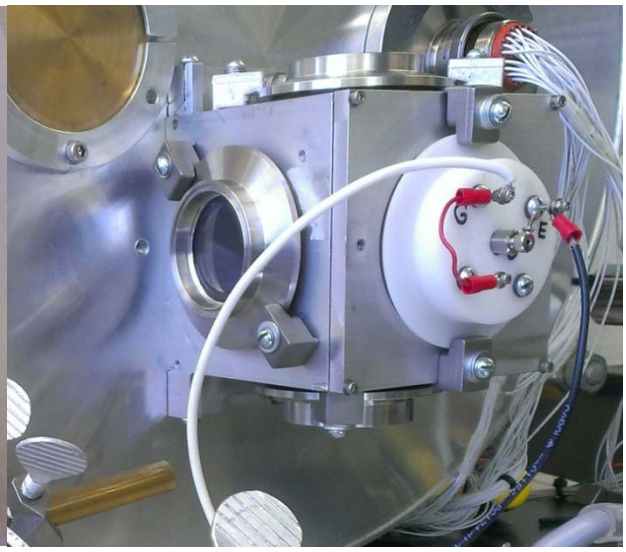

Figure 125. Electrical connections for the setup

The fluid is electrified by means of a wire which is also taken out of the chamber in a similar manner. As the fluid is electrically conducting, the emitter is going to be in the same potential as the fluid. As it can be seen in Figure 126, two terminals are connected to each other and they are connected to ground whereas the third one which is the emitter is connected to high voltage. According to Table 4, this combination will turn the electrospray ON. A hole was made in the whole setup such that the emitter tip could be seen. The images are magnified using a microscopic camera. Also, the chamber where the setup is installed (the small cube seen in Figure 126) is illuminated using a light. In Figure 127, the vacuum chamber with all these accessories can be seen. For high voltage generation, the high voltage source designed by Prof. Manuel Gamero is used. There are two multimeters attached in this circuit that measure the voltage applied to the emitter and the current flowing in the circuit. The images from the microscope can be seen in the computer.

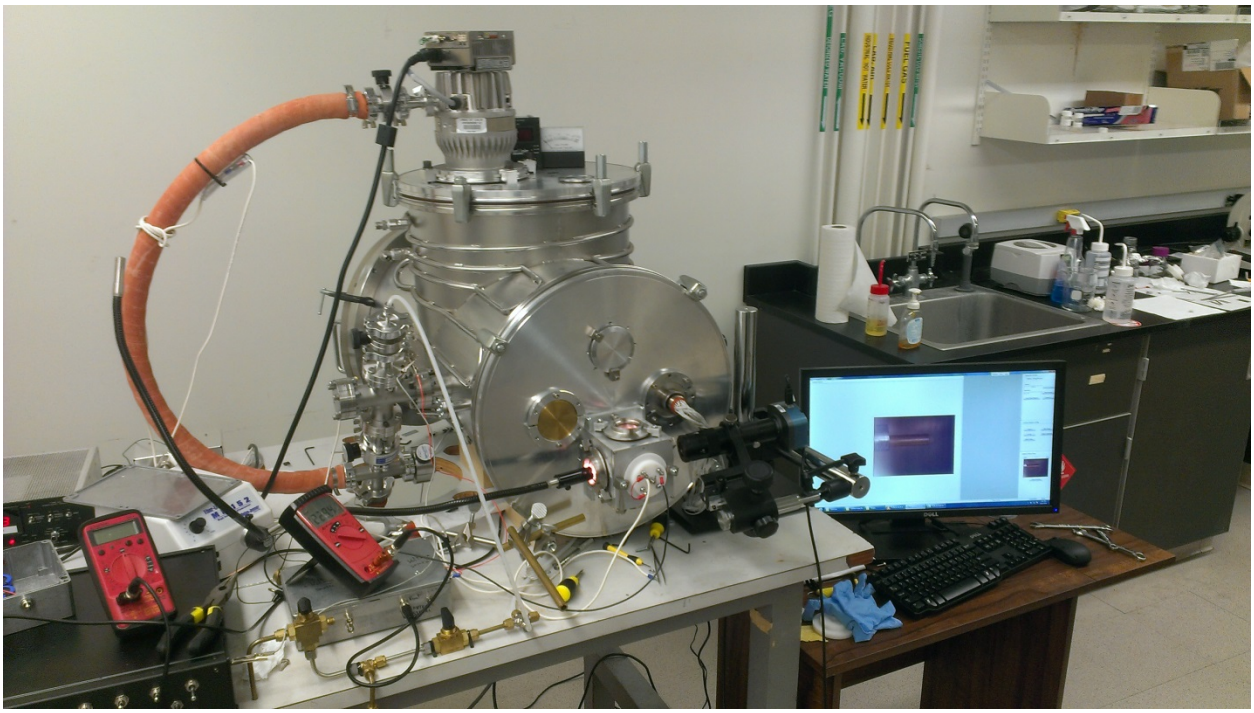

Figure 127. Vacuum chamber and other accessories used to run and visualize the passive feeding experiment.

4.3.3.2 Failed Attempts

Once the setup is in a complete vacuum, the emitter voltage is slowly turned on till the liquid in the emitter tip starts moving and a spray is formed. The maximum voltage allowed by the high voltage source is 3000 V, so this value shall not be exceeded in any case. As the subtitle says, there were many failed attempts before a perfect spray was formed. Some major problems that prevented the formation of a stable electrospray are explained below.

- No electric field seen

Due to different reasons, even though we apply certain voltage in the source, there might not be an electric field created between the emitter and the internal extractor. A very common error leading to this could be a loose connection between the voltage supply and the emitter/extractor. Also, sometimes while the setup is brought to vacuum from atmospheric pressure, there can be a cloud of propellant between the emitter and the internal extractor

which causes a short circuit and hence no electric field will be seen. In addition to this, the propellant cloud can cause oxidation of the extractors and make them electrically non-conducting. Black copper oxide (CuO) is a common oxide formed as the extractor is made of brass: a zinc-copper alloy. In Figure 128, we can see the inner surface of the internal extractor oxidized and the oxide is also diffused in the thruster's base. Some white spots above the black surface was seen which is probably Zinc Oxide (ZnO). Lastly, the phenomenon of outgassing can occur while bringing the chamber into vacuum and some very tiny particles can block the fluid passage and eventually disrupt the spray formation.

Figure 128. Oxidized internal extractor

To get rid of above stated problems, we should bring the chamber back into atmospheric pressure, remove the setup, and clean all the components using Acetone. High pressure air should also be blown into the emitter to remove any tiny particles stuck inside it. After this, the experiment can be run again.

- Bubble in the emitter

In the current setup, high voltage is applied in the propellant tank and the propellant, which is in high voltage, breaks into spray when reaches the emitters' tip. There have been many cases when there is a huge air bubble inside the emitter which separates the propellant into two parts. This bubble interrupts the high voltage chain and hence, the propellant that is near the emitter tip is no longer electrified resulting in a lack of spray formation. Even though most of the time the air bubble is pulled out by the pressure difference given that the whole chamber is in vacuum, sometimes the pressure difference is not enough and the bubble remains there

making us helpless. Figure 129 shows how a bubble travels through an emitter eventually stopping in a spray formation.

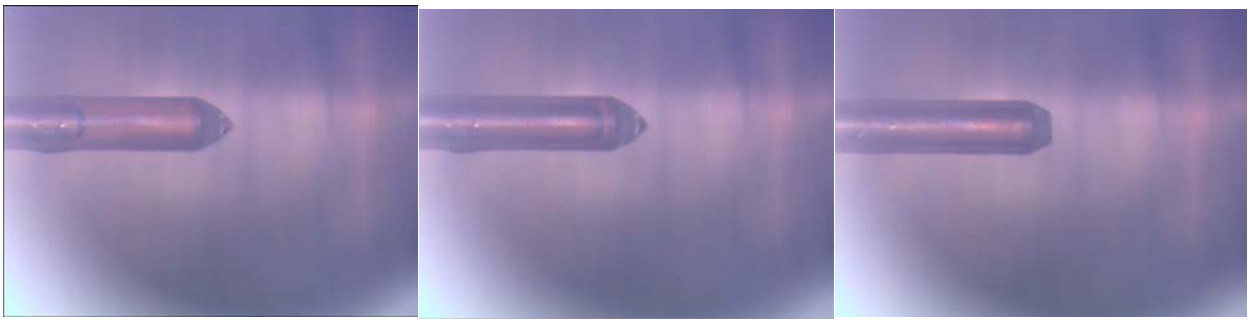

Figure 129. Images showing an air bubble travelling through the emitter and disrupting the spray

These bubbles could have been formed inside the propellant tank because of the presence of humidity in the propellant or because of a small leak somewhere in the vacuum chamber that allows air to enter the chamber. To solve this problem, all the fittings in the vacuum chamber were re-checked and later the setup was left in vacuum overnight so that the humidity from the propellant could be removed. The next day, the experiment was run and we could still be having the same problem. In this case, chances might be that the emitter was not completely dry when we set the experiment up and a small liquid film trapped inside it might have trapped an air bubble between itself and the propellant flowing into the emitter through capillary action. At this point, we bring the vacuum chamber into atmospheric pressure, remove all the setup, check the emitter and, before running a new experiment, blow air at high pressure from the emitter till a continuous bubble flow can be seen inside the propellant tank. This assures us that there is no such liquid film present inside the emitter and hence we will have a continuous propellant line from the tank til the emitter tip. In my case, even after doing this, the same problem existed for many days. At this point there was no other option other than to continue to repeat the same process and until it would eventually work. The only option left is applying the high voltage right at the emitter tip and not in the propellant tank so that a bubble wouldn't be a problem anymore as the small liquid trapped in

the emitter tip could be removed by electrospraying it. The two possible options to do this are either electrifying the tip of the silica emitter or using metallic emitters. As electrifying the emitter required knowledge of how to use some machines to do it and is also tedious, we decide to move forward with the metallic emitters. A disadvantage of metallic emitters is that they are opaque. Therefore, we can't see what's going on near the emitter tip. But, the Taylor cone formed can be visible and also the current read in the multimeter gives us an idea of if a spray is formed there. We use a stainless steel emitter with internal diameter of $0.007\ in/\ 177.8\ \mu m$.

If we apply a high voltage between the emitter and the internal extractor when a bubble is present, there can be an electric arc which would eventually destroy the emitter tip. The electric arc has been a huge problem, especially in case of the metallic emitters, as at many times, we don't realize that a bubble is coming and all of a sudden there is a huge electric arc that destroys the whole emitter and sometimes the electronic components that build up the high voltage source. A close-up view of an emitter destroyed by various electric arcs is presented in Figure 130.

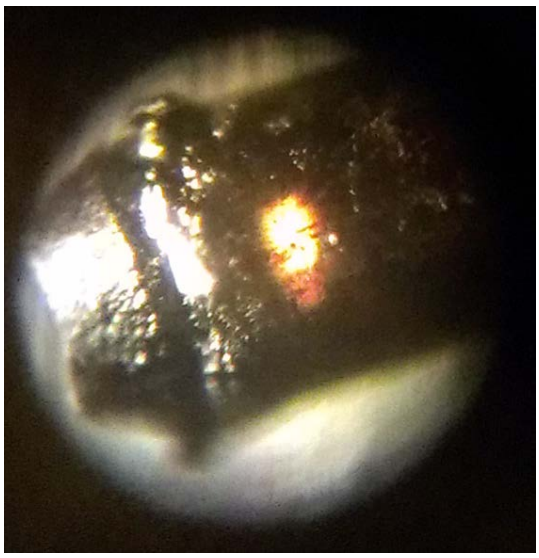

Figure 130. An emitter destroyed by electric arcs

Because the problem with the bubble and the arcs kept existing, we decided to try a new propellant, Emi-Otf (1-butyl-3-methylimidazolium tetrafluoroborate), and finally the setup worked with the silica emitter. After many trials, Emi-Im worked with the metallic emitter and the experimental results are going to be presented in the next subtopic.

4.3.3.3 Experimental Results

The first stable spray we were able to form was with Emi-Otf as propellant and silica emitter of internal diameter 200 μm. The spray started forming when the voltage applied at the emitter was between 1982 V and 2450 V. As it can be seen in Figure 131, there is a small bump right at the edge of the emitter (the part seen after that is the cone formed by the propellant). It is because the external surface of the emitter is wet by the propellant. Table 13 lists the beam current produced for various voltages and Figure 132 graphs those values. As we can see, the current produced varies from 130 to 1060 nA.

Table 13. Current vs Voltage for Emi-Otf with externally-wet silica emitter

Voltage (V)	Current (nA)
1982	130
2012	198
2043	266
2072	353
2100	396
2150	460
2201	510
2334	710
2374	880
2450	1060

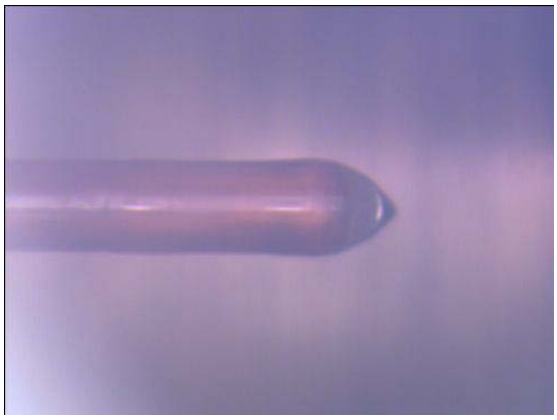

Figure 131. Electrospray formed in an externally-wet Silica emitter

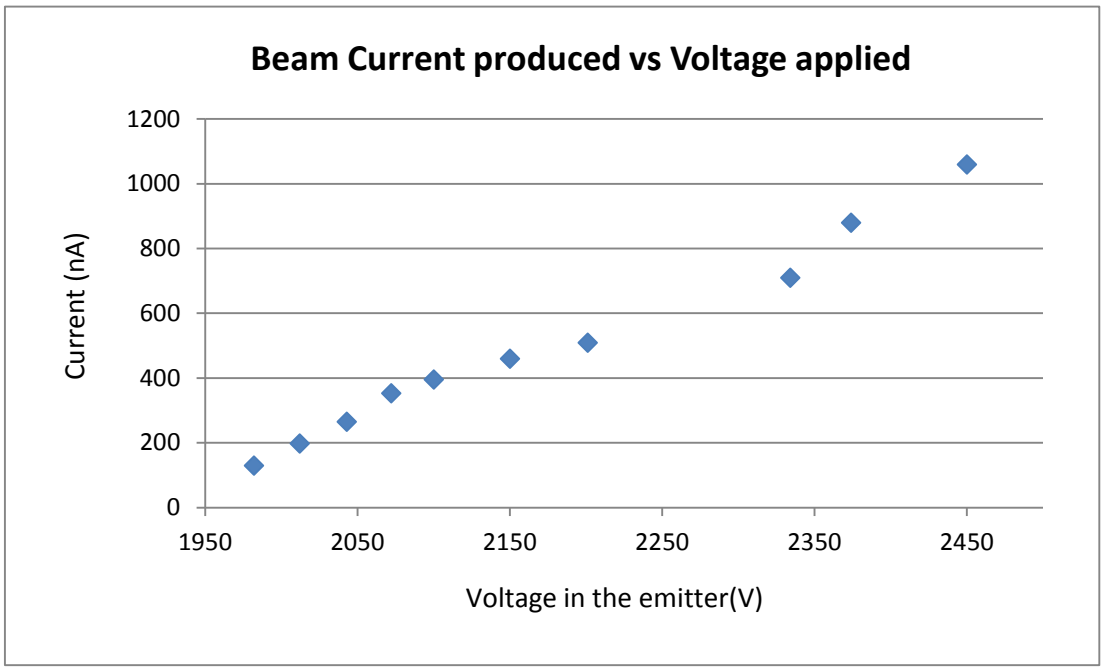

Figure 132. Beam Current produced at different voltages using an externally-wet silica emitter and Emi-Otf as the propellant.

When the experiment was repeated under similar conditions, the Taylor cone formed was found to be pretty different as seen in Figure 133. Unlike the previous case, the cone is small and is originated from a tiny area in the center of the emitter. Also, as it can be seen in Figure 134 and Table 14, the spray is formed at different voltages and also the corresponding current is different. The reason behind this is that the electric field created between the emitter and the internal extractor is not only affected by the voltage applied through the high voltage source, it also depends on other factors like the roughness of the emitter tip, presence of liquid in the outer surface, etc. Comparing Table 13 and Table 14, we can see that when the emitter is externally wet, smaller voltages applied produce bigger beam currents i.e. the electric field created is stronger than when the emitter is not externally wet. And it seems to be correct as when the emitter is wet, there is more surface area of propellant and hence the electric field created is stronger.

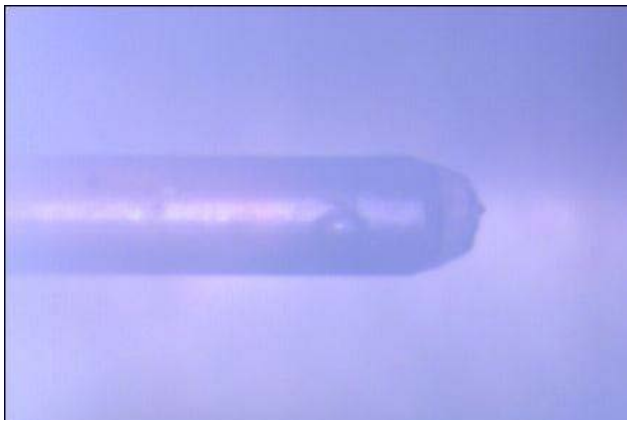

Figure 133. Electrospray formed in a Silica emitter

Table 14. Current vs Voltage for Emi-Otf with silica emitter

Voltage (V)	Current (nA)
2374	516
2403	588
2455	724
2503	876
2555	1030
2586	1147

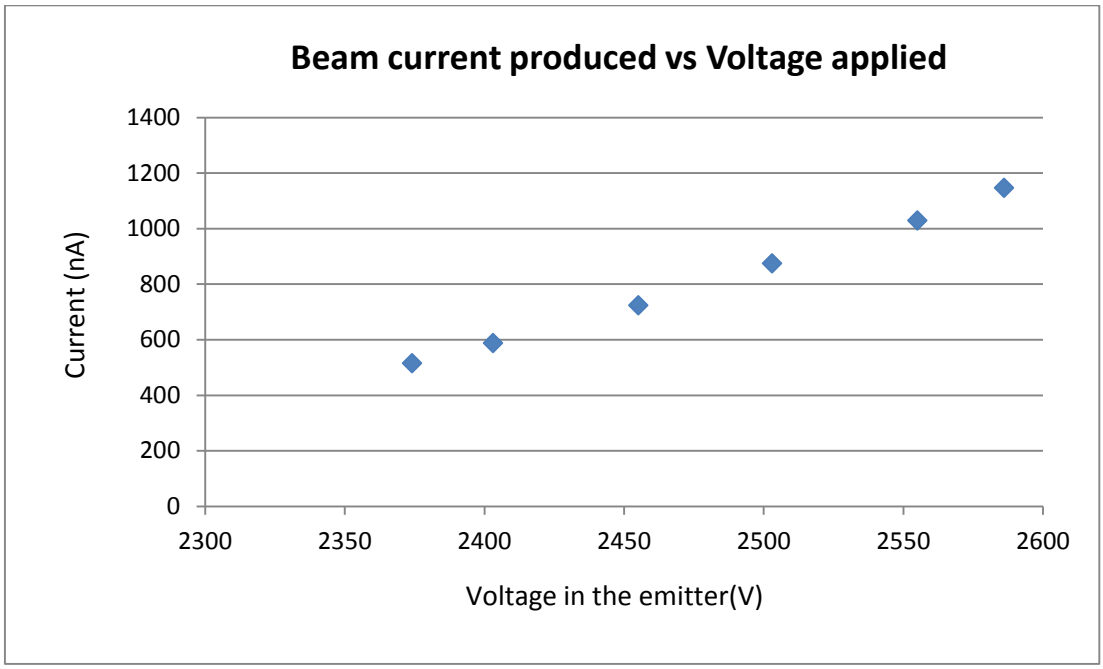

Figure 134. Beam Current produced at different voltages using a silica emitter and Emi-Otf as the propellant.

The final version of the satellite will have metallic emitters as they have less chances of malfunctioning due to bubble formation inside the emitter. They are also more than the silica emitters. The passive feeding experiment was also tested with the metallic emitter. The emitter is made of stainless steel and has an internal diameter of 177.8 μm. The beam currents produced for different voltages applied in the emitter are listed in Table 15. Comparing Table 15 with Table

14, it can be seen that when a metallic emitter is used, more beam current produced for a similar applied voltage. This could also be because of the electric field produced while using the metallic emitter is stronger in comparison to while using the silica emitter, as the uniformity/value of the electric field does not depend anymore in the distribution of propellant around the emitter tip. Figure 136 is the corresponding graph designed. A small jump can be noticed in the current produced when the voltage applied is around 2450 V. This jump occurs as the number of Taylor cones produced from the liquid surface increases from one to two and therefore there is more beam current. In other words, the electric field produced is so big that the ions extracted by a single cone are not enough to balance it, so multiple cones arise from the liquid surface. Figure 135 has an image of the metallic emitter tip with the spray formed.

Table 15. Current vs Voltage for Emi-Otf with metallic emitter

Voltage (V)	Current (nA)
2359	549
2379	589
2398	727
2419	814
2438	889
2458	1188
2480	1262
2500	1337
2521	1412
2541	1477
2561	1534
2580	1596

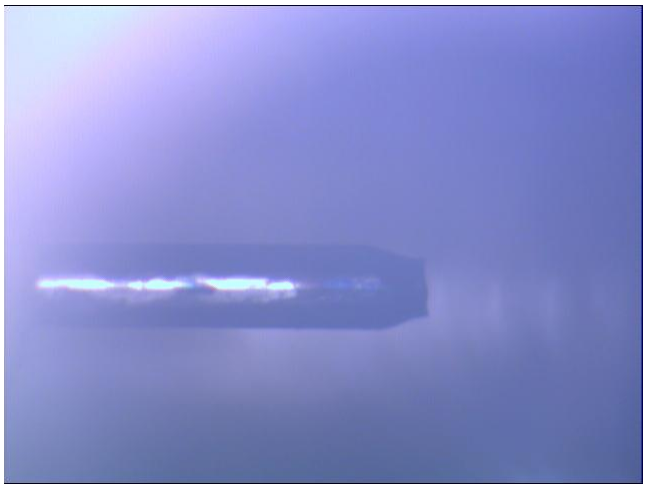

Figure 135. Electrospray formed in a metallic emitter

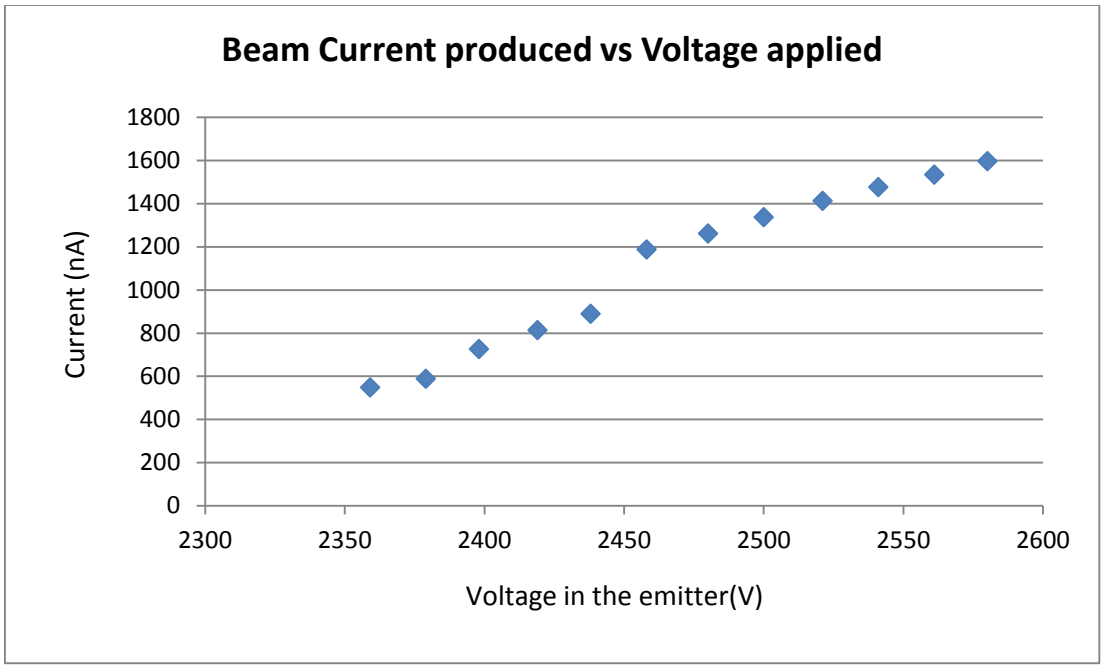

Figure 136. Beam Current produced at different voltages using a metallic emitter and Emi-Otf as the propellant.

In order to find out how much thrust can each of these emitters give, it is necessary to know the propellant mass flow rate. In order to find out the mass flow rate, either a time of flight experiment has to be done or we have to use another propellant whose mass flow rate has been already calculated for similar experiments. We decide to move forward with Emi-Im which is a classical liquid in electrospraying and we have found out its mass flow rate earlier. Now, the passive feeding experiment was repeated using Emi-Im as propellant and the stainless steel emitter of internal diameter 177.8 µm. The values of beam current produced for different voltages are given in Table 16 and the corresponding graph is presented in Figure 137.

Table 16. Current vs Voltage for Emi-Im with metallic emitter

Voltage (V)	Current (nA)
2397	410
2421	454
2440	476
2461	506
2483	541
2501	575
2523	932
2540	987
2560	1053
2580	1111
2599	1515
2623	1560
2644	1634

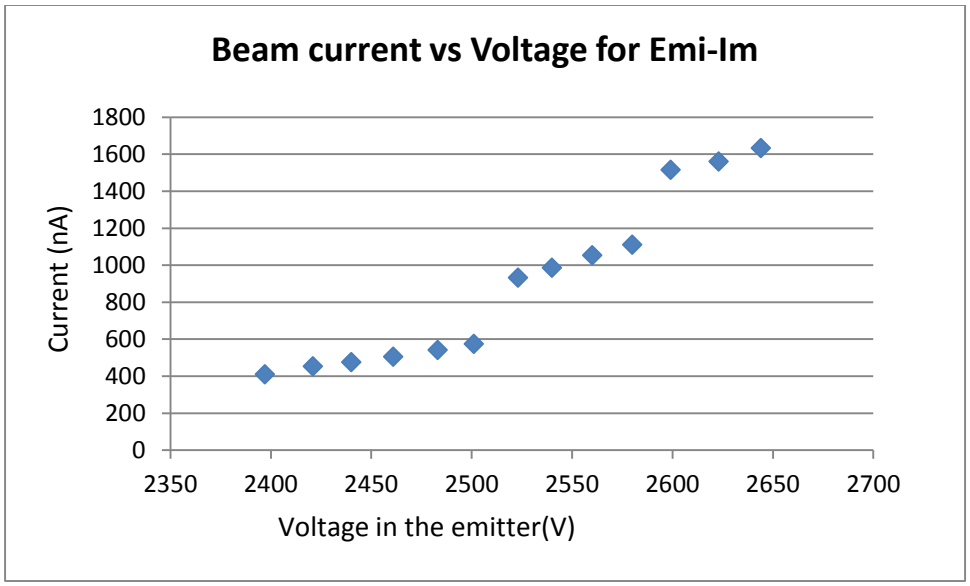

Figure 137. Beam Current produced at different voltages using a metallic emitter and Emi-Im as the propellant.

As it can be noticed in the graph, there is a jump in the current produced between 2500 V and 2520 V and there is another jump produced between 2580 and 2600 V. These jumps are formed as the number of Taylor cones formed from the liquid surface increases. The first jump indicates that the number of Taylor cones produced increases from one to two and the second jump indicates that there are three Taylor cones forming from the liquid surface.

In order to calculate the force, we need to find the mass flow rate of the propellant. As a first approximation, we will take the mass flow rate obtained from the Time-Of-Flight experiment for zero pressure difference which is $\dot{m} = 6.84E - 10\ kg/s$ according to 7.3.4.1.We know that the kinetic energy of the liquid sprayed is equal to the charge of the particles multiplied by the acceleration voltage applied.

$$qV_{acc} = \frac{1}{2}mv^2 \rightarrow I * t * V_{acc} = \frac{1}{2}m * \left(\frac{T}{\dot{m}}\right)^2 \rightarrow T = \sqrt{2 * I * V_{acc} * \dot{m}}$$

Where $Charge(q) = I * t\ with\ I = Current\ flowing$

$V_{acc} = acceleration\ voltage$

$$v = velocity\ of\ the\ particles = \frac{T}{\dot{m}}\ where\ T = Thrust\ and\ \dot{m} = mass\ flow\ rate$$

If we take $V_{acc} = 2500\ V, I = 575\ nA$. With these values, the thrust obtained from one thruster is: $T = 1.4\ \mu N$.

4.3.4 ACS Testing

Once all the previous tests were done and found working, we assemble wholly the thruster components with the electronics and hang the satellite inside a vacuum chamber using the tungsten wire previously chosen. Figure 138 shows the image of the satellite hung inside the vacuum chamber ready to perform the Attitude Control System (ACS) testing.

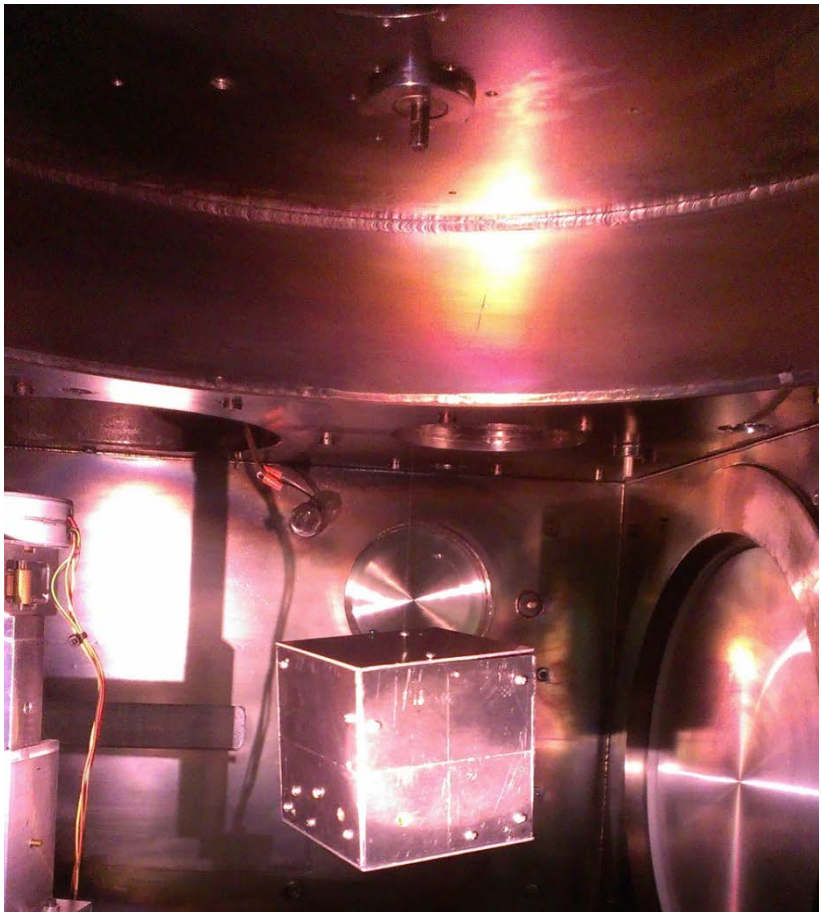

Figure 138. Satellite hung inside the vacuum chamber with a Tungsten wire of diameter 0.003"

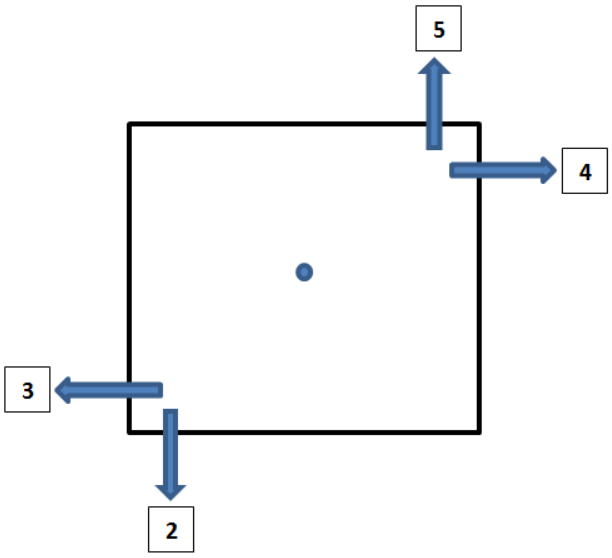

Figure 139. Top view of thruster configuration with the pins connected to the Arduino

Table 17. Angle turned by the satellite with time right after it was hung

Time	Angle turned(degrees)
14:20 pm	720
14:50 pm	150
15:20 pm	95
15:50 pm	60
16:20 pm	30
16:50 pm	10

Once the satellite is hung, it starts rotating on the axis defined by the tungsten wire. As there is no damping system introduced, it takes a lot of time to come to rest. The test was performed on 5th November 2014 and Table 17 shows the total angle turned by the satellite with respect to time. As it can be seen, it took the satellite almost three hours to come into rest. After this, the mechanical pump was turned on to put the satellite into vacuum. It was seen that due to the air being extracted from the chamber, the satellite started rotating again. After waiting for almost an hour with the satellite in a complete vacuum, the satellite was rotating very slightly and we decided to run the thruster system. First of all, the Arduino pin turning the high voltage supply was turned on after turning the main power button ON (Pin 1 in Figure 113). Now, the circuit has high voltage in it, the emitters are in high voltage (2500 V) and the internal extractors are in 909.09 V as explained in 4.1.1.2. Hence, the voltage difference is not enough to form a spray which means there is no thrust being generated. Figure 139 gives the top view of the satellite with the thrusters and pins of Arduino each of them are connected. As it can be seen in the figure, the central dot represents the wire respect to which the rotation is going to occur. Hence, thrusters 2 and 5 will

rotate the satellite in an anti-clockwise direction and thrusters 3 and 4 will rotate the satellite in a clockwise direction. Secondly, the pair of pins 2 and 5 was turned on and the movement of satellite was being observed. Once we had performed this step, the LabView program controlling the setup was frozen and no signals were being obtained. We waited for a while, tried restarting the system but it still didn't work. Then, we brought the vacuum chamber into atmospheric pressure and removed the satellite from the wire. The outer surface of satellite was warm and the battery was dead. Later we realized that the Arduino and the WiFi Shield were not working anymore. It is supposed that either these microcontrollers aren't supposed to work in vacuum or there was an electric discharge between some points in the high voltage and the Arduino because of which they stopped working. So, the next step would be buy a new set of microcontrollers and test them in vacuum if they work, try to re-analyze the electronic circuit built, test each components separately in vacuum and continue with the ACS testing. Because of time limit, I couldn't proceed with this debugging process and some other student in the Electric Propulsion Laboratory will continue with this experiment.

5. CONCLUSIONS

From the chapters of Conductivity measurement and Time-Of-Flight technique, the following conclusions can be drawn:

As given in Table 3, FORMAMIDE G (4% EAN) and FORMAMIDE 2 (25% Emi Im) have almost the same electric conductivity (approximately 1 Si/m). According to Figure 81 - Figure 86, FORMAMIDE G gives higher thrust and specific impulse than FORMAMIDE 2 for the similar flow rates. Similarly, FORMAMIDE H (7% EAN) and FORMAMIDE 1 (50% Emi Im) have almost the same electric conductivity (approximately 1.5 Si/m) but FORMAMIDE H gives higher thrust and specific impulse than FORMAMIDE 1 for the similar flow rates. Hence, for use in Space Propulsion, a mixture of EAN with Formamide is better than a mixture of Emi Im with Formamide as higher thrust and specific impulse is obtained from fluids of similar conductivity. However, it should not be forgotten that the mixtures with EAN provide lower spray efficiencies than the mixtures with Emi Im.

As explained in section 3.6.3, EAN (Ethyl ammonium nitrate) and Emi BF4 (1-ethyl-3-methylimidazolium tetra fluoroborate) are the liquids that provide the higher values of Specific Impulse and Thrust among the ones we analyzed. Moreover, both of them are molten salts and have very low vapor pressure which is desired in Colloid thrusters' use. On the other hand, the viscosity of Emi BF4 at room temperature is 43 centipoise whereas EAN has viscosity of 28 centipoise. Also, according to Table 2, the electric conductivity of EAN is 2.03 Si/m at 19.8ºC and that of Emi BF4 is 1.31 Si/m at 19.9ºC. As EAN and Emi BF4 give similar values of thrust and Isp, they have similar vapor pressures but EAN has lower viscosity and higher electric conductivity than the Emi BF4, I would say EAN is the best propellant among all the propellants studied for its use in Space Propulsion.

Similarly, from the chapter of ACS control in CubeSat, the following conclusions can be drawn:

A set of thruster systems and the corresponding circuit board that would fit inside the CubeSat was fabricated using tools available in the machine shop and the laboratory. As the elements to design were very tiny, extra caution had to be applied while fabricating them. Another point to take into account while designing the parts in Solidworks is to know the resources available for fabrication. Sometimes the designs made can seem easier and better but are not feasible if they can't be made using the machines we had access to.

While designing the electronic board and testing the electronic components, we realized that making a prototype of a theoretical circuit doesn't always gives the results we expect. In setups like ours where we have limitations of power and we have a high voltage circuit, many times hit and trial methods had to be used to find the correct combination of resistors that would make the desired voltage divider. Moreover, as the resistance in the circuit was comparable to that of the high voltage probe, it was never sure if the value we were reading in the multimeter was the correct one or not as the probe's introduction in the circuit would change the circuit we were analyzing.

During the passive feeding test, we encountered many problems which were eventually solved and we were able to see a stable electrospray formed. We proved that the thruster design we have made works for its use in the satellite. Bubble formation and electric discharge were one of the main problems in this testing and it was found that these problems were reduced while using metallic emitters compared to using silica emitters.

Assembling different parts together was more time consuming as interferences between various components had to be solved. Unfortunately, we couldn't finish the final testing as the microcontroller stopped working. There could be many reasons behind it but we think that some electrical discharges between high voltage points in the circuit and the microcontroller might have

destroyed the microcontroller. This situation could have been avoided if we had tested each and every component of the satellite in vacuum separately because it also might be that some of the electronic components we used were not to be used in a vacuum. But, after proving that one thruster works with passive feeding, we can say that the ACS testing would have worked if we had properly designed and tested the electronic board and the microcontroller.

As the satellite we made was for testing purposes, we tried to use cheap materials and designed the components so that we could fabricate it in our laboratory facilities. But, if this thruster system is meant to be integrated in a real satellite, all these components can be designed such that they occupy very small space and are light. The thruster system could be made even smaller with appropriate machines to fabricate, a smaller and better battery and microcontroller could be used and also the propellant feeding system could be made smaller and more efficient. This way, there would be enough space to integrate all other components of the satellite. On the other hand, the thruster configuration could be changed to four thrusters in each corner of the satellite such that the fourth one could be a redundant one. Hence, we can conclude that giving a proper attitude control to a CubeSat using passively fed electrospray thrusters is feasible.

6. REFERENCES

[1] Swartout M. “The First One Hundred CubeSats: A Statistical Look”, *Journal of small satellites,*Vol.2, No.2, pp.213-233

[2] 2013 annual report on CubeSats- National Science Foundation <http://www.nsf.gov/geo/ags/uars/cubesat/nsf-nasa-annual-report-cubesat-2013.pdf> (7 November,2014)

[3] Larson, W; Wertz, J. (2006). *Space Mission Analysis and Design* (3rd edition).Microcosm Press, Springer

[4] Gamero-Castaño, M. & Hruby, V. “Electrospray as a source of nanoparticles for efficient colloid thrusters”, *Journal of Propulsion and Power*, 17, 977-987 (2001)

[5] Kaltashov, I.A & Eyles, S.J, *Mass Spectrometry in Biophysics* (1st Edition). John Wiley and Sons

[6] Matthews J.A., Wnek, G.E., Simpson, D.G., Bowlin, G.L., “Electrospinning of Collagen Nanofibers”, *Biomacromolecules,* 3, 232-238 (2002)

[7] Gamero-Castaño, M.,Borrajo-Pelaez, R., Torrents A.,Zheng, J.G., “Amorphization of hard crystalline materials by electrosprayed nanodroplet impact”, *Journal of Applied Physics,* 116, (2014)

[8] Timp, G.,Howard, R.E., Mankiewich, P.M., *Nanotechnology* (1st Edition). Springer-Verlag

[9] Hartman, R.P.A., Brunner, D.J. ,Camelot, D.M.A., Marijnessen, J.C.M., and Scarlett, B., “Jet Break-Up in ELectrohydrodynamic Atomization in the Cone-Jet Mode, Physical Modeling of the Liquid Cone and Jet,” *Journal of Aerosol Sciences,* Vol.30, No.7, 1999, pp.823-849

[10] D. Garoz, C. Bueno, C. Larriba, S. Castro, I. Romero-Sanz, J. Fernandez de la Mora, Y.Yoshida, and G. Saito, “*Taylor cones of ionic liquids from capillary tubes as sources of pure ions: The role of Surface tension and electrical conductivity*”, J.Appl. Phys. 102, 064913 (2007)

[11] Ziemer John K., Colleen M., Anderson M., Plett G., Gamero-Castano M. “*Colloid Thruster Propellant Stability after Radiation Exposure*”, AIAA 2003

[12] Ortiz-Berrocal L. (1998). *Elasticidad* (3rd edition).Mc Graw-Hill

7. ANNEXES

7.1 Arduino Code

```
#include <SPI.h>
#include <WiFi.h>
#include <WiFiUdp.h>

int status = WL_IDLE_STATUS;
char ssid[] = "EG3116"; //  Network SSID
char pass[] = "gamerolab";    // Network Password

unsigned int localPort = 2382;      // local port to listen on

char packetBuffer[255]; //buffer to hold incoming packet
WiFiUDP Udp;
void setup()
{
  // Serial.begin(9600);
  // Initialize ports used for satellite control
  pinMode(0, OUTPUT);
  pinMode(1, OUTPUT);
  pinMode(2, OUTPUT);
  pinMode(3, OUTPUT);
  pinMode(5, OUTPUT);
  //  Set all pins to low except the first one which has to be HIGH
```

```
digitalWrite(0, HIGH);
digitalWrite(1, LOW);
digitalWrite(2, LOW);
digitalWrite(3, LOW);
digitalWrite(5, LOW);
// check for the presence of the shield:
if (WiFi.status() == WL_NO_SHIELD)
{
  //Serial.println("WiFi shield not present");
  // don't continue:
  while (true);
}
// attempt to connect to WiFi network:
while (status != WL_CONNECTED)
{
  //Serial.print("Attempting to connect to SSID: ");
  //Serial.println(ssid);
  // Connect to WPA/WPA2 network. Change this line if using open or WEP network:
  status = WiFi.begin(ssid, pass);
  // wait 10 seconds for connection:
  delay(10000);
}
//Serial.println("Connected to WiFi");
//printWifiStatus();
//Serial.println("\nWaiting for packets...");
// if you get a connection, report back via serial:
```

```
  Udp.begin(localPort);   // Begins listening for incoming packets
}
void loop()
{
  // if there's data available, read a packet
  int packetSize = Udp.parsePacket();
  if(packetSize)
  {
    /*
    Serial.print("Received packet of size ");
    Serial.println(packetSize);
    Serial.print("From ");
    IPAddress remoteIp = Udp.remoteIP();
    Serial.print(remoteIp);
    Serial.print(", port ");
    Serial.println(Udp.remotePort());
    */
    // read the packet into packetBuffer
    int len = Udp.read(packetBuffer, 255);
    if (len > 0) packetBuffer[len] = 0;
    //Serial.println("Contents:");
    String packet = packetBuffer;
   // Serial.println(packet);
    int indexPosition = packet.indexOf("P");
    char power = packet.charAt(indexPosition + 1);
    if(power == 'F')   // Sets all pins to low except the first one if power switch is off
```

```
{
  digitalWrite(0, HIGH);
  digitalWrite(1, LOW);
  digitalWrite(2, LOW);
  digitalWrite(3, LOW);
  digitalWrite(5, LOW);
}
else if(power == 'T')
{
  for(int i=1; i<9; i++)     // This loop turns the pins on or off based on received string data
  {
     String num;
     num+=i;
     indexPosition = packet.indexOf(num);

     char PinState = packet.charAt(indexPosition + 1);
     int Pin;
     switch(i)      //  assigns the  pin to be controlled
     {
       case 1:
         Pin = 0;
         break;
       case 2:
         Pin = 1;
         break;
       case 3:
```

```
        Pin = 2;
        break;
      case 4:
        Pin = 3;
        break;
      case 5:
        Pin = 5;
        break;
    }

    if(PinState == 'T')
    {
      digitalWrite(Pin, HIGH);
    }
    else if(PinState == 'F')
    {
      digitalWrite(Pin, LOW);
    }
  }
}

int xaccel = analogRead(0)-233;    // read accelerations and adjust for offset
int yaccel = analogRead(1)-224;
int zaccel = analogRead(2)-234;
int currentVoltage = analogRead(3);
delay(1);     // a delay is usually necessary for analogRead to work correctly
```

```
    String acceleration = "x";
    acceleration += xaccel;
    acceleration += "y";
    acceleration += yaccel;
    acceleration += "z";
    acceleration += zaccel;
    acceleration += "v";
    acceleration += currentVoltage;
    // send a reply, to the IP address and port that sent us the packet we received
    Udp.beginPacket(Udp.remoteIP(), Udp.remotePort());
    Udp.print(acceleration);
    Udp.endPacket();
  }
}
```

7.2 Conductivity Measurement of Propellants

For all the liquids, the length of the tube used is 0.46m and the diameter of the tube used is 200μm.

$$L = 0.46\ m$$

$$D = 200\ \mu m$$

What we will be measuring in the Electrometer is Voltage and it has to be multiplied by the Gain of the Circuit in order to find out the Current in Amperes.

For all cases

$$I(A) = 0.909E-06 \cdot I(V)$$

7.2.1 EAN

Lab Temperature: 19.8 ºC. The data acquired are:

Table 18. Current obtained for certain voltages: EAN

V (v)	I (v)	I (A)
1.045	0.0802	7.29E-08
2.701	0.3089	2.81E-07
3.925	0.467	4.25E-07
5.61	0.725	6.59E-07
7.16	0.963	8.75E-07
8.64	1.186	1.08E-06
10.09	1.421	1.29E-06
12.05	1.734	1.58E-06
14.29	2.089	1.9E-06

The Current vs. Voltage graph is:

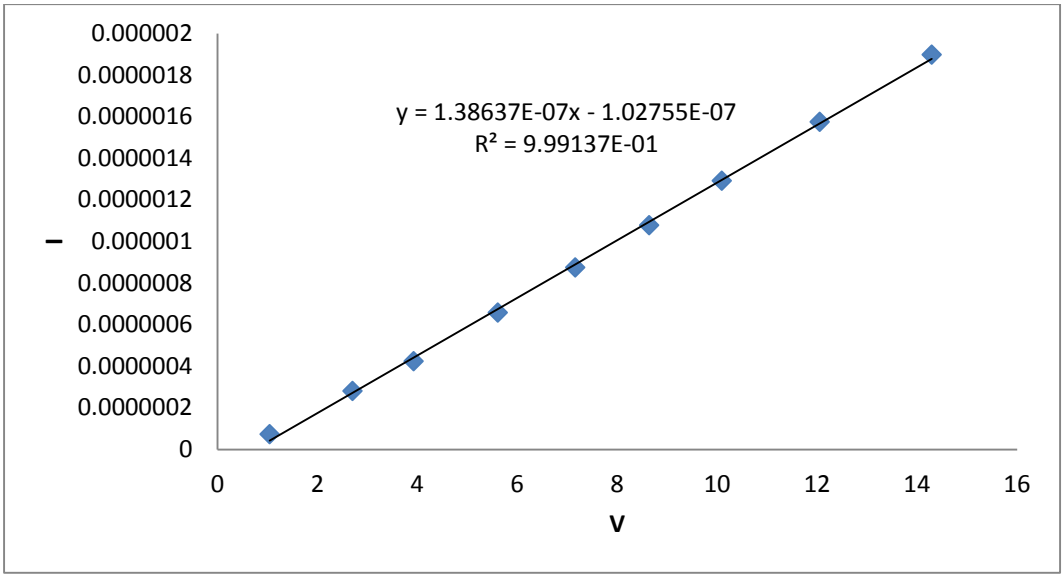

Figure 140. Current vs. Voltage graph: EAN

Conductivity calculation:

Table 19. Conductivity calculation: EAN

I/V	1.39E-07
L (m)	0.46
A (m^2)	3.1416E-08
Conductivity (Si/m)	2.02996

7.2.2 Emi IM

Lab Temperature: 20.2ºC .The data acquired are:

Table 20. Current obtained for certain voltages: Emi IM

V (v)	I (v)	I (A)
1.08	0.0457	4.15E-08
2.735	0.135	1.23E-07
3.941	0.1955	1.78E-07
5.55	0.2857	2.6E-07
6.98	0.366	3.33E-07
8.73	0.47	4.27E-07
10.52	0.578	5.25E-07
14.36	0.809	7.35E-07

The current vs. Voltage graph is:

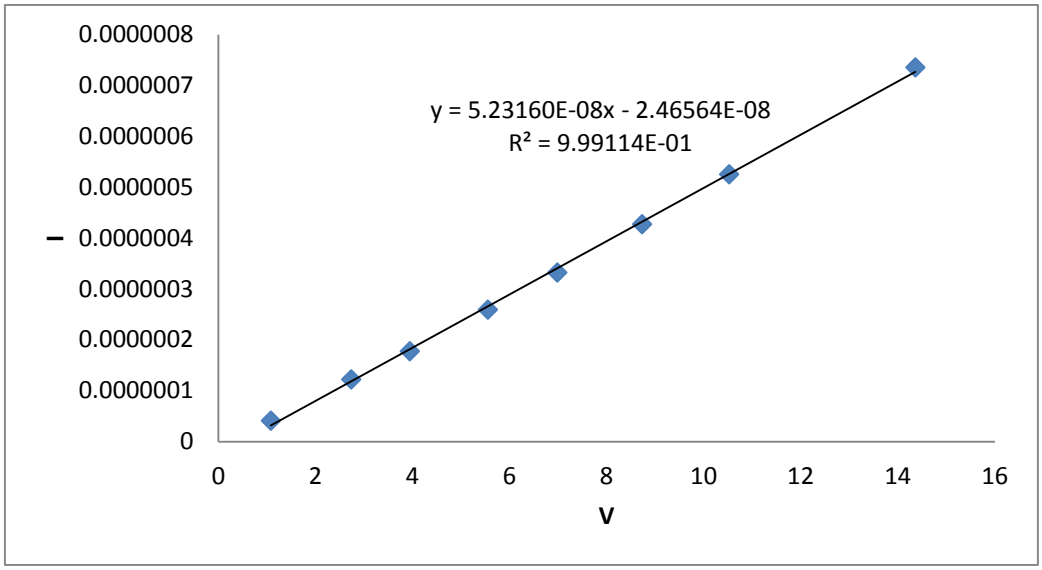

Figure 141. Current vs. Voltage graph: Emi IM

Conductivity calculation:

Table 21. Conductivity calculation: Emi IM

I/V	5.23E-08
L (m)	0.46
A (m^2)	3.1416E-08
Conductivity (Si/m)	0.76602

7.2.3 Emi BF4

Lab Temperature: 19.9ºC . The data acquired are:

Table 22. Current obtained for certain voltages: Emi BF4

V (v)	I (v)	I (A)
1.037	0.0753	6.84E-08
2.729	0.2318	2.11E-07
4.025	0.347	3.15E-07
5.64	0.506	4.6E-07
7.17	0.656	5.96E-07
8.57	0.796	7.24E-07
10.22	0.962	8.74E-07
12.01	1.146	1.04E-06
14.13	1.353	1.23E-06

The current vs. Voltage graph is:

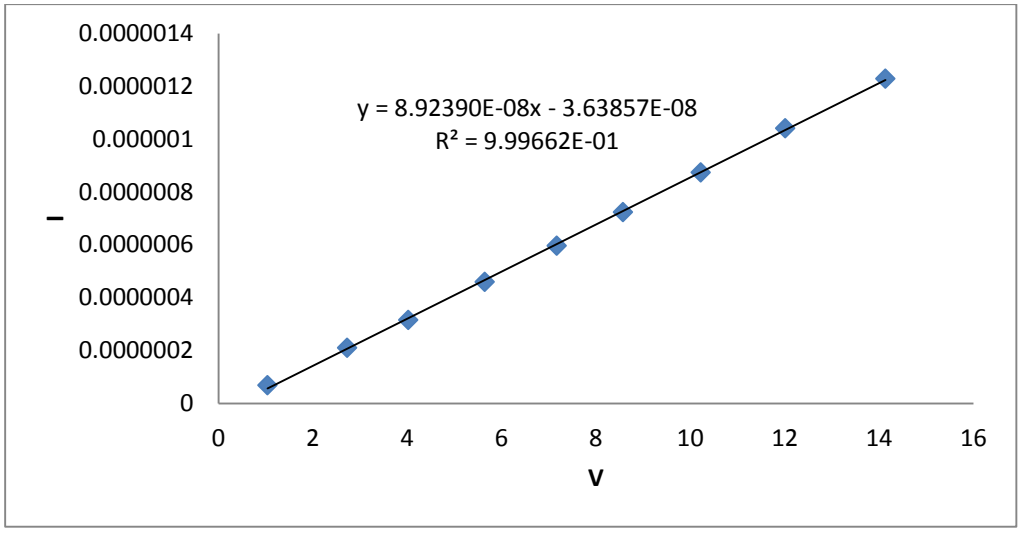

Figure 142. Current vs. Voltage graph: Emi BF4

Conductivity calculation:

Table 23. Conductivity calculation: Emi BF4

I/V	8.92E-08
L (m)	0.46
A (m^2)	3.1416E-08
Conductivity (Si/m)	1.30666

7.2.4 Emi TF

Lab Temperature: 19.7ºC. The data acquired are:

Table 24. Current obtained for certain voltages: Emi TF

V (v)	I (v)	I (A)
1.07	0.0413	3.75E-08
2.782	0.1379	1.25E-07
4.051	0.2131	1.94E-07
5.54	0.3058	2.78E-07
7.05	0.4	3.64E-07
9.24	0.532	4.84E-07
11.08	0.645	5.86E-07
12.77	0.739	6.72E-07
14.29	0.83	7.54E-07

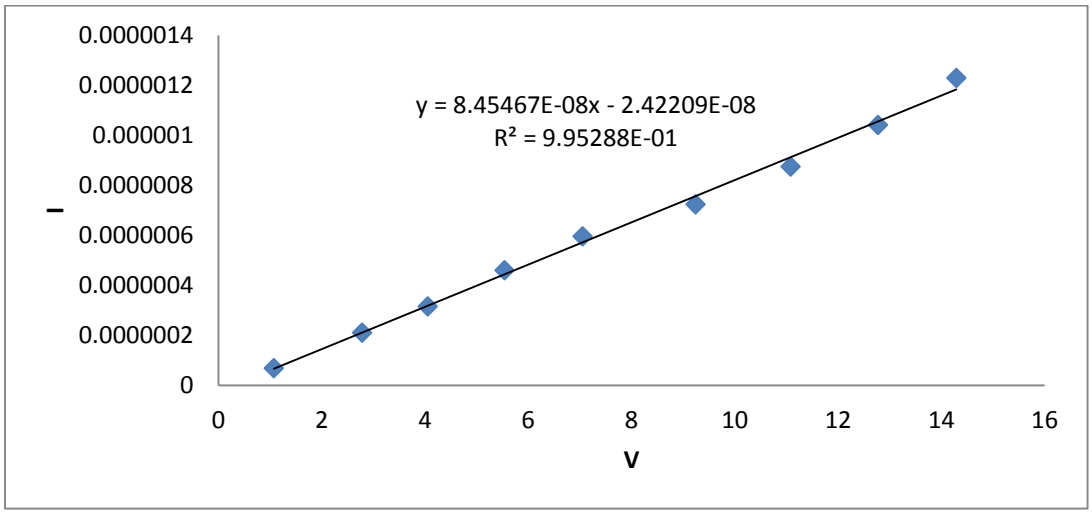

Figure 143. Current vs. Voltage graph: Emi TF

The current vs. Voltage graph is shown in Figure 143.

Conductivity calculation:

Table 25. Conductivity calculation: Emi TF

I/V	8.45E-08
L (m)	0.46
A (m^2)	3.1416E-08
Conductivity (Si/m)	1.23795

7.2.5 TES

Lab Temperature: 19.9ºC.The data acquired are:

Table 26. Current obtained for certain voltages: TES

V (v)	I (v)	I (A)
1.08	0.0359	3.26E-08
2.43	0.0952	8.65E-08
4.21	0.1749	1.59E-07
6.05	0.2544	2.31E-07
8.13	0.358	3.25E-07
9.75	0.44	4E-07
11.35	0.521	4.74E-07
13.1	0.607	5.52E-07
14.41	0.674	6.13E-07

The current vs. Voltage graph is:

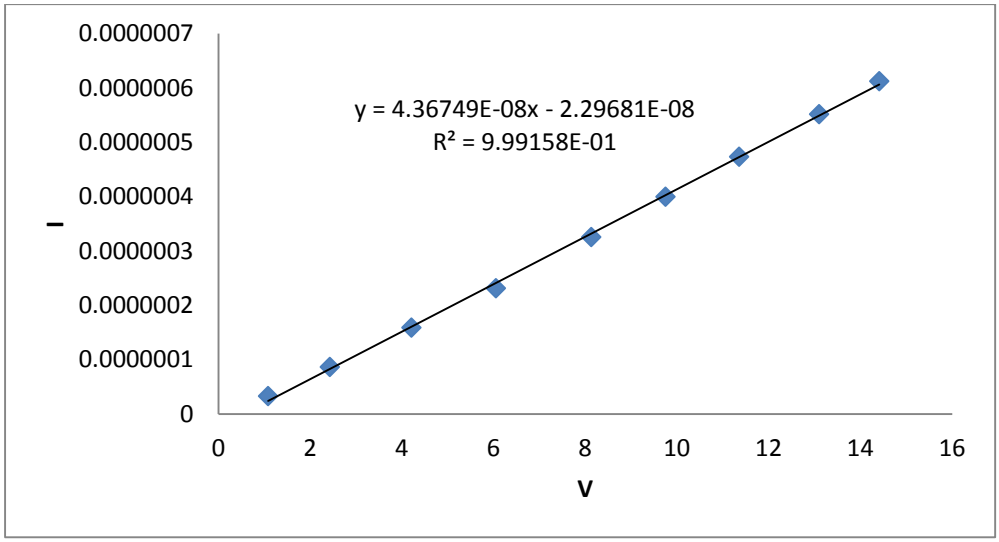

Figure 144. Current vs. Voltage graph: TES

Conductivity calculation:

Table 27. Conductivity calculation: TES

I/V	4.37E-08
L (m)	0.46
A (m^2)	3.1416E-08
Conductivity (Si/m)	0.63950

7.2.6 Formamide G

Lab Temperature: 22.8ºC.The data acquired are:

Table 28. Current obtained for certain voltages: Formamide G

V (v)	I (v)	I (A)
1.061	0.072	6.54E-08
2.59	0.177	1.61E-07
4.24	0.29	2.64E-07
6.19	0.432	3.93E-07
7.59	0.533	4.84E-07
9.14	0.645	5.86E-07
10.48	0.745	6.77E-07
13.09	0.934	8.49E-07
14.53	1.041	9.46E-07

The current vs. Voltage graph is:

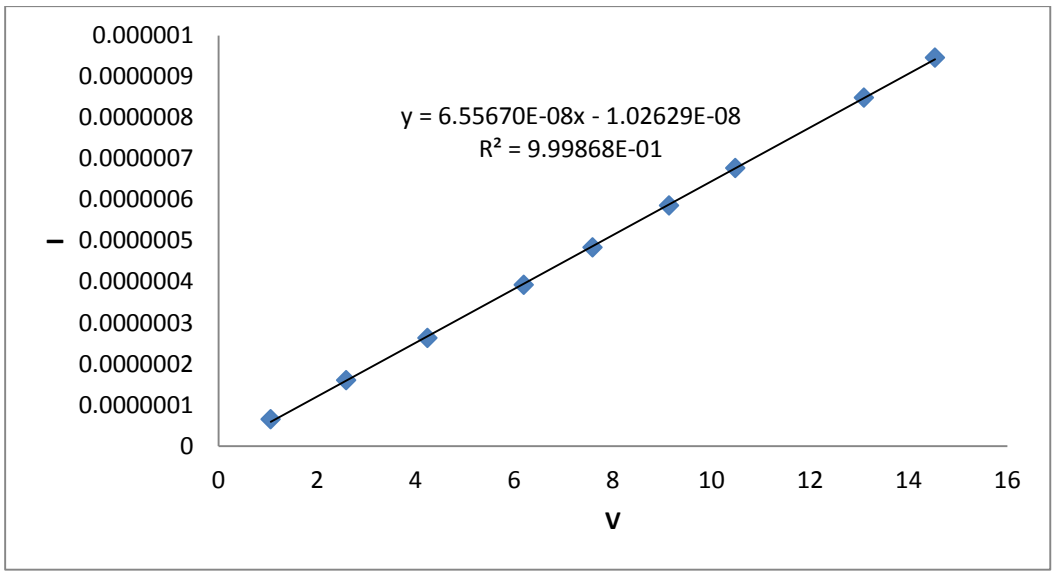

Figure 145. Current vs. Voltage graph: Formamide G

Conductivity calculation:

Table 29. Conductivity calculation: Formamide G

I/V	6.56E-08
L (m)	0.46
A (m^2)	3.1416E-08
Conductivity (Si/m)	0.96005

7.2.7 Formamide H

Lab Temperature: 20.2ºC.The data acquired are:

Table 30. Current obtained for certain voltages: Formamide H

V (v)	I (v)	I (A)
1.03	0.1044	9.49E-08
2.621	0.2079	1.89E-07
3.899	0.407	3.7E-07
5.58	0.588	5.34E-07
7.04	0.748	6.8E-07
9.55	1.032	9.38E-07
11.76	1.284	1.17E-06
14.09	1.55	1.41E-06

The current vs. Voltage graph is:

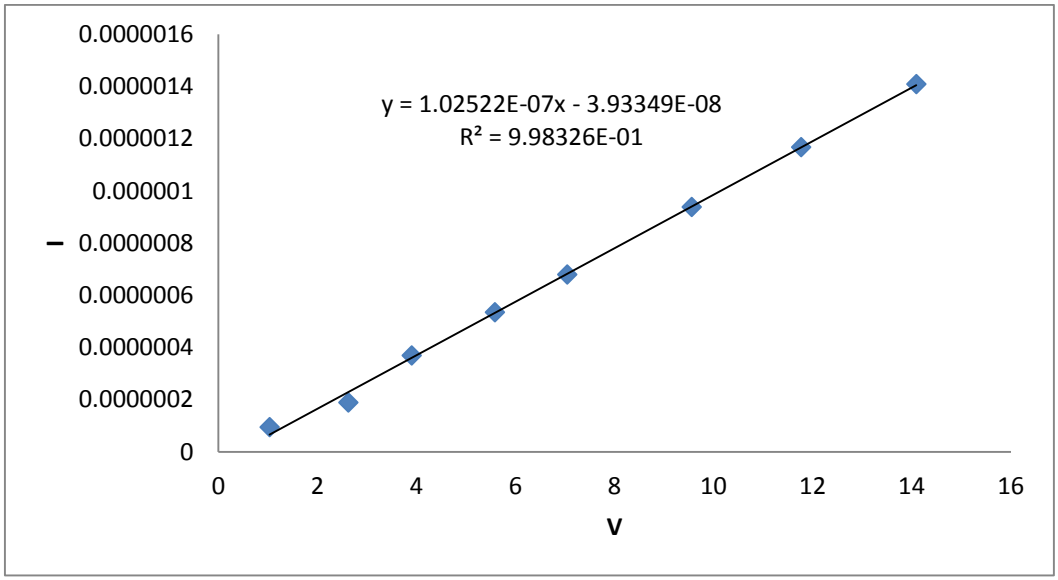

Figure 146. Current vs. Voltage graph: Formamide H

Conductivity calculation:

Table 31. Conductivity calculation: Formamide H

I/V	1.03E-07
L (m)	0.46
A (m^2)	3.1416E-08
Conductivity (Si/m)	1.50115

7.3 Time-Of-Flight Measurement

7.3.1 TOF Formulae

7.3.1.1 Charge to Mass Ratio

We know that the kinetic energy gained by the charged particles is equal to the total potential energy due to the potential difference applied between the emitter and the extractor.

$$\frac{1}{2}mv^2 = q \cdot V_A$$

The velocity of every particle is the ratio of emitter-collector distance to time required to complete this distance or time of flight.

$$v = \frac{L}{t_f}$$

Hence,

$$\boldsymbol{\frac{q}{m} = \frac{1}{2V_A}\left(\frac{L}{t_f}\right)^2}$$

7.3.1.2 Mass Flow rate

We know that current is the rate of change of charge.

$$I = \frac{q}{t} = \frac{q}{m} \cdot \frac{m}{t} = \frac{q}{m} \cdot \dot{m}$$

i.e.

$$dI = \frac{q}{m} \cdot d\dot{m} = \frac{1}{2V_A}\left(\frac{L}{t}\right)^2 . d\dot{m} \rightarrow$$

$$d\dot{m} = 2\,V_A\left(\frac{t}{L}\right)^2\left(\frac{dI}{dt}\right)dt \;\rightarrow d\dot{m} = 2\,V_A\left(\frac{t}{L}\right)^2 I'(t)dt$$

Integrating on both sides from $t = 0\ to\ t = \infty$,

$$\int_{t\,=\,0}^{t\,=\,\infty} d\dot{m} = \dot{m} = \int_{t=0}^{t\,=\,\infty} 2\,V_A\left(\frac{t}{L}\right)^2 I'(t)dt \;=\; \frac{2\,V_A}{L^2}\cdot\int_{t=0}^{t\,=\,\infty} t^2 I'(t)dt$$

Say $Int = \int_{t=0}^{t\,=\,\infty} t^2 I'(t)dt$. Now integrating on parts,

$$Int = \left[t^2\int I'(t)dt - \int\left(\frac{d}{dt}(t^2)\cdot\int I'(t)dt\right)dt\right]_{t=0}^{t=\,\infty} = \left[t^2 I(t) - \int 2t\cdot I(t)dt\right]_{t=0}^{t=\,\infty}$$

$$For\ time(t) = 0, \qquad t \rightarrow 0\ and$$

$$for\ time(t) = \infty, \qquad I(t) \rightarrow 0$$

Hence,

$$Int = -\int_{t=0}^{t=\,\infty} 2t\cdot I(t)dt$$

which leads to:

$$\boldsymbol{\dot{m} = -\frac{4V_A}{L^2}\int_{t=o}^{t=\,\infty} t\cdot I(t)dt}$$

7.3.1.3 Thrust

We know that,

$$dT = vd\dot{m} = \frac{L}{t}\cdot 2\,V_A\left(\frac{t}{L}\right)^2 I'(t)dt \;=\; 2\,V_A\frac{t}{L}I'(t)dt$$

Integrating on both sides from $time(t) = 0\ to\ time(t) = \infty$

$$T = \int_{t=0}^{t=\infty} 2\,V_A \frac{t}{L} I'(t)dt$$

Integrating by parts,

$$T = \frac{2V_A}{L}\left[t\int I'(t)dt - \int \left(\frac{d}{dt}(t)\cdot\int I'(t)dt\right)dt\right]_{t=0}^{t=\infty} = \frac{2V_A}{L}\left[t\cdot I(t) - \int I(t)dt\right]_{t=0}^{t=\infty}$$

$$For\ time(t) = 0, \qquad t \to 0\ and$$

$$for\ time(t) = \infty, \qquad I(t) \to 0$$

Hence,

$$\boldsymbol{T = -\frac{2V_A}{L}\int_{t=0}^{t=\infty} I(t)dt}$$

7.3.1.4 Efficiency

For an electrospray, efficiency is the ratio of Kinetic Energy produced to the Power involved to produce it.

$$\eta = \frac{\frac{1}{2}\dot{m}v^2}{P} = \frac{\frac{1}{2}\dot{m}v^2}{I\cdot V_A}$$

We know that $T = \dot{m}v$, then

$$\boldsymbol{\eta = \frac{1}{2}\frac{T^2}{\dot{m}IV_A}}$$

7.3.2 Relation between Needle Voltage and Voltage at source

Using an electrometer, the voltage difference at the needle is noted down for various values of voltages applied at source.

Table 32. Values of voltage at needle for various source voltages

Voltage at Source(V)	Voltage at Needle(V)
103	96
529	488
799	744
992	920
1281	1200
1426	1320
1638	1520
1838	1700
2050	1900

Now the graph obtained is:

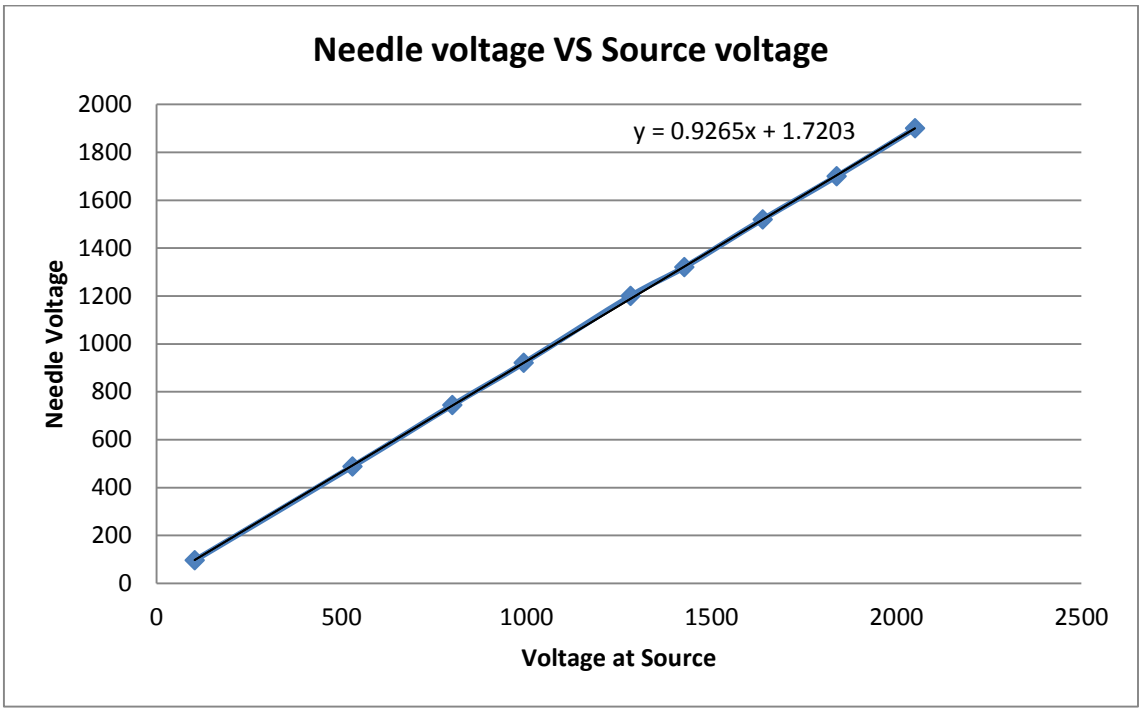

Figure 147. Relation between Needle voltage and Voltage at source.

Hence, $\boldsymbol{Needle\ voltage = 0.9265 * Source\ voltage + 1.7203}$

7.3.3 Programming Codes developed

7.3.3.1 Code to see all the graphs and a particular graph

```
% To see all the graphs
clear all; clc;
filelist = dir('*.txt');
n = length(filelist);
            for i = 1:1:n
                S3 = reading_filename (i,filelist);
                T4 = arrange_data(i,filelist,S3);
                plot(T4(:,1),T4(:,2));
                hold on;
            end
            hold off
%% To see a particular graph
% to find which is erroneous, filelist(p).name where p is the erroneous one
clear all; clc;
filelist = dir('EmiIm_1_1755_208_574_102_2_19.txt'); % An example
n = length(filelist);
S3 = reading_filename (1,filelist);
T4 = arrange_data(1,filelist,S3);
plot(T4(:,1),T4(:,2));
```

7.3.3.2 Function 'reading_filename'

```
function SS = reading_filename(k, filelist)
% filelist = dir('*.txt');( If you want to call the filelist here)
[tok, remain] = strtok(filelist(k).name, '_');
[tok, remain] = strtok(remain, '.');
ttok = tok*1;
```

```
 s_n = 0; V = 0; I = 0; P = 0; j= 2;num1 = 0; num2 =0; len = 0;
for i = 2:1:length(ttok)
    p = ttok(i);
    q = char(p);
    if j ==i
        if q ~=95
            r = str2num(q);
            s_n = s_n*10+r;
            j = j+1;
        end
    end
    if j ==i-1
        if q ~=95
            r = str2num(q);
            V = V*10+r;
            j = j+1;
        end
    end
    if j ==i-2
        if q ~=95
            r = str2num(q);
            I = I*10+r;
            j = j+1;
        end
    end
    if j ==i-3
        if q ~=95
            r = str2num(q);
            P = P*10+r;
```

```
            j = j+1;
        end
    end
    if j ==i-4
        if q ~=95
            r = str2num(q);
            len = len*10+r;
            j = j+1;
        end
    end
    if j ==i-5
        if q ~=95
            r = str2num(q);
            num1 = num1*10+r;
            j = j+1;
        end
    end
    if j ==i-6
        if q ~=95
            r = str2num(q);
            num2 = num2*10+r;
            j = j+1;
        end
    end
 SS(1) = s_n; SS(2) = V; SS(3) = I; SS(4) = P; SS(5) = len; SS(6) = num1;
SS(7) = num2;
 end
```

7.3.3.3 Function 'arrange_data'

```
function T = arrange_data (i,filelist,S1)
Iamm = S1(3)*1.01e-09; %From the relation that 1mV = 1.01nA  (as it will be
shown in volts)
    S = load(filelist(i).name);
    ns = length(S);
    %To calculate the offset
    tt = 0;
        for j = ns-49:1:ns
            tt = tt+S(j,2);
        end
    offset = tt/50;
    %Done with offset, now we'r gonna apply the offset to all the data.
    SS(:,2) = S(:,2)-offset;
    SS(:,1) = S(:,1);
    %Conversion factor alpha calculation
    tt = 0;
        for k = 1:1:50
         tt = tt+SS(k,2);
        end
    totvolt= tt/50;
    alpha = Iamm/totvolt;  %Multiplying with this alpha, we will get the
current values in Amperes
    SSS(:,2) = SS(:,2)*alpha; %We just converted voltage into current value
    SSS(:,1) = SS(:,1);
    %Now we have to find the position where time = 0
        for l = 1:1:ns
            if S(l,1) == 0
```

```
                pos = l;
            end
        end
    %Now we're gonna define a new matrix T which will have the corrected
values
    n = ns-pos+1;
    T = zeros(n,2);
        for m = 1:1:n
            T(m,1) = SSS(pos-1+m,1);
            T(m,2) = SSS(pos-1+m,2);
         end
```

7.3.3.4 Main Code

```
% This code calculates the average and prints the curve for various
% flowrates
clear all; clc;
filelist = dir('*.txt');
n = length(filelist);
for i = 1:1:n
    S1 = reading_filename(i,filelist);
    T1 = arrange_data(i,filelist,S1);
    S2(i,:) = S1(:);
    T2(i,:,:) = T1(:,:);
end
i= 1;
p = 1;
j = 2;
while i <= n    && p<=max(S2(:,1))
    T3(p,:,:) = T2(i,:,:);
```

```
while j <= n
    if S2(j,1) == S2(i,1)
        T3(p,:,:) = T3(p,:,:) + T2(j,:,:);
       j = j+1;
    else
        T3(p,:,:) = T3(p,:,:)/(j-i);
        %All stuffs to calculate Thrust,Isp,etc
        L = S2(i,5)/1000;
        Vacc = 0.9265*S2(i,2)+1.7203; % Using the regression line
        SM(:,2) = T3(p,:,2).*T3(p,:,1);
        SM(:,1) = T3(p,:,1);
        T4(:,2) = T3(p,:,2);
        T4(:,1) = T3(p,:,1);
        integm = calc_integral(SM);
        integt = calc_integral(T4);
        Thrust = integt*2*Vacc/L;
        Flowrate = integm*4*Vacc/(L*L);
        Isp = Thrust/(Flowrate*9.81);
        S3(p,1) = S2(i,1); %serial number
        S3(p,2) = Vacc; %Vacc
        S3(p,3) = S2(i,3); %Iamm
        S3(p,4) = S2(i,4); %Pressure
        S3(p,5) = S2(i,5); %Length of flight
        S3(p,6) = Thrust;
        S3(p,7) = Isp;
        S3(p,8) = Flowrate;
        i = j;
        j = n+1;
    end
```

```
    if j == n
        T3(p,:,:) = T3(p,:,:)/(j-i);
        %All stuffs to calculate Thrust,Isp,etc
        L = S2(i,5)/1000;
        Vacc = 0.9265*S2(i,2)+1.7203; % Using the regression line
        SM(:,2) = T3(p,:,2).*T3(p,:,1);
        SM(:,1) = T3(p,:,1);
        T4(:,2) = T3(p,:,2);
        T4(:,1) = T3(p,:,1);
        integm = calc_integral(SM);
        integt = calc_integral(T4);
        Thrust = integt*2*Vacc/L;
        Flowrate = integm*4*Vacc/(L*L);
        Isp = Thrust/(Flowrate*9.81);
        S3(p,1) = S2(i,1); %serial number
        S3(p,2) = Vacc; %Vacc
        S3(p,3) = S2(i,3); %Iamm
        S3(p,4) = S2(i,4); %Pressure
        S3(p,5) = S2(i,5); %Length of flight
        S3(p,6) = Thrust;
        S3(p,7) = Isp;
        S3(p,8) = Flowrate;
        i = j;
        j = n+1;
    end
end
p = p+1;
j = i+1;
%disp('iteracion n=%d',i)
```

```
end
%% To print the graphics
hold off;
for i = 1:1:max(S2(:,1))
    plot(T3(i,:,1),T3(i,:,2));
  hold on;
end
%xlswrite('filename',value interested to import) to take results to excel
```

7.3.3.5 Function 'calc_integral'

```
function integ = calc_integral(S)
n = length(S);
sum = 0;
for i = 1:1:n-1
    sum = sum + 0.5*[S(i+1,1)-S(i,1)]*[S(i+1,2)+S(i,2)];
end
integ = sum;
```

7.3.3.6 Program to calculate the accumulated Thrust and Mass flow rate

```
% This code calculates the accumulation of thrust and mass flow rate
clear all; clc;
filelist = dir('*.txt');
n = length(filelist);
for i = 1:1:n
    S1 = reading_filename(i,filelist);
    T1 = arrange_data(i,filelist,S1);
    S2(i,:) = S1(:);
    T2(i,:,:) = T1(:,:);
end
```

```
i= 1;
p = 1;
j = 2;
while i <= n    && p<=max(S2(:,1))
    T3(p,:,:) = T2(i,:,:);
    while j <= n
        if S2(j,1) == S2(i,1)
            T3(p,:,:) = T3(p,:,:) + T2(j,:,:);
           j = j+1;
        else
            T3(p,:,:) = T3(p,:,:)/(j-i);
            L = S2(i,5)/1000;
            Vacc = 0.9265*S2(i,2)+1.7203; % Using the regression line
            Km = 4*Vacc/(L*L);
            Kt = 2*Vacc/L;
            KK = 2*Vacc/(L*L);
            SM(:,2) = T3(p,:,2).*T3(p,:,1);
            SM(:,1) = T3(p,:,1);
            T4(:,2) = T3(p,:,2);
            T4(:,1) = T3(p,:,1);
            nn = length(SM);

            integ_time = zeros(nn,2);
            integ_time(:,1) = SM(:,1);
            sum = 0;
            for i = 1:1:nn-1
                 integ_time(i,2) = sum;
                    sum = sum + 0.5*[SM(i+1,1)-SM(i,1)]*[SM(i+1,2)+SM(i,2)];
```

```
    end
    integ_time(nn,2) = sum;
    integ_time(:,2) = integ_time(:,2).*Km;
    T7(p,:,1) = integ_time(:,1).*integ_time(:,1).*KK;
    T7(p,:,2) = integ_time(:,2);

    integ_thr = zeros(nn,2);
    integ_thr(:,1) = T4(:,1);
    sum = 0;
    for i = 1:1:nn-1
     integ_thr(i,2) = sum;
        sum = sum + 0.5*[T4(i+1,1)-T4(i,1)]*[T4(i+1,2)+T4(i,2)];
    end
    integ_thr(nn,2) = sum;
    integ_thr(:,2) = integ_thr(:,2).*Kt;
    T8(p,:,1) = integ_thr(:,1).*integ_thr(:,1).*KK;
    T8(p,:,2) = integ_thr(:,2);

    i = j;
    j = n+1;
end
if j == n
    T3(p,:,:) = T3(p,:,:)/(j-i);
    L = S2(i,5)/1000;
    Vacc = 0.9265*S2(i,2)+1.7203; % Using the regression line
    SM(:,2) = T3(p,:,2).*T3(p,:,1);
    SM(:,1) = T3(p,:,1);
    T4(:,2) = T3(p,:,2);
```

```
T4(:,1) = T3(p,:,1);
Km = 4*Vacc/(L*L);
Kt = 2*Vacc/L;
KK = 2*Vacc/(L*L);
nn = length(SM);

integ_time = zeros(nn,2);
integ_time(:,1) = SM(:,1);
sum = 0;
for i = 1:1:nn-1
     integ_time(i,2) = sum;
        sum = sum + 0.5*[SM(i+1,1)-SM(i,1)]*[SM(i+1,2)+SM(i,2)];
end
integ_time(nn,2) = sum;
integ_time(:,2) = integ_time(:,2).*Km;
T7(p,:,1) = integ_time(:,1).*integ_time(:,1).*KK;
T7(p,:,2) = integ_time(:,2);

integ_thr = zeros(nn,2);
integ_thr(:,1) = T4(:,1);
sum = 0;
for i = 1:1:nn-1
 integ_thr(i,2) = sum;
    sum = sum + 0.5*[T4(i+1,1)-T4(i,1)]*[T4(i+1,2)+T4(i,2)];
end
integ_thr(nn,2) = sum;
integ_thr(:,2) = integ_thr(:,2).*Kt;
T8(p,:,1) = integ_thr(:,1).*integ_thr(:,1).*KK;
```

```
            T8(p,:,2) = integ_thr(:,2);
            i = j;
            j = n+1;
        end
    end
    p = p+1;
    j = i+1;
    %disp('iteracion n=%d',i)
end

%% To print the graphs of mass flow rate
hold off;
for i = 1:1:max(S2(:,1))
    plot(T7(i,:,1),T7(i,:,2));
  hold on;
end

%% To print the graphs of thrust
hold off;
for i = 1:1:max(S2(:,1))
    plot(T8(i,:,1),T8(i,:,2));
  hold on;
end
```

7.3.4 Measurement of Thrust and Specific Impulse

After analyzing the data obtained from the oscilloscope using the MATLAB codes described above, important parameters like thrust, specific impulse, mass flow rate, etc. for each liquid is found which is later passed to a document in excel for post processing of the data. These data are presented in this Annex for each liquid separately.

Note: the values in red are those which are neglected for the calculation due to the instability of the cone-jet.

7.3.4.1 Emi Im

Table 33. Acceleration Voltage, Beam Current, Pressure difference, TOF length and Thrust given by different experiments for Emi Im.

S.N	Vacc	I(nA)	I(real)	ΔP	L	Thrust
1	1627.7278	208	210.08	-574	102	2.7982E-07
2	1627.7278	240	242.4	-492	102	3.8458E-07
3	1627.7278	254	256.54	-445	102	4.3094E-07
4	1627.7278	266	268.66	-399	102	4.7719E-07
5	1627.7278	280	282.8	-357	102	5.2166E-07
6	1627.7278	293	295.93	-304	102	5.6961E-07
7	1627.7278	306	309.06	-246	102	6.1734E-07
8	1627.7278	315	318.15	-205	102	6.5323E-07
9	1627.7278	327	330.27	-150	102	7.0054E-07
10	1627.7278	337	340.37	-96	102	7.422E-07
11	1627.7278	346	349.46	-44	102	7.7972E-07
12	1627.7278	353	356.53	0	102	8.0602E-07
13	1627.7278	360	363.6	49	102	8.3694E-07
14	1627.7278	370	373.7	97	102	8.7325E-07
15	1627.7278	375	378.75	156	102	9.0419E-07
16	1627.7278	385	388.85	201	102	9.3475E-07
17	1627.7278	392	395.92	256	102	9.6849E-07
18	1627.7278	400	404	299	102	1.0014E-06
19	1627.7278	408	412.08	351	102	1.0385E-06
20	1627.7278	415	419.15	400	102	1.0738E-06
21	1627.7278	423	427.23	449	102	1.1103E-06
22	1627.7278	430	434.3	497	102	1.1483E-06
23	1627.7278	438	442.38	552	102	1.1859E-06
24	1627.7278	445	449.45	605	102	1.2194E-06

25	1627.7278	449	453.49	655	102	1.2602E-06
26	1627.7278	450	454.5	704	102	1.2903E-06
27	1627.7278	459	463.59	751	102	1.326E-06

Table 34. Specific impulse, mass flow rate, Efficiency and Thrust error given by different experiments for Emi Im.

S.N	Isp	m_f	m_f(1e-10)	Thrust(μN)	Efficiency(η)	Thrust error
1	194.343168	1.4677E-10	1.46769685	0.27981736	78.00	13.22
2	169.033871	2.3192E-10	2.31923867	0.38458132	80.81	11.24
3	164.323523	2.6733E-10	2.67328626	0.43093742	83.18	9.65
4	152.009656	3.2E-10	3.19998774	0.47718688	81.36	10.86
5	147.952059	3.5941E-10	3.59413942	0.52165688	82.24	10.27
6	142.258087	4.0816E-10	4.08157841	0.56960542	82.51	10.09
7	139.149727	4.5225E-10	4.52246657	0.61734329	83.76	9.27
8	133.009722	5.0063E-10	5.00625053	0.65322827	82.30	10.23
9	128.664999	5.5502E-10	5.5501717	0.70054469	82.24	10.27
10	123.636826	6.1193E-10	6.11934059	0.74220091	81.24	10.95
11	121.658331	6.5332E-10	6.53323159	0.77972043	81.80	10.57
12	120.106602	6.8409E-10	6.84085578	0.80602093	81.82	10.55
13	118.301477	7.2116E-10	7.21163751	0.83693757	82.06	10.39
14	115.79381	7.6875E-10	7.68749068	0.87325072	81.54	10.74
15	112.802932	8.1709E-10	8.17091871	0.90419122	81.15	11.01
16	111.633863	8.5355E-10	8.53552458	0.93474936	80.87	11.20
17	108.803187	9.0737E-10	9.07366248	0.96848577	80.20	11.66
18	107.75369	9.4738E-10	9.47378166	1.00143907	80.49	11.46
19	105.771081	1.0009E-09	10.0086523	1.03851208	80.33	11.58
20	103.885001	1.0537E-09	10.5368838	1.07382632	80.20	11.66
21	101.582456	1.1142E-09	11.142175	1.11034436	79.56	12.12
22	99.4149915	1.1774E-09	11.7742298	1.14829479	79.21	12.36
23	97.696128	1.2374E-09	12.3736105	1.18588561	78.92	12.57
24	96.9422886	1.2822E-09	12.8219483	1.21937222	79.25	12.33
25	94.5922568	1.3581E-09	13.5807882	1.2602293	79.21	12.36
26	91.9264409	1.4308E-09	14.3080447	1.29029716	78.64	12.76
27	90.8739265	1.4874E-09	14.874493	1.32602121	78.33	12.99

7.3.4.2 EAN

Table 35. Acceleration Voltage, Beam Current, Pressure difference, TOF length and Thrust given by different experiments for EAN.

S.N	Vacc	I(nA)	I(real)	ΔP	L	Thrust
1	1800.0568	655	661.55	-606	102	4.4008E-07
2	1800.0568	678	684.78	-541	102	5.4843E-07
3	1800.0568	696	702.96	-493	102	6.2371E-07
4	1800.0568	711	718.11	-442	102	6.8676E-07
5	1800.0568	730	737.3	-395	102	7.5172E-07
6	1800.0568	744	751.44	-349	102	7.9888E-07
7	1800.0568	762	769.62	-305	102	8.5555E-07
8	1800.0568	787	794.87	-247	102	9.2431E-07
9	1800.0568	809	817.09	-191	102	9.9054E-07
10	1800.0568	819	827.19	-150	102	1.0287E-06
11	1800.0568	835	843.35	-96	102	1.0793E-06
12	1800.0568	853	861.53	-44	102	1.1415E-06
13	1800.0568	866	874.66	5	102	1.1917E-06
14	1800.0568	881	889.81	55	102	1.248E-06
15	1800.0568	902	911.02	102	102	1.2999E-06
16	1800.0568	913	922.13	150	102	1.3451E-06
17	1800.0568	935	944.35	207	102	1.4099E-06
18	1800.0568	956	965.56	291	102	1.4842E-06
19	1800.0568	961	970.61	334	102	1.5402E-06
20	1800.0568	961	970.61	352	102	1.5416E-06
21	1800.0568	974	983.74	402	102	1.58E-06
22	1800.0568	988	997.88	451	102	1.6231E-06
23	1800.0568	1001	1011.01	497	102	1.667E-06
24	1800.0568	1016	1026.16	552	102	1.7106E-06
25	1800.0568	1029	1039.29	605	102	1.7557E-06
26	1800.0568	1041	1051.41	655	102	1.7943E-06
27	1800.0568	1054	1064.54	703	102	1.8268E-06
28	1800.0568	1063	1073.63	749	102	1.8586E-06

Table 36. Specific impulse, mass flow rate, Efficiency and Thrust error given by different experiments for EAN.

S.N	Isp	m_f	m_f(1e-10)	Thrust(μN)	Efficiency(η)	Thrust error
1	488.175323	9.1894E-11	0.91894398	0.440082266	88.49	6.30
2	353.222846	1.5827E-10	1.58272591	0.548432906	77.09	13.90

3	342.777145	1.8548E-10	1.85483276	0.623714189	82.87	9.85
4	310.462843	2.2549E-10	2.25488105	0.686755703	80.90	11.18
5	296.126461	2.5877E-10	2.58769138	0.751724496	82.27	10.25
6	296.878798	2.743E-10	2.74303663	0.798876781	86.00	7.83
7	270.331508	3.2261E-10	3.22609569	0.855545123	81.89	10.51
8	267.352313	3.5242E-10	3.52424694	0.924313477	84.71	8.65
9	247.1939	4.0848E-10	4.08476671	0.990544553	81.66	10.66
10	241.138109	4.3487E-10	4.34873898	1.028722408	81.72	10.62
11	241.972366	4.5467E-10	4.54669138	1.079270371	84.38	8.86
12	231.829507	5.0194E-10	5.01943909	1.141544661	83.70	9.30
13	223.653044	5.4313E-10	5.43132051	1.19165147	83.03	9.74
14	211.482202	6.0156E-10	6.01562394	1.248025645	80.83	11.23
15	211.860682	6.2546E-10	6.25458767	1.299924288	82.37	10.18
16	205.437886	6.6744E-10	6.67443197	1.345128755	81.66	10.66
17	197.16964	7.2891E-10	7.28914608	1.409891538	80.21	11.65
18	189.825556	7.9702E-10	7.97019193	1.484200135	79.51	12.15
19	184.297426	8.519E-10	8.51901988	1.540202799	79.69	12.02
20	183.834236	8.5484E-10	8.54837206	1.541625259	79.56	12.11
21	184.563293	8.7267E-10	8.72669689	1.580025982	80.78	11.27
22	179.937824	9.1949E-10	9.19488982	1.623072805	79.75	11.98
23	174.772106	9.7229E-10	9.72293424	1.667011042	78.53	12.85
24	174.16287	1.0012E-09	10.0120517	1.710596832	79.11	12.43
25	171.584138	1.043E-09	10.4303109	1.755672072	78.98	12.52
26	169.25241	1.0806E-09	10.8063734	1.794253663	78.70	12.72
27	166.911899	1.1157E-09	11.1566268	1.826792472	78.05	13.19
28	163.716992	1.1573E-09	11.5726225	1.858636891	77.23	13.79

7.3.4.3 Emi BF4

Table 37.Acceleration Voltage, Beam Current, Pressure difference, TOF length and Thrust given by different experiments for Emi BF4.

S.N	Vacc	I(nA)	I(real)	ΔP	L	Thrust
1	1916.7958	1203	1215.03	-358	102	8.85664E-07
2	1916.7958	1216	1228.16	-331	102	1.13174E-06
3	1916.7958	1214	1226.14	-300	102	9.56648E-07
4	1916.7958	1194	1205.94	-268	102	1.1222E-06
5	1916.7958	1172	1183.72	-225	102	1.10076E-06
6	1916.7958	1100	1111	-200	102	1.10551E-06
7	1916.7958	1030	1040.3	-149	102	1.15781E-06

8	1916.7958	898	906.98	-95	102	1.17517E-06
9	1916.7958	890	898.9	-55	102	1.24586E-06
10	1916.7958	895	903.95	5	102	1.30865E-06
11	1916.7958	902	911.02	53	102	1.3525E-06
12	1916.7958	910	919.1	101	102	1.39165E-06
13	1916.7958	920	929.2	148	102	1.4533E-06
14	1916.7958	925	934.25	181	102	1.48458E-06
15	1916.7958	930	939.3	204	102	1.51525E-06
16	1916.7958	934	943.34	234	102	1.53686E-06
17	1916.7958	940	949.4	269	102	1.57404E-06
18	1916.7958	948	957.48	290	102	1.59824E-06
19	1916.7958	950	959.5	300	102	1.60076E-06
20	1916.7958	957	966.57	330	102	1.63671E-06
21	1916.7958	960	969.6	351	102	1.66234E-06
22	1916.7958	968	977.68	380	102	1.69846E-06
23	1916.7958	971	980.71	400	102	1.71439E-06
24	1916.7958	978	987.78	439	102	1.75598E-06
25	1916.7958	985	994.85	476	102	1.79151E-06
26	1916.7958	992	1001.92	503	102	1.81671E-06
27	1916.7958	998	1007.98	530	102	1.83854E-06
28	1916.7958	1008	1018.08	565	102	1.88142E-06
29	1916.7958	1017	1027.17	606	102	1.93802E-06
30	1916.7958	1025	1035.25	649	102	1.87641E-06
31	1916.7958	1044	1054.44	698	102	1.98244E-06
32	1916.7958	1059	1069.59	752	102	1.9924E-06

Table 38. Specific impulse, mass flow rate, Efficiency and Thrust error given by different experiments for Emi BF4.

S.N	Isp	m_f	m_f(1e-10)	Thrust(μN)	Efficiency(η)	Thrust error
1	329.2206532	2.7423E-10	2.74228596	0.88566365	61.41	27.61
2	347.1121329	3.3236E-10	3.3235849	1.13173717	81.85	10.53
3	286.5455274	3.4032E-10	3.40321542	0.95664781	57.21	32.21
4	304.941659	3.7513E-10	3.75133442	1.12220332	72.61	17.35
5	292.0721391	3.8418E-10	3.84180573	1.10076481	69.50	19.95
6	263.8352356	4.2713E-10	4.27132385	1.10551415	67.18	22.00
7	241.6412718	4.8842E-10	4.88422483	1.15780592	68.82	20.54
8	221.2731129	5.4138E-10	5.41381096	1.17517012	73.37	16.75
9	220.7853092	5.7522E-10	5.7521674	1.24586417	78.31	13.01
10	210.0921942	6.3496E-10	6.34958842	1.30865298	77.83	13.35

11	213.5651018	6.4556E-10	6.45560721	1.35249726	81.13	11.02
12	214.9879031	6.5985E-10	6.598548	1.39165445	83.30	9.57
13	201.8961142	7.3377E-10	7.33767202	1.45329997	80.80	11.25
14	199.040901	7.6031E-10	7.6031489	1.48458419	80.94	11.15
15	193.6263752	7.9772E-10	7.97720061	1.51524911	79.93	11.85
16	195.0890429	8.0303E-10	8.0303243	1.53686234	81.33	10.88
17	196.771287	8.1543E-10	8.15429082	1.57404422	83.48	9.45
18	190.2982449	8.5613E-10	8.5612928	1.59824421	81.29	10.92
19	193.3887974	8.4377E-10	8.43774803	1.60076239	82.56	10.06
20	186.2706393	8.9569E-10	8.95692035	1.63671147	80.71	11.31
21	184.8951438	9.1649E-10	9.16486438	1.66234268	81.12	11.03
22	180.0641552	9.6152E-10	9.61519043	1.69845547	80.05	11.77
23	183.2510183	9.5366E-10	9.53663541	1.71439379	81.97	10.45
24	177.8968968	1.0062E-09	10.0619788	1.75598489	80.93	11.16
25	175.4125695	1.0411E-09	10.4109214	1.79150855	80.83	11.23
26	177.7636889	1.0418E-09	10.4177126	1.81670509	82.48	10.11
27	177.1543663	1.0579E-09	10.5791833	1.83853969	82.69	9.97
28	172.6307256	1.111E-09	11.1096054	1.88141992	81.64	10.68
29	171.5284607	1.1517E-09	11.5173806	1.93802296	82.82	9.89
30	166.3155389	1.1501E-09	11.5007331	1.87640836	77.14	13.86
31	166.1090049	1.2166E-09	12.1657282	1.9824411	79.92	11.86
32	164.2416963	1.2366E-09	12.3658368	1.99239728	78.29	13.02

7.3.4.4 Emi TF

Table 39. Acceleration Voltage, Beam Current, Pressure difference, TOF length and Thrust given by different experiments for Emi TF.

S.N	Vacc	I(nA)	I(real)	ΔP	L	Thrust
1	2047.4323	343	346.43	-474	102	6.45592E-07
2	2047.4323	354	357.54	-442	102	6.32081E-07
3	2047.4323	370	373.7	-396	102	6.50916E-07
4	2047.4323	382	385.82	-365	102	6.89649E-07
5	2047.4323	404	408.04	-306	102	7.67396E-07
6	2047.4323	422	426.22	-248	102	8.31585E-07
7	2047.4323	435	439.35	-206	102	8.78613E-07
8	2047.4323	454	458.54	-150	102	9.38129E-07
9	2047.4323	468	472.68	-110	102	9.84755E-07
10	2047.4323	481	485.81	-58	102	1.03465E-06
11	2047.4323	495	499.95	-7	102	1.0842E-06
12	2047.4323	502	507.02	28	102	1.11457E-06

13	2047.4323	512	517.12	77	102	1.14661E-06
14	2047.4323	523	528.23	113	102	1.18882E-06
15	2047.4323	532	537.32	147	102	1.22259E-06
16	2047.4323	545	550.45	193	102	1.27068E-06
17	2047.4323	560	565.6	249	102	1.31873E-06
18	2047.4323	566	571.66	292	102	1.35494E-06
19	2047.4323	581	586.81	344	102	1.40846E-06
20	2047.4323	593	598.93	393	102	1.44739E-06
21	2047.4323	602	608.02	443	102	1.49269E-06
22	2047.4323	614	620.14	490	102	1.53707E-06
23	2047.4323	625	631.25	547	102	1.57894E-06
24	2047.4323	635	641.35	574	102	1.61454E-06
25	2047.4323	643	649.43	619	102	1.65077E-06
26	2047.4323	650	656.5	654	102	1.6723E-06
27	2047.4323	657	663.57	697	102	1.70952E-06
28	2047.4323	666	672.66	751	102	1.74784E-06

Table 40. Specific impulse, mass flow rate, efficiency and thrust error given by different experiments for Emi TF.

S.N	Isp	m_f	m_f(1e-10)	Thrust(μN)	Efficiency(η)	Thrust error
1	156.621363	4.20183E-10	4.20182875	0.64559232	69.92	19.59
2	185.263587	3.47787E-10	3.47787245	0.63208099	78.46	12.89
3	194.964065	3.40331E-10	3.40331023	0.65091625	81.36	10.87
4	197.989593	3.55072E-10	3.55072199	0.68964889	84.78	8.60
5	179.558321	4.35657E-10	4.35657442	0.76739626	80.90	11.18
6	171.959805	4.92959E-10	4.92958705	0.8315847	80.38	11.54
7	164.422973	5.44711E-10	5.44710687	0.87861255	78.77	12.67
8	162.388856	5.88894E-10	5.8889428	0.93812901	79.59	12.09
9	157.546014	6.37165E-10	6.37165064	0.98475542	78.63	12.77
10	153.772365	6.85875E-10	6.85875416	1.0346478	78.46	12.90
11	150.589955	7.33913E-10	7.33912586	1.08419986	78.24	13.06
12	146.808693	7.73903E-10	7.7390327	1.11457028	77.31	13.73
13	148.149554	7.88947E-10	7.8894662	1.1466133	78.70	12.73
14	143.398812	8.45088E-10	8.4508843	1.18882168	77.32	13.73
15	142.23975	8.76177E-10	8.761775	1.22259351	77.54	13.57
16	138.760033	9.33477E-10	9.33476895	1.27068229	76.74	14.15
17	138.020385	9.73963E-10	9.73962783	1.31872611	77.09	13.89
18	134.859143	1.02417E-09	10.2416933	1.35494345	76.58	14.28

19	131.361661	1.09297E-09	10.9296824	1.40846215	75.53	15.06
20	132.048931	1.11733E-09	11.1733371	1.44739411	76.45	14.37
21	128.316731	1.18582E-09	11.8581874	1.49269337	75.47	15.11
22	127.293435	1.23089E-09	12.308918	1.5370744	75.59	15.02
23	125.913685	1.27827E-09	12.7827397	1.57894094	75.45	15.12
24	125.507297	1.31133E-09	13.1132648	1.61454003	75.69	14.94
25	123.480403	1.36276E-09	13.627644	1.65077478	75.19	15.32
26	123.370642	1.38176E-09	13.8176192	1.67229947	75.29	15.25
27	121.013932	1.44002E-09	14.4002076	1.70951586	74.69	15.71
28	119.540436	1.49045E-09	14.9045337	1.74784226	74.41	15.92

7.3.4.5 TES

Table 41. Acceleration Voltage, Beam Current, Pressure difference, TOF length and Thrust given by different experiments for TES.

S.N	Vacc	I(nA)	I(real)	ΔP	L	Thrust
1	1767.6293	221	223.21	-421	102	4.92647E-07
2	1767.6293	244	246.44	-352	102	5.19356E-07
3	1767.6293	255	257.55	-291	102	5.66932E-07
4	1767.6293	266	268.66	-247	102	6.11964E-07
5	1767.6293	274	276.74	-203	102	6.516E-07
6	1767.6293	286	288.86	-149	102	6.93956E-07
7	1767.6293	295	297.95	-94	102	7.39147E-07
8	1767.6293	305	308.05	-42	102	7.87667E-07
9	1767.6293	310	313.1	-3	102	8.07996E-07
10	1767.6293	324	327.24	52	102	8.63113E-07
11	1767.6293	330	333.3	100	102	8.94254E-07
12	1767.6293	338	341.38	151	102	9.29788E-07
13	1767.6293	343	346.43	189	102	9.56787E-07
14	1767.6293	351	354.51	238	102	9.90205E-07
15	1767.6293	360	363.6	290	102	1.03972E-06
16	1767.6293	366	369.66	335	102	1.06198E-06
17	1767.6293	372	375.72	378	102	1.09391E-06
18	1767.6293	379	382.79	428	102	1.12272E-06
19	1767.6293	383	386.83	461	102	1.15045E-06
20	1767.6293	388	391.88	490	102	1.1684E-06
21	1767.6293	393	396.93	521	102	1.1977E-06
22	1767.6293	398	401.98	551	102	1.22052E-06
23	1767.6293	402	406.02	581	102	1.24073E-06

24	1767.6293	406	410.06	609	102	1.25922E-06
25	1767.6293	410	414.1	637	102	1.28138E-06
26	1767.6293	414	418.14	664	102	1.29577E-06
27	1767.6293	417	421.17	689	102	1.31198E-06
28	1767.6293	421	425.21	724	102	1.33192E-06

Table 42. Specific impulse, mass flow rate, Efficiency and Thrust error given by different experiments for TES.

S.N	Isp	m_f	m_f(1e-10)	Thrust(μN)	Efficiency(η)	Thrust error
1	126.559677	3.968E-10	3.96799601	0.49264672	77.51	13.58
2	142.419995	3.7173E-10	3.71727763	0.51935578	83.29	9.58
3	138.242715	4.1804E-10	4.18041719	0.56693189	84.44	8.82
4	132.299515	4.7152E-10	4.71518753	0.6119645	83.62	9.35
5	126.488006	5.2512E-10	5.25124692	0.65159958	82.64	10.00
6	124.516878	5.6811E-10	5.68113176	0.69395625	83.01	9.76
7	119.889713	6.2846E-10	6.28463213	0.73914695	82.53	10.08
8	117.069043	6.8585E-10	6.8585351	0.78766662	83.06	9.72
9	116.245643	7.0854E-10	7.08538443	0.80799582	83.24	9.60
10	113.182697	7.7735E-10	7.77353275	0.86311264	82.84	9.87
11	110.53341	8.247E-10	8.24704559	0.89425416	82.29	10.23
12	108.675635	8.7213E-10	8.7213323	0.9297882	82.13	10.34
13	107.528778	9.0703E-10	9.07029457	0.95678666	82.41	10.16
14	106.607383	9.4682E-10	9.46823192	0.99020514	82.63	10.01
15	102.616214	1.0328E-09	10.328334	1.0397173	81.42	10.82
16	102.881588	1.0522E-09	10.5223235	1.06198484	82.02	10.42
17	101.60712	1.0975E-09	10.9745556	1.09390621	82.09	10.37
18	100.366458	1.1403E-09	11.4028671	1.12272054	81.69	10.64
19	98.8709446	1.1861E-09	11.8612673	1.15045275	81.60	10.71
20	98.4888881	1.2093E-09	12.0929873	1.1683954	81.48	10.78
21	96.6510992	1.2632E-09	12.632003	1.19769994	80.93	11.16
22	96.4783916	1.2896E-09	12.8957317	1.22052042	81.29	10.92
23	96.0474274	1.3168E-09	13.1681238	1.24073389	81.45	10.81
24	95.0707222	1.3502E-09	13.5015966	1.25921801	81.01	11.10
25	93.95094	1.3903E-09	13.9029781	1.2813801	80.67	11.34
26	93.9063946	1.4066E-09	14.0657475	1.29576722	80.75	11.28
27	93.5964249	1.4289E-09	14.2889326	1.31198254	80.91	11.18
28	92.9315505	1.461E-09	14.609868	1.33192105	80.78	11.26

7.3.4.6 FORMAMIDE 1

Table 43. Acceleration Voltage, Beam Current, Pressure difference, TOF length and Thrust given by different experiments for FORMAMIDE 1.

S.N	Vacc	I(nA)	I(real)	ΔP	L	Thrust
1	1598.0798	205	207.05	-701	102	2.4122E-07
2	1598.0798	277	279.77	-663	102	4.3402E-07
3	1598.0798	356	359.56	-602	102	6.9603E-07
4	1598.0798	420	424.2	-542	102	9.2356E-07
5	1598.0798	464	468.64	-500	102	1.0802E-06
6	1598.0798	514	519.14	-443	102	1.2638E-06
7	1598.0798	547	552.47	-403	102	1.3914E-06
8	1598.0798	588	593.88	-351	102	1.544E-06
9	1598.0798	625	631.25	-303	102	1.6779E-06
10	1598.0798	671	677.71	-242	102	1.8293E-06
11	1598.0798	702	709.02	-197	102	1.9142E-06
12	1598.0798	761	768.61	-140	102	2.0722E-06
13	1598.0798	803	811.03	-98	102	2.1711E-06
14	1598.0798	842	850.42	-44	102	2.275E-06
15	1598.0798	891	899.91	7	102	2.3808E-06
16	1598.0798	935	944.35	58	102	2.4854E-06
17	1598.0798	995	1004.95	107	102	2.5901E-06
18	1598.0798	1068	1078.68	176	102	2.7372E-06
19	1598.0798	1169	1180.69	253	102	2.9146E-06
20	1598.0798	1240	1252.4	305	102	3.0369E-06
21	1598.0798	1310	1323.1	356	102	3.1432E-06
22	1598.0798	1382	1395.82	415	102	3.2818E-06
23	1598.0798	1431	1445.31	453	102	3.3501E-06
24	1598.0798	1501	1516.01	507	102	3.486E-06

Table 44. Specific impulse, mass flow rate, Efficiency and Thrust error given by different experiments for FORMAMIDE 1.

S.N	Isp	m_f	m_f(1e-10)	Thrust(μN)	Efficiency(η)	Thrust error
1	215.368589	1.1417E-10	1.14172207	0.24121914	77.01	13.95
2	186.787843	2.3686E-10	2.36862662	0.43402447	88.94	6.03
3	148.522518	4.7771E-10	4.77712058	0.69602929	88.24	6.45
4	128.650477	7.3179E-10	7.31788426	0.92356176	85.97	7.85
5	120.385507	9.1464E-10	9.14637099	1.08016979	85.17	8.36
6	111.064019	1.1599E-09	11.5989889	1.26375395	82.98	9.78

7	106.504783	1.3317E-09	13.3167832	1.39135339	82.33	10.21
8	101.632284	1.5486E-09	15.4864522	1.54401896	81.10	11.04
9	97.1328376	1.7609E-09	17.6088959	1.67790439	79.25	12.33
10	92.5055589	2.0158E-09	20.1575186	1.82925356	76.64	14.23
11	90.2192004	2.1628E-09	21.628112	1.91419683	74.76	15.66
12	86.5536213	2.4405E-09	24.4046854	2.07217993	71.62	18.16
13	84.9647911	2.6048E-09	26.0482676	2.17113509	69.81	19.68
14	81.9719582	2.8291E-09	28.2914031	2.27503878	67.31	21.89
15	80.3766002	3.0194E-09	30.1944682	2.38081705	65.27	23.78
16	78.3118889	3.2352E-09	32.3521786	2.48542257	63.26	25.73
17	76.4514603	3.4535E-09	34.5346914	2.59006327	60.48	28.59
18	74.2094923	3.7599E-09	37.5989751	2.73718704	57.80	31.54
19	72.1460951	4.1181E-09	41.1808865	2.91459039	54.66	35.25
20	70.7891012	4.3732E-09	43.7319182	3.03692406	52.69	37.77
21	69.5759221	4.6051E-09	46.0510051	3.14316436	50.73	40.40
22	68.2738991	4.8999E-09	48.9986302	3.28176631	49.27	42.47
23	67.813836	5.0359E-09	50.3589701	3.35014927	48.25	43.97
24	66.8733135	5.3138E-09	53.1380984	3.48600382	47.20	45.56

7.3.4.7 FORMAMIDE 2

Table 45. Acceleration Voltage, Beam Current, Pressure difference, TOF length and Thrust given by different experiments for FORMAMIDE 2.

S.N	Vacc	I(nA)	I(real)	ΔP	L	Thrust
1	1593.4473	170	171.7	-722	102	1.3753E-07
2	1593.4473	280	282.8	-660	102	5.5303E-07
3	1593.4473	356	359.56	-603	102	8.5901E-07
4	1593.4473	412	416.12	-549	102	1.1155E-06
5	1593.4473	467	471.67	-499	102	1.3568E-06
6	1593.4473	522	527.22	-436	102	1.6165E-06
7	1593.4473	557	562.57	-389	102	1.7915E-06
8	1593.4473	591	596.91	-343	102	1.9432E-06
9	1593.4473	628	634.28	-300	102	2.0894E-06
10	1593.4473	681	687.81	-242	102	2.2611E-06
11	1593.4473	725	732.25	-201	102	2.3849E-06
12	1593.4473	778	785.78	-145	102	2.5228E-06
13	1593.4473	832	840.32	-104	102	2.662E-06
14	1593.4473	890	898.9	-50	102	2.7983E-06
15	1593.4473	944	953.44	3	102	2.9206E-06

16	1593.4473	1011	1021.11	58	102	3.0818E-06
17	1593.4473	1069	1079.69	109	102	3.2096E-06
18	1593.4473	1119	1130.19	157	102	3.3125E-06
19	1593.4473	1164	1175.64	204	102	3.4166E-06
20	1593.4473	1210	1222.1	249	102	3.5409E-06
21	1593.4473	1272	1284.72	305	102	3.6808E-06
22	1593.4473	1324	1337.24	348	102	3.8083E-06

Table 46. Specific impulse, mass flow rate, Efficiency and Thrust error given by different experiments for FORMAMIDE 2.

S.N	Isp	m_f	m_f(1e-10)	Thrust(μN)	Efficiency(η)	Thrust error
1	284.101713	4.9345E-11	0.49344817	0.13752587	70.05	19.48
2	158.536931	3.5559E-10	3.55587538	0.55302655	95.43	2.36
3	129.016542	6.7871E-10	6.78709881	0.8590107	94.88	2.66
4	111.333148	1.0213E-09	10.2133465	1.11547942	91.87	4.33
5	102.108605	1.3545E-09	13.544841	1.35676696	90.41	5.17
6	93.5421932	1.7616E-09	17.6158483	1.61651641	88.29	6.43
7	88.4469367	2.0647E-09	20.6472645	1.79148974	86.70	7.40
8	84.6591713	2.3398E-09	23.3980359	1.94322202	84.84	8.57
9	81.3512588	2.6181E-09	26.1808982	2.08938189	82.49	10.10
10	77.4554065	2.9758E-09	29.7575571	2.26109089	78.38	12.95
11	75.0023848	3.2414E-09	32.4136855	2.38491274	75.20	15.32
12	72.0352603	3.57E-09	35.6997697	2.522781	71.19	18.52
13	69.9370646	3.88E-09	38.799696	2.66197965	68.20	21.09
14	67.9020373	4.2009E-09	42.0085464	2.79826903	65.07	23.97
15	65.9589457	4.5136E-09	45.1362879	2.92057626	62.19	26.80
16	64.3338114	4.883E-09	48.8304785	3.08176323	59.77	29.35
17	63.022068	5.1914E-09	51.9140616	3.20956862	57.67	31.68
18	61.7880662	5.4649E-09	54.6491549	3.31250896	55.75	33.94
19	60.8443027	5.7241E-09	57.2414428	3.41664218	54.43	35.54
20	59.9199336	6.0239E-09	60.2391395	3.54094426	53.44	36.79
21	58.9999979	6.3595E-09	63.595355	3.68083542	52.03	38.63
22	58.3977331	6.6476E-09	66.4763528	3.80830901	51.19	39.76

7.3.4.8 FORMAMIDE G

Table 47. Acceleration Voltage, Beam Current, Pressure difference, TOF length and Thrust given by different experiments for FORMAMIDE G.

S.N	Vacc	I(nA)	I(real)	ΔP	L	Thrust
1	1933.4728	223	225.23	-725	102	1.11931E-07
2	1933.4728	396	399.96	-640	102	8.44877E-07
3	1933.4728	475	479.75	-588	102	1.18856E-06
4	1933.4728	545	550.45	-536	102	1.50186E-06
5	1933.4728	610	616.1	-486	102	1.79663E-06
6	1933.4728	684	690.84	-424	102	2.09968E-06
7	1933.4728	728	735.28	-393	102	2.24968E-06
8	1933.4728	781	788.81	-350	102	2.41665E-06
9	1933.4728	856	864.56	-299	102	2.62871E-06
10	1933.4728	930	939.3	-249	102	2.82744E-06
11	1933.4728	1001	1011.01	-199	102	3.01543E-06
12	1933.4728	1082	1092.82	-145	102	3.24612E-06
13	1933.4728	1150	1161.5	-101	102	3.43831E-06
14	1933.4728	1220	1232.2	-50	102	3.63804E-06
15	1933.4728	1303	1316.03	6	102	3.88174E-06
16	1933.4728	1370	1383.7	49	102	4.06823E-06
17	1933.4728	1520	1535.2	145	102	4.51796E-06
18	1933.4728	1586	1601.86	201	102	4.75233E-06
19	1933.4728	1660	1676.6	249	102	4.98065E-06
20	1933.4728	1740	1757.4	308	102	5.2492E-06
21	1933.4728	1811	1829.11	352	102	5.47753E-06
22	1933.4728	1860	1878.6	397	102	5.6397E-06
23	1933.4728	1942	1961.42	453	102	5.91374E-06
24	1933.4728	2010	2030.1	506	102	6.14901E-06
25	1933.4728	2087	2107.87	562	102	6.40196E-06
26	1933.4728	2140	2161.4	600	102	6.57341E-06
27	1933.4728	2262	2284.62	713	102	6.97633E-06
28	1933.4728	2388	2411.88	811	102	7.41088E-06

Table 48. Specific impulse, mass flow rate, efficiency and thrust error given by different experiments for FORMAMIDE G

S.N	Isp	m_f	m_f(1e-10)	Thrust(μN)	Efficiency(η)	Thrust error
1	1469.33214	7.76534E-12	0.07765344	0.11193082	185.24	-26.53
2	181.40618	4.74758E-10	4.74758051	0.84487688	97.21	1.42

3	151.528015	7.99577E-10	7.99576752	1.18856271	95.24	2.47
4	135.831422	1.12709E-09	11.2709289	1.50185832	94.02	3.13
5	123.697362	1.48057E-09	14.8057222	1.79663164	91.51	4.54
6	111.903652	1.91266E-09	19.1266469	2.09967515	86.28	7.66
7	107.023299	2.14275E-09	21.4275477	2.24967516	83.07	9.72
8	100.518241	2.45075E-09	24.5075234	2.41664753	78.12	13.14
9	94.6018735	2.83253E-09	28.3253012	2.62871366	72.97	17.06
10	89.7613712	3.21096E-09	32.1095832	2.82743841	68.55	20.78
11	85.6791606	3.58761E-09	35.8761201	3.01543298	64.83	24.20
12	82.1559836	4.02769E-09	40.2769129	3.24611859	61.91	27.09
13	79.6265265	4.40167E-09	44.0167166	3.43830519	59.80	29.32
14	77.6921709	4.77333E-09	47.733328	3.63804427	58.19	31.09
15	75.5918134	5.23459E-09	52.3458807	3.88173857	56.56	32.96
16	74.2567396	5.58472E-09	55.8471648	4.06823483	55.39	34.37
17	71.864653	6.40853E-09	64.0852827	4.51796274	53.65	36.52
18	70.7307104	6.84903E-09	68.4903427	4.75232756	53.23	37.06
19	69.8271246	7.27098E-09	72.7098476	4.98065432	52.62	37.85
20	69.0239533	7.75219E-09	77.5219151	5.24920254	52.30	38.27
21	68.7462302	8.12207E-09	81.2207078	5.47752874	52.23	38.37
22	68.117345	8.43975E-09	84.3974665	5.63970165	51.88	38.84
23	67.3783705	8.94691E-09	89.4690948	5.91374446	51.54	39.30
24	67.1516527	9.33425E-09	93.3424958	6.14900891	51.60	39.21
25	66.9699967	9.74459E-09	97.4458522	6.40195538	51.60	39.21
26	66.8276536	1.00269E-08	100.268728	6.57341004	51.56	39.27
27	66.5922345	1.06791E-08	106.790921	6.9763286	51.59	39.23
28	66.6792344	1.13295E-08	113.294823	7.41087824	51.98	38.71

.

7.3.4.9 FORMAMIDE H

Table 49. Acceleration Voltage, Beam Current, Pressure difference, TOF length and Thrust given by different experiments for FORMAMIDE H.

S.N	Vacc	I(nA)	I(real)	ΔP	L	Thrust
1	1933.4728	314	317.14	-730	102	1.04923E-07
2	1933.4728	372	375.72	-690	102	4.94688E-07
3	1933.4728	494	498.94	-642	102	9.2132E-07
4	1933.4728	573	578.73	-602	102	1.19376E-06
5	1933.4728	733	740.33	-521	102	1.7013E-06

6	1933.4728	828	836.28	-480	102	1.91761E-06
7	1933.4728	990	999.9	-410	102	2.23605E-06
8	1933.4728	1123	1134.23	-357	102	2.47301E-06
9	1933.4728	1282	1294.82	-297	102	2.7623E-06
10	1933.4728	1430	1444.3	-242	102	3.04138E-06
11	1933.4728	1554	1569.54	-194	102	3.30376E-06
12	1933.4728	1683	1699.83	-147	102	3.57553E-06
13	1933.4728	1803	1821.03	-101	102	3.84339E-06
14	1933.4728	1944	1963.44	-48	102	4.16298E-06
15	1933.4728	2051	2071.51	0	102	4.44063E-06
16	1933.4728	2198	2219.98	55	102	4.80269E-06
17	1933.4728	2308	2331.08	105	102	5.06549E-06
18	1933.4728	2444	2468.44	158	102	5.41116E-06
19	1933.4728	2558	2583.58	205	102	5.70658E-06
20	1933.4728	2674	2700.74	250	102	6.03914E-06
21	1933.4728	2791	2818.91	307	102	6.37658E-06
22	1933.4728	2899	2927.99	352	102	6.67331E-06
23	1933.4728	3016	3046.16	407	102	6.96262E-06
24	1933.4728	3096	3126.96	448	102	7.19651E-06
25	1933.4728	3240	3272.4	509	102	7.60123E-06
26	1933.4728	3338	3371.38	558	102	7.86E-06
27	1933.4728	3460	3494.6	618	102	8.21717E-06
28	1933.4728	3640	3676.4	710	102	8.69928E-06

Table 50. Specific impulse, mass flow rate, Efficiency and Thrust error given by different experiments for FORMAMIDE H.

S.N	Isp	m_f	m_f(1e-10)	Thrust(μN)	Efficiency(η)	Thrust error
1	1315.06771	8.13302E-12	0.08133021	0.10492259	110.37	-4.82
2	307.881773	1.63787E-10	1.6378664	0.4946881	102.84	-1.39
3	191.424643	4.90618E-10	4.90618376	0.92132035	89.67	5.60
4	177.26274	6.86487E-10	6.86486689	1.1937643	92.76	3.83
5	142.539052	1.21669E-09	12.166867	1.70130288	83.10	9.70
6	130.980576	1.4924E-09	14.9239718	1.91761016	76.19	14.56
7	115.169944	1.97913E-09	19.7912939	2.23605433	65.34	23.71
8	107.876851	2.33684E-09	23.3684102	2.4730132	59.67	29.46
9	101.2907	2.77992E-09	27.7992336	2.76230355	54.82	35.06
10	97.0600279	3.19419E-09	31.9419488	3.041381	51.85	38.87
11	93.6110199	3.5976E-09	35.9759544	3.30375861	49.99	41.44
12	91.6393121	3.97731E-09	39.7731476	3.575533	48.90	43.00

13	89.6683347	4.36924E-09	43.6924187	3.84338773	48.01	44.32
14	88.2415426	4.80908E-09	48.0908421	4.1629815	47.46	45.15
15	86.4055049	5.23883E-09	52.3882508	4.44062723	46.99	45.88
16	85.2223499	5.74463E-09	57.4462678	4.80268753	46.77	46.22
17	84.5379466	6.10803E-09	61.080259	5.06549129	46.60	46.48
18	83.8573856	6.57779E-09	65.7778682	5.41115681	46.63	46.44
19	83.4293367	6.9725E-09	69.7249856	5.70658422	46.75	46.26
20	82.2744254	7.4824E-09	74.8240162	6.03913698	46.67	46.38
21	81.848047	7.94165E-09	79.4164842	6.37658253	46.97	45.91
22	81.6528459	8.33107E-09	83.3106858	6.67330606	47.21	45.54
23	81.6700432	8.69043E-09	86.9042873	6.96262483	47.36	45.31
24	81.8805404	8.95926E-09	89.5926299	7.19651099	47.81	44.63
25	81.4496094	9.51319E-09	95.1318908	7.6012347	48.00	44.34
26	82.0545093	9.76452E-09	97.6452057	7.85999708	48.53	43.55
27	81.4310593	1.02864E-08	102.864004	8.21717467	48.58	43.48
28	82.4285315	1.07581E-08	107.58127	8.69927858	49.48	42.16

7.4 Dimensions of thruster head

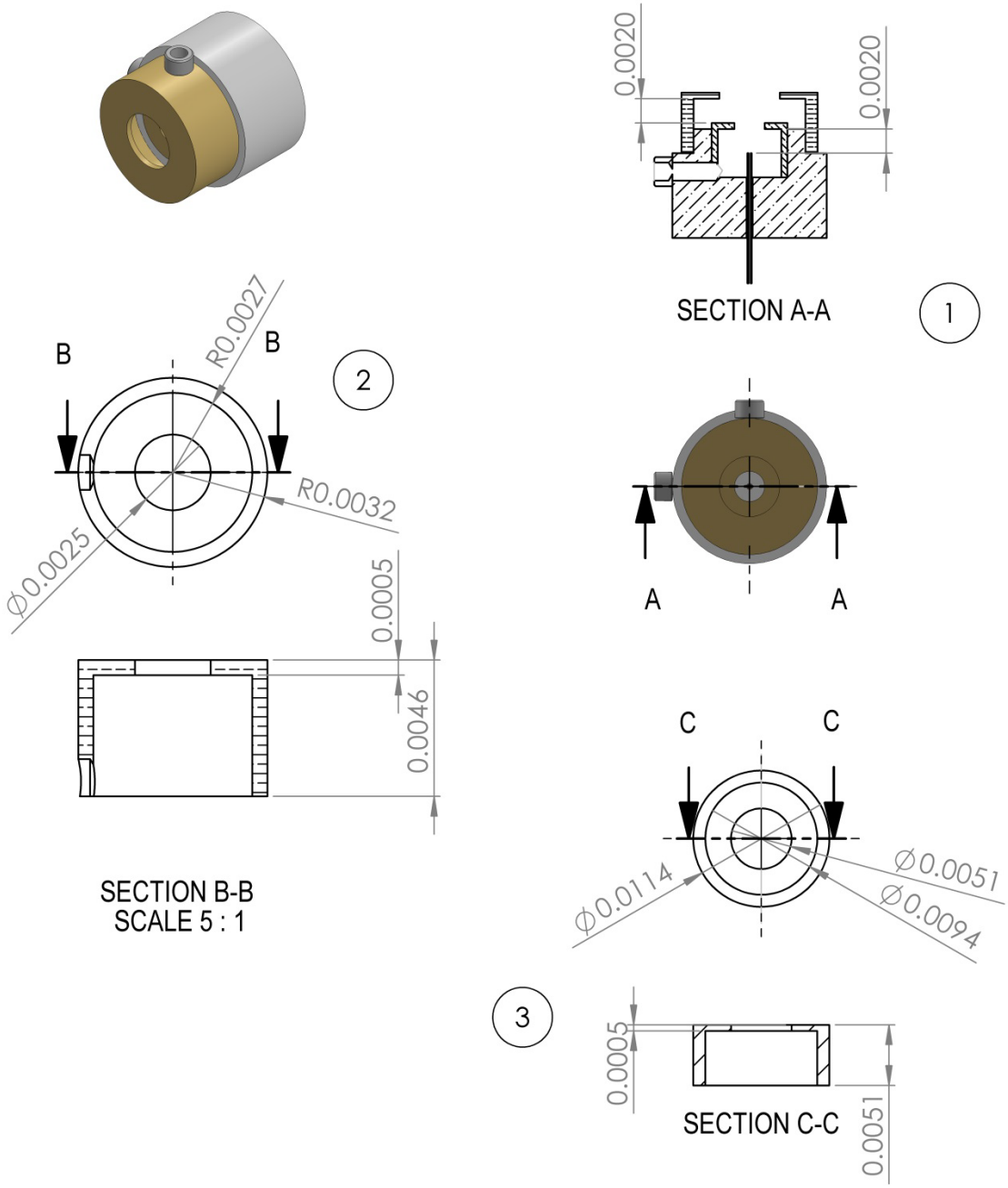

TITLE	SCALE	COMPONENTS	MATERIALS	AUTHOR
Thruster Head	2:1	1:Thruster Head 2:Internal Extractor 3: External Extractor	1: Brass & Teflon 2 & 3: Brass	N. Timilsina

Figure 148. Dimensions of the components of thruster heads and the distance between them in the assembly